FINITE ELEMENT STUDY OF TUNNEL-SOIL-PILE INTERACTION

by

Cheng Ch'ng Yih B. Eng. (Hons)

A thesis submitted in partial fulfillment of the
requirements for the degree of

Masters of Engineering

National University of Singapore

2003

ACKNOWLEDGEMENTS

The author wishes to express his sincere gratitude and thanks to his supervisor, Dr Ganeswara Rao Dasari, who has been an endless source of ideas and inspiration. His guidance and help rendered throughout the candidature of the author is much appreciated. The author also wishes to thank his co-supervisors, A/P Leung Chun Fai and Prof Chow Yean Khow for their encouragement and advice given, especially during the fortnightly meetings.

The assistance of Mr. Yeo Eng Hee from the Supercomputing and Visualisation Unit and Mr. Kwa Lam Koon from the Engineering Information Technology Unit for facilitating the use of computational resources is also acknowledged.

The completion of this thesis would also not be possible without the invaluable support of a dear friend, Ms. Chew Puey Lu. Last but not least, the author wishes to extend his thanks to all friends and family who has provided moral support without whom the completion of this thesis would not have been possible.

FINITE ELEMENT STUDY OF TUNNEL-SOIL-PILE INTERACTION

Cheng Ch'ng Yih

National University of Singapore

ABSTRACT

This study was initiated to assess the effects of tunneling induced ground movements on adjacent pile foundations. Current methods of analyzing such interaction behaviour involve a two stage uncoupled approach which is subject to major limitations. A novel kinematic FE model, called Displacement Controlled Model (DCM) which simulates soil convergence around the excavated tunnel boundary is first developed to obtain the realistic displacement field around a deforming tunnel. This model was subsequently applied to the analysis of tunnel-soil-pile interaction in three-dimensional (3D) space.

Computed ground movements from the back analysis of numerous greenfield case histories are in good agreement with field data thus verifying the usefulness of the DCM developed for this study. A strain dependant constitutive model accounting for stiffness non-linearity was used to obtain realistic ground movement profiles. Subsurface soil displacements and shape are also predicted to a reasonable degree of accuracy. Emphasis was placed on obtaining correct displacement shape as it is important for assessing induced bending stresses in structures and services. Realistic computed displacement magnitudes and shape around a deforming tunnel indicate the suitability of the method in analyzing complex tunnel-soil-structure problems.

Sixty five tunnel-soil-pile interaction parametric analyses were performed to investigate in detail the various factors affecting the performance of single piles. Computed induced pile bending moments (*BM*) and axial forces (*P*) generally agrees in trend with current findings. The study reveals that for piles in close proximity to the tunnel (less than 1 tunnel diameter), the induced *BM* could be close to its ultimate capacity. When the pile head is fixed (rotation and displacement) computed results indicate that the pile may fail in tension depending on pile geometry, soil type and relative position of the pile tip with respect to tunnel axis level. This is due to the small relative displacements required to fully mobilize skin friction even at small volume loss magnitudes.

Back analyses of two case histories indicate fair agreement between computed and test results with regards to maximum induced pile *BM* and *P*. The first analysis corresponded to a single pile centrifuge test while the second was performed for a two by two pile group field case.

TABLE OF CONTENT

LIST OF FIGURES

LIST OF TABLES

NOTATIONS AND ABBREVEATIONS

English alphabet, upper case

BM = induced pile bending moment

C = soil cover above tunnel

D_p = pile diameter

D_t = excavated tunnel diameter

E = Young's modulus

E_p = pile Young's modulus

E_pI = pile flexural stiffness

G = soil shear modulus

G_p = difference between cutter head and tunnel lining diameter (Gap Parameter Method)

K = trough width parameter

K_o = coefficient of earth pressure at rest

L_p = pile length

P = induced pile axial force

R = excavated tunnel radius

R_o = overconsolidation ratio defined as p_c'/p'

S = soil settlement induced by tunneling

U^*_{3D} = parameter accounting for three dimensional heading effects (Gap Parameter Method)

V_l = tunnel volume loss

X = horizontal distance between pile and tunnel centre

Y_p = pile tip level relative to tunnel axis level (positive for pile tip above tunnel axis)

English alphabet, lower case

a = radius of point sink

f_{cu} = concrete crushing stress

g = gravitational acceleration constant ($9.81 ms^{-2}$)

i = horizontal distance from tunnel centre to point of inflexion of the settlement trough

n = parameter controlling rate of stiffness degradation within small strain region

p' = mean normal effective stress

p_c' = preconsolidation pressure

x = horizontal offset from tunnel centre

r = radial distance from point sink

u_1 = pile displacement in the transverse tunnel direction

u_3 = pile displacement in the vertical direction

z = depth below ground surface

z_0 = depth to tunnel axis level

Greek alphabet

ε_q = deviatoric strain

ϖ = parameter accounting for workmanship quality (Gap Parameter Method)

ϕ' = effective friction angle of soil

β = parameter denoting focus point of tunnel (DCM)

μ = coefficient of friction

γ = slip displacement for interface element

τ = skin friction / shear stress

τ_1 = skin friction mobilized along pile longitudinal axis

τ_2 = skin friction mobilized transverse to pile longitudinal axis

ν = Poisson ratio

σ' = soil effective stress

Subscripts

cr = cracking moment

equi = $\sqrt{\tau_1^{\,2} + \tau_2^{\,2}}$ = equivalent shear stress

h = horizontal direction

lim = limiting elastic slip or skin friction

max = maximum magnitude

min = minimum magnitude

nc = normally consolidated

oc = over consolidated

sec = secant stiffness

tan = tangent stiffness

ult = ultimate bending moment or tensile force

v = vertical direction

CHAPTER 1

INTRODUCTION

1.1 Background

Recent advances in tunneling technology have enabled underground space to be exploited to a greater extent as numerous techniques and machines are available to efficiently excavate through almost any soil condition. This advancement is reflected in the large number of tunnel excavation projects proceeding concurrently throughout the world, mostly in densely populated areas where land is scarce. It is therefore inevitable that some form of tunnel-soil-structure interaction will occur as the zone of influence caused by tunneling induced ground movements affects close proximity structures, foundations and services. Although such circumstances are inherently undesirable, tunnel construction in such areas may be dictated by geographical and or economic constraints.

A form of tunnel-soil-structure interaction that has recently received much attention concerns the effect of tunneling induced ground movements on piles. This is mainly attributed to the fact that more tunnels are being excavated close to piled foundations (Lee et al., 1994, Coutts and Wang, 2000, Tham and Deutscher, 2000) which consequently results in additional lateral and vertical forces induced on the pile. Depending on the fixity conditions at the pile head and relative position of the pile and its tip to the tunnel, failure could be induced to the deep foundation by exceeding a combination of serviceability and/or ultimate limit states.

To avoid the hazard of damaging close proximity piles, a method is required to systematically and reliably assess the performance of piles subjected to tunneling induced ground movements. The effect of construction method, ground conditions, soil type and pile-tunnel geometry should be accounted for in order to obtain realistic predictions that are suitable for decision making purposes.

Current methods of analyzing pile performance subjected to tunneling induced ground movement involves a two stage uncoupled approach where greenfield soil movements are approximated by a quasi-analytical method (Loganathan and Poulos, 1998), subsequently applying the obtained free field ground movements on soil elements surrounding the pile via boundary element programs (Chen et al., 1999, Loganathan et al., 2001). In these numerical programs, the pile is either modeled as a beam or elastic continuum while the soil is modeled as an elastic continuum. Although simple and easy to use, this approach to estimating pile performance subjected to tunneling induced ground movements does not account for coupled interaction where induced pile axial loads could result in additional moments depending on the magnitude of pile deformation under lateral loading (Chen and Poulos, 1999). This suggests that a more rigorous approach to analyzing tunnel-soil-pile interaction is required to obtain a better understanding and insight into the various factors affecting piled foundations.

One such tool to analyse complex tunnel-soil-pile interaction in a more rigorous manner is the FE method where coupled interaction is simulated. Although tunneling is essentially a 3D problem, 3D FE analysis (construction sequence modeled) is resource intensive. Assuming experienced tunnellers and good construction technique are present in a tunnel excavation project, the most severe loading on a close proximity pile would correspond to the case in

which tunnel face has past the pile location, ie. uniform displacements along tunnel boundary in the longitudinal direction. 3D FE studies by Mroueh and Shahrour (2002) and field data from Coutts and Wang (2000) supports this intuitive assumption as although pile bending is inevitably induced in the longitudinal tunnel direction, maximum bending moments are developed in the transverse tunnel direction when tunnel heading has passed the pile location. Thus the problem can be simplified to a 3D FE analysis in geometry but with uniform soil displacements along the tunnel boundary in the longitudinal direction.

Plane strain tunnel excavation is commonly simulated using the FE method by various techniques such as the Convergence Confinement Method (Panet and Guenot, 1982), Volume Loss Method and Gap Parameter Method (Lee et al., 1992). In these methods, soil convergence around the tunnel is simulated by releasing insitu soil stresses from equilibrium conditions, hence the term "stress based". This is performed by (i) removing elements that form the excavated tunnel or (ii) releasing fixities around the excavated tunnel boundary. Although widely accepted, the application of the above mentioned methods to 2D FE tunnel analyses usually result in incorrect displacement profiles. Computed settlement troughs are wider than field data coupled with high far field settlements while subsurface displacements are unreliable due to the incorrect surface settlement trough.

This shortcoming can be partly improved by using advanced soil constitutive models as in Lee and Rowe (1989), Stallebrass et al. (1996), Addenbrooke et al. (1997), Simpson (1996). As noted by Stallebrass et al. (1996) and observed in NATM tunnelling studies by Dasari et al. (1996), the inclusion of advanced soil models have only resulted in limited success. This limited success may be sufficient for ground movement prediction, but may not be so for tunnel-soil-pile interaction as the induced forces in the pile are sensitive to deformed shape.

This therefore suggests a need for an improved method capable of predicting the displacement field around a converging tunnel to an acceptable degree of accuracy before meaningful FE analysis of tunnel-soil-pile interaction study can be performed.

1.2 Objectives and Scope of Study

Due to the inherent nature of the problem where a pile is cast/driven long before a tunnel is excavated along side, it is very difficult to instrument the pile to obtain induced bending moments and axial forces. Therefore, numerical tools could be used to gain insight into the problem. This study intends to provide a reliable and sound numerical method to predict pile responses subjected to tunneling induced ground movement to supplement the few documented field cases available.

The objectives of the present research study are as follows:

(a) To develop a novel Displacement Based Model (DCM) capable of predicting plane strain tunneling induced ground movements accurately using FE methods.

(b) To obtain realistic and reasonable predictions of pile structural performance using the DCM in 3D tunnel-soil-pile interaction studies.

The scope of the research encompasses three main parts. The first part involves developing a new FE model to obtain the correct plane strain displacement field around the tunnel by assuming a deformation mechanism around the excavated tunnel. Numerous greenfield tunnel case histories in clay are back analysed to verify the applicability of the method. The tunnels located are at various tunnel cover to tunnel diameter (C/D_i) ratios thus providing an adequate collection of cases to verify the developed method.

In the second part of this study, DCM was used for tunnel-soil-pile interaction analysis to study the various factors influencing pile performance when subjected to tunneling induced ground movements. A hypothetical pile and tunnel problem was analysed while varying the below mentioned factors:

i) soil stiffness

ii) volume loss (V_l)

iii) pile head fixity conditions (rotation and displacement)

iv) pile length, ie. pile tip position relative to tunnel axis level (Y_p)

v) pile horizontal distance from tunnel (X)

C/D_t ratio, pile diameter (D_p) and pile Young's modulus (E_p) were assumed constant for all analyses. The parameters investigated are induced bending moments and axial forces, in particular their maximum magnitudes.

Finally, DCM was applied to back analyse two tunnel-soil-pile case histories; one from centrifuge testing and the other from a field project.

1.3 Organisation of Thesis

Chapter 2 presents a review of the literature relevant to the study of this thesis. This review covers the various popular methods available to predict plane strain tunneling induced ground movements and the limitations associated with each method. Also reviewed are the research efforts in the area of tunnel-soil-pile interaction.

The development of the DCM is fully discussed in Chapter 3 with justifications behind the various assumptions employed in the method. The applicability of the method is verified by comparison with published field and centrifuge data of tunnels excavated in greenfield conditions. Comparisons are also made with existing methods used to predict the displacement field around a deforming tunnel.

Chapter 4 presents a detailed study on tunnel-soil-pile interaction. The impact of various factors on pile performance is presented to develop a deeper understanding of the problem.

The suitability of the DCM to predict/simulate tunnel-soil-pile interaction is verified in Chapter 5 by back analysing and comparing computed results with a published centrifuge test and field case history.

Conclusions of findings presented in this thesis are summarised in Chapter 6 along with suggestions for further work.

CHAPTER 2

BACKGROUND THEORY AND LITERATURE REVIEW

2.1 Introduction

The prediction of tunneling induced ground movements is necessary and important to prevent potential damage to pre-existing structures, foundations and services in the form of serviceability (displacements) or ultimate limit states (stress). The engineer responsible for design and construction of the tunnel should be able to predict these movements to a reasonable degree of accuracy with the aid of numerous methods that are available to him. The selection of method would largely depend on the complexity and severity of the tunnel-soil-structure interaction anticipated from the tunnel excavation project and the resources available to the engineer.

This chapter briefly discusses the features of various methods employed to predict tunneling induced ground behaviour with the intention of justifying the necessity of FE methods in analysing tunnel-soil-pile interaction problems and why a new model is required to simulate 2D FE tunneling. Published efforts and current advances in the area of tunnel-soil-pile interaction are also presented.

2.2 Tunnelling Induced Ground Movements

Various methods are available to the engineer to predict soil deformation due to tunnel excavation. These methods can be generally categorized as; (i) empirical, (ii) analytical and (iii) numerical to which each has its merits and limitations.

2.2.1 Empirical Methods

For the case of a greenfield tunnel excavation, Peck's (1969) representation of the transverse settlement trough in the shape of a Gaussian distribution curve (Figure 2.1) is arguably the most popular empirical method used to provide a preliminary estimate of the surface settlement profile. The method offers the advantage of simplicity with only 2 parameters required as input. The method needs an estimate of volume loss (V_l) and the trough width parameter (i) to obtain S_{max} and subsequently the settlement profile. Settlements are generally negligible beyond an offset of 3i from the tunnel centerline for Peck's proposed curve.

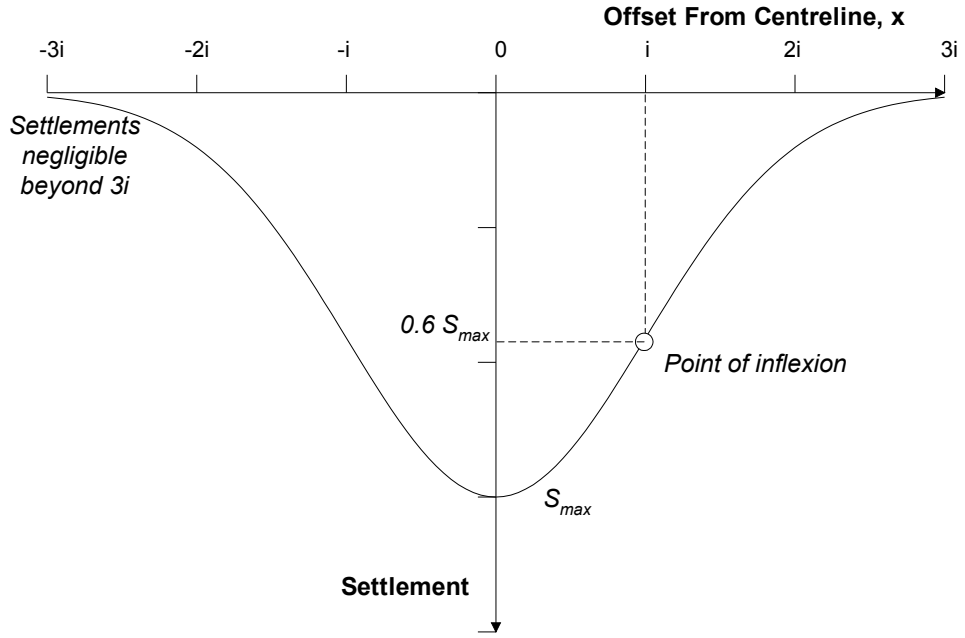

Fig. 2.1. Gaussian curve approximating transverse surface settlement trough

The surface settlement trough and volume loss is approximated by the following equations;

$$S = S_{\max} \exp\left(-\frac{x^2}{2i^2}\right) \tag{2.1}$$

$$V = \sqrt{2\pi} i S_{\max} \tag{2.2}$$

Estimates of volume loss are made by the engineer based on experience, taking into account the effects of ground conditions, contractor and or operator experience and construction technique. Unlike volume loss, the trough width parameter is relatively easier to quantify as it is largely independent of construction method and operator experience (Fujita, 1981; O'Reilly and New, 1982). Numerous estimates of trough width parameters have been put forward by researchers based on their collection of field data. However, a comprehensive summary by Lake et al. (1992) on tunneling data from many countries has shown that the general variations of *i* are as such:

- Approximate relationship $i = Kz_o$
- Clays (soft and stiff) K = 0.4-0.6
- Sands and gravels K = 0.25-0.45

where z_o is the depth to tunnel axis level. This study complements the various proposals that *K* can be assumed as 0.5 for tunnels excavated in clays (O'Reilly and New, 1982; Mair et al., 1993).

Subsurface settlement profiles are also reasonably approximated by a Gaussian distribution curve in a similar way as surface settlements. Mair et al. (1993) proposed that at a depth z below the ground surface, above a tunnel depth of z_o, the trough width parameter for tunnels constructed in clays can be expressed as:

$$i = K(z_o - z) \tag{2.3}$$

$$K = \frac{0.175 + 0.325\left(1 - z/z_o\right)}{\left(1 - z/z_o\right)} \tag{2.4}$$

The variation of *K* presented above was obtained from a best fit line to field data from numerous tunneling projects (Figure 2.2). Trough width parameter is shown to increase with depth and would be under predicted should a constant value be assumed. Similar patterns of increase in *K* was observed in studies by Moh et al. (1996) and Dyer et al. (1996) irrespective of the soil conditions encountered. Recent centrifuge studies by Grant and Taylor (2000) show that the proposed variation of *K* with depth for clays by Mair et al. (1993) provide a good fit to data obtained from tests within a certain range between ground surface and tunnel axis level (Figure 2.3). Data showed larger trough width values at the surface and lower values nearing tunnel axis level compared to corresponding magnitudes obtained using Mair's (1993) proposed variation.

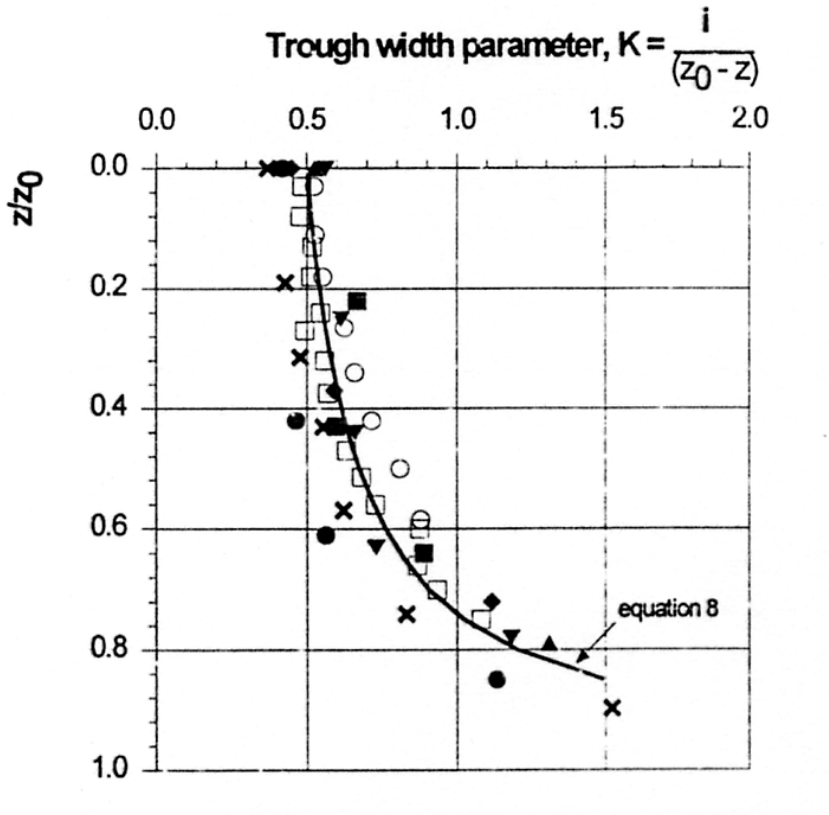

Fig. 2.2. Variation of trough width parameter *K* with depth for subsurface settlement profiles above tunnels in clays (Mair et al., 1993)

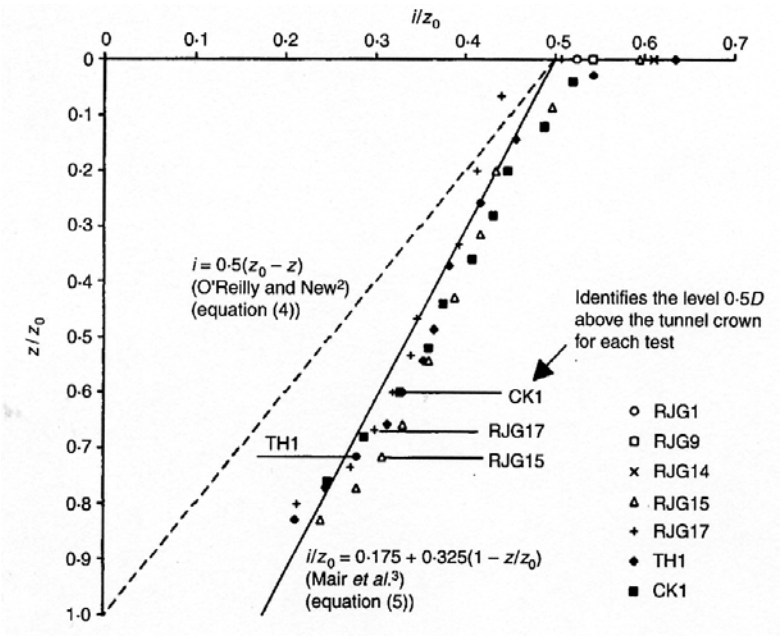

Fig. 2.3. Variation of normalized *i* parameter with depth (Grant and Taylor, 2000)

Horizontal movements can be predicted by assuming a particular focus point along the tunnel centre line. Attewell (1978) and O'Reilly and New (1982) proposed a convergence point at the tunnel centre for tunnels in clays while Taylor (1995) demonstrated that for constant volume conditions, the application of Equation 2.2 to represent the variation of K with depth would yield a convergence point $\frac{0.175}{0.325} z_o$ below tunnel axis level.

- Convergence point at tunnel centre

$$S_h = \frac{x}{z_o} S_v$$

$$S_h = 1.65 S_{h\max} \frac{x}{i} \exp\left(-\frac{x^2}{2i^2}\right) \qquad (2.5)$$

- Convergence point at $\frac{0.175}{0.325} z_o$ below tunnel axis level

$$S_h = 0.65 \frac{x}{z_o} S_v$$

$$S_h = 1.07 S_{h\max} \frac{x}{i} \exp\left(-\frac{x^2}{2i^2} \right) \qquad (2.6)$$

Empirical predictions of subsurface horizontal movements are 35% less for the latter case compared to the former.

Although simple and efficient to use, empirical methods suffer from certain limitations. They are unable to directly account for the effect of (i) varying soil properties, (ii) different ground conditions, (iii) construction method and most important to this study, (iv) tunnel-soil-structure interaction.

2.2.2 Analytical and Quasi-Analytical Methods

Closed form solutions represent a theoretically based method to obtain predictions of displacements and corresponding stress-strain field around a deforming tunnel. Equilibrium conditions, boundary conditions and constitutive models are required to derive these solutions thus producing a sound and consistent method to determine tunnel deformation behaviour. There also exist methods that build on established closed form solutions which are termed as quasi-analytical methods in this study. These methods are modified to incorporate observations from field data thus adding varying degrees of empiricism into the solutions.

Sagaseta (1987) presented an analytical solution to predict tunneling induced ground movements for a weightless incompressible soil by simulating ground loss around a tunnel in the form of a point sink. The tunnel is first assumed to be located within an elastic infinite medium where it collapses uniformly. Plane strain displacements around the sink with centre at coordinates (x_o, y_o) can be estimated by the following equations:

$$S_x = -\frac{(x - x_o)}{2}\left(\frac{a}{r}\right)^2 \tag{2.7}$$

$$S_y = -\frac{(z - z_o)}{2}\left(\frac{a}{r}\right)^2 \tag{2.8}$$

where a is the radius of the point sink with area (πa^2) equal to predicted ground loss and $r = \left[(x - x_o)^2 + (z - z_o)^2\right]^{\frac{1}{2}}$. The free ground surface is simulated by introducing a virtual image to eliminate normal or shear stresses at the surface. Corresponding final displacements at the free surface are thus twice those obtained in Equations 2.7 and 2.8. Back analysis of the Caracas Metro tunnel (Sagaseta, 1987) show wider trough width and high far field settlements when compared with field data. This is mainly attributed to the uniform convergence of soil when assuming a point sink.

Solutions derived by Sagaseta (1987) are subsequently extended by Verrujit and Booker (1996) to account for compressible materials and the ovalisation of the excavated tunnel boundary. The method provides improved solutions of settlement profiles as narrower trough widths result as a consequence of the ovalisation effect. However, the choice of ovalisation parameter (δ) value is unclear as no attempt is made to provide recommendations or guidelines.

Loganathan and Poulos (1998) presented a quasi-analytical method to predict tunneling induced ground movements based on solutions presented by Sagaseta (1987) and Verrujit and Booker (1996). Although the method has been successfully used to back analyse numerous case histories in clay, calculated results have to be treated with caution as the method does not satisfy volumetric constancy for undrained conditions. The method consistently yields smaller settlement trough volumes than the prescribed input tunnel face loss. This is due to the assumed empirical distribution of ground loss with horizontal and vertical distance from tunnel center as shown in the equation below:

$$\varepsilon_{x,z} = \varepsilon_0 \exp\left\{\left[\frac{1.38x^2}{(H+R)^2} + \frac{0.69z^2}{H^2}\right]\right\} \tag{2.9}$$

The assumed ground loss distribution as shown in Equation 2.9 attempts to indirectly model the effect of nonuniform soil convergence around a deforming tunnel as shown in Figure 2.4. Complete solutions to predict the displacement field around a tunnel excavation are as given below:

$$u_z = R^2\left\{-\frac{z-H}{x^2+(z-H)^2} + (3-4v)\frac{z+H}{x^2+(z+H)^2} - \frac{2z\left[x^2-(z+H)^2\right]}{\left[x^2+(z+H)^2\right]^2}\right\}. \\ \varepsilon.\exp\left\{-\left[\frac{1.38x^2}{(H+R)^2} + \frac{0.69z^2}{H^2}\right]\right\} \tag{2.10}$$

$$u_x = -R^2 x\left\{-\frac{1}{x^2+(z-H)^2} + \frac{3-4v}{x^2+(z+H)^2} - \frac{4z(z+H)}{\left[x^2+(z+H)^2\right]^2}\right\}. \\ \varepsilon.\exp\left\{-\left[\frac{1.38x^2}{(H+R)^2} + \frac{0.69z^2}{H^2}\right]\right\} \tag{2.11}$$

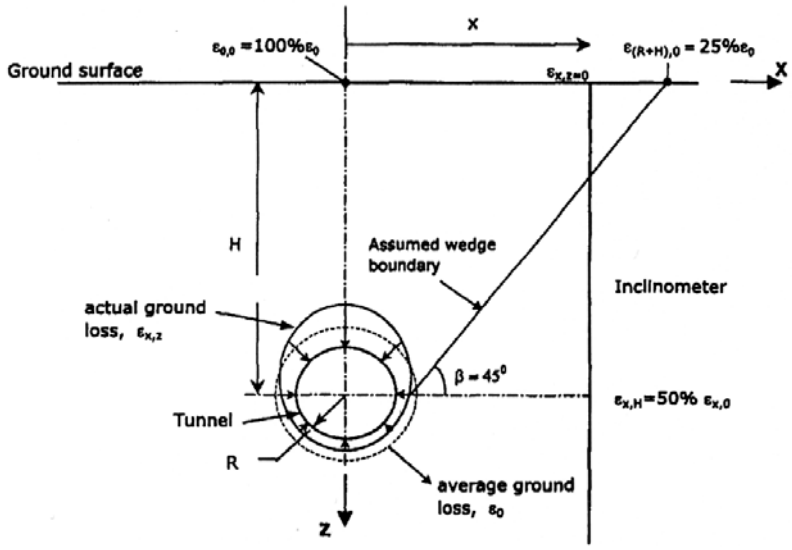

Fig. 2.4. Non-uniform soil displacement around tunnel boundary (Loganathan and Poulos, 1998)

Although attractive as a predictive tool, analytical methods are mathematically limited in the efforts required to derive solutions accounting for material nonlinear behaviour and complex geometries. This limitation is reflected in the small number of analytical solutions available to predict tunneling induced ground movements where only linear elastic, isotropic, homogeneous soil is considered. Analytical methods are unable to account for tunnel-soil-structure interaction from the practical perspective thus being limited in application to greenfield conditions. Care has to be exercised when employing quasi-analytical methods to predict displacements as certain important conditions necessary in the derivation of analytical solutions are violated (eg. volume loss is not conserved for undrained cases (Loganathan and Poulos, 1998)) when empirical assumptions are introduced.

2.2.3 Numerical Methods

Recent advances in the field of computational power and efficiency has enabled complex numerical modeling of tunnel excavation problems to be executed with relative ease. FE

methods represent one of the popular numerical schemes used by researchers and engineers to assess tunneling induced ground movements.

2.2.3.1. Techniques Simulating Plane Strain Tunnelling

It is well known that two-dimensional plane strain finite element simulation of tunnelling with simple soil models, predicts (i) large displacements, and (ii) incorrect shape of settlement trough. The prediction of large displacements is due to the inability of plane strain models to simulate three-dimensional arching effects in front of the tunnel heading. To solve this, three popular FE techniques can be used:

(i) Convergence-Confinement method (Panet and Guenot, 1982)

(ii) Volume loss method

(iii) Gap parameter method (Lee and Rowe, 1991).

In methods (i) and (ii), a proportion of the initial equilibrium radial stress around the tunnel boundary is reduced to match maximum surface settlements or ground loss. The amount of reduction is usually between 20%-40% and can be calibrated to give measured volume loss. These methods have been applied to predict ground movements due to tunnelling (Addenbrooke et al., 1997; Simpson et al., 1996; Stallebrass et al., 1994).

In the Gap parameter method, soil inside the tunnel is excavated and the tunnel allowed to deform under self-weight until the vertical settlement of the tunnel crown equals a predetermined gap value, and then lining elements are activated. Comprehensive guidelines

have been provided to calculate the gap parameter (Lee et al., 1992) which is summarised in the following equation:

$$GAP = G_p + U_{3D}^* + \varpi \qquad (2.12)$$

G_p represents the difference between cutter head and outer lining diameter while U_{3D}^* and ϖ accounts for 3D heading effects and workmanship quality. The method is originally restricted to analyses of tunnelling in soft ground as it assumes complete tail void closure (Rowe and Lee, 1983) and but was later modified (Lee et al., 1992) to account for grouting by setting G_p to zero. However, the use of Gap Parameter method in FE analysis appears to be unclear due to inconsistencies between the theoretical and FE applied definition of the parameter.

2.2.3.2. Soil Constitutive Models

It should be noted that these methods, Convergence-Confinement, Volume loss, and Gap parameter, only address the problem of large displacement prediction and not the correct shape of settlement trough. These techniques used to simulate 2D FE tunnelling tend to predict significantly wider surface settlement troughs accompanied with large far field displacement compared to field measurements when isotropic elastic soil models are used. This shortcoming can be partly improved by using advanced soil constitutive models as in Lee and Rowe (1989), Stallebrass et al. (1996), Addenbrooke et al. (1997), Kovacevic et al. (1996), Dasari et al. (1996).

In numerical studies by Stallebrass et al. (1996), a three surface kinematic hardening model (3-SKH) was used to back analyse centrifuge tunneling test data performed in heavily overconsolidated kaolin clay. The tunneling process was modelled by decreasing tunnel pressure from equilibrium conditions to zero. Despite being simulated in great detail, computed results revealed significantly wider settlement troughs and high far field settlements as shown in Figure 2.5.

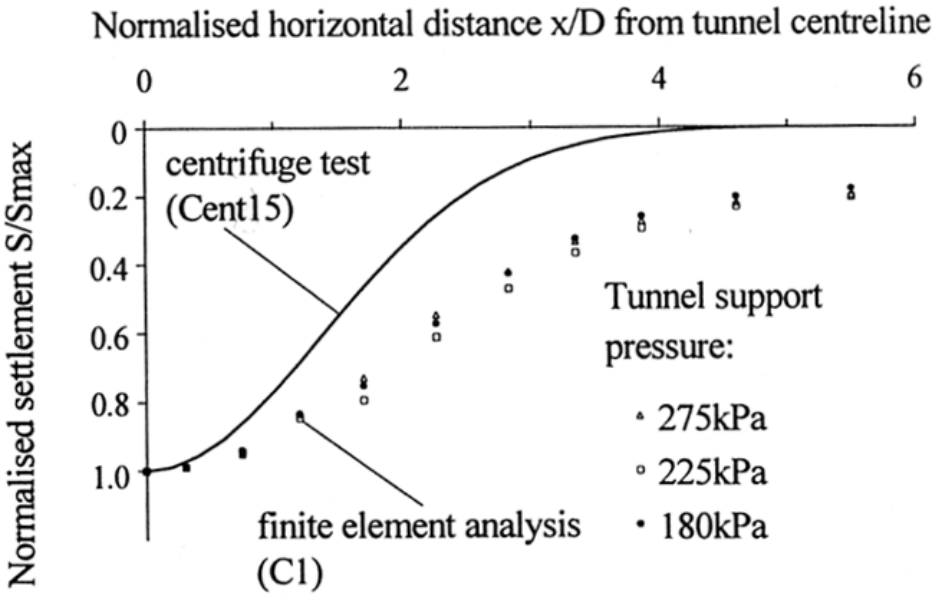

Fig. 2.5. Wider surface settlement trough in FE analysis (Stallebrass et al., 1996)

Similar results were also observed in the Heathrow Trial Tunnel (Type 2) simulation by Dasari et al. (1996). A strain dependant modified cam-clay model was assigned to the London Clay layer in the 2D and 3D analysis of the NATM constructed tunnel. A comparison of the predicted settlement trough with field data is as shown in Figure 2.6.

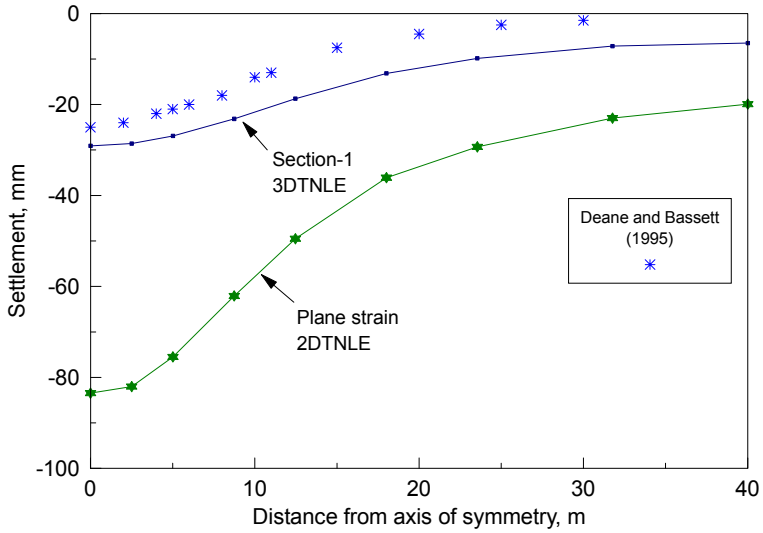

Fig. 2.6. Surface settlement trough from 2D and 3D FE analysis (Dasari et al., 1996)

2.2.3.3. Implications

It is generally acknowledged that the inclusion of sophisticated soil constitutive models in FE analysis of tunnel problems is necessary to produce realistic predictions of soil behaviour subjected to tunneling induced ground movements. These models have been developed based on actual soil behaviour from laboratory test data thus limiting the degree of improvements and modifications that could be made to the constitutive models to obtain better predictions of tunneling induced ground movements. It is clear that even with the aid of advanced soil models, the prediction of correct settlement profile shape is difficult. This would therefore imply that improvements in the method/way tunnel excavation is simulated are required.

2.3 Tunnel-Soil-Pile Interaction

There has been relatively few published literature in the area of piled foundations subjected to tunneling induced soil movements compared to other sources of soil movements (eg.

excavation, embankment loading). This could be partially due to the low potential of having to tunnel nearby piled foundations in the past where underground space was still relatively free of services and pre-existing structures. However, with the growing number of obstructions being encountered underground in congested metropolises, this lack of understanding in the area of tunnel-soil-pile interaction cannot be ignored anymore due to the possible hazards involved.

Figure 2.7 shows three possible failure mechanisms that could be induced on piled foundations as identified by the author in this study. The mechanisms are explained with respect to a triangular zone of large displacements similar to that observed/proposed in works by Cording and Hansmire (1975), Morton and King (1979) and Jacobsz (2001). This zone is defined by a line extending upwards at an angle $45°+\phi/2$ from the springline of the excavated tunnel boundary to the ground surface. For undrained cases in clays, this angle is 45° as ϕ is zero.

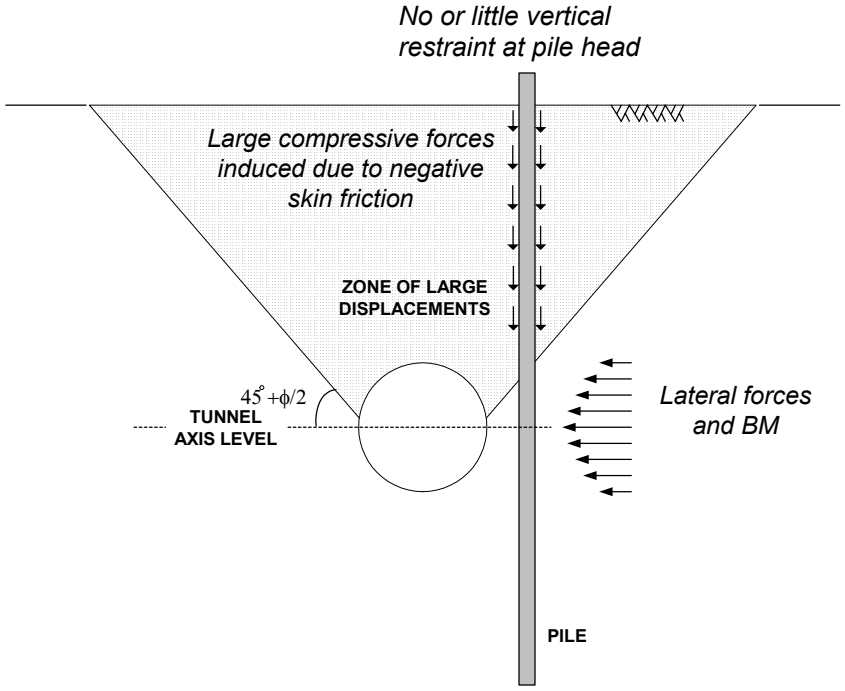

(I)

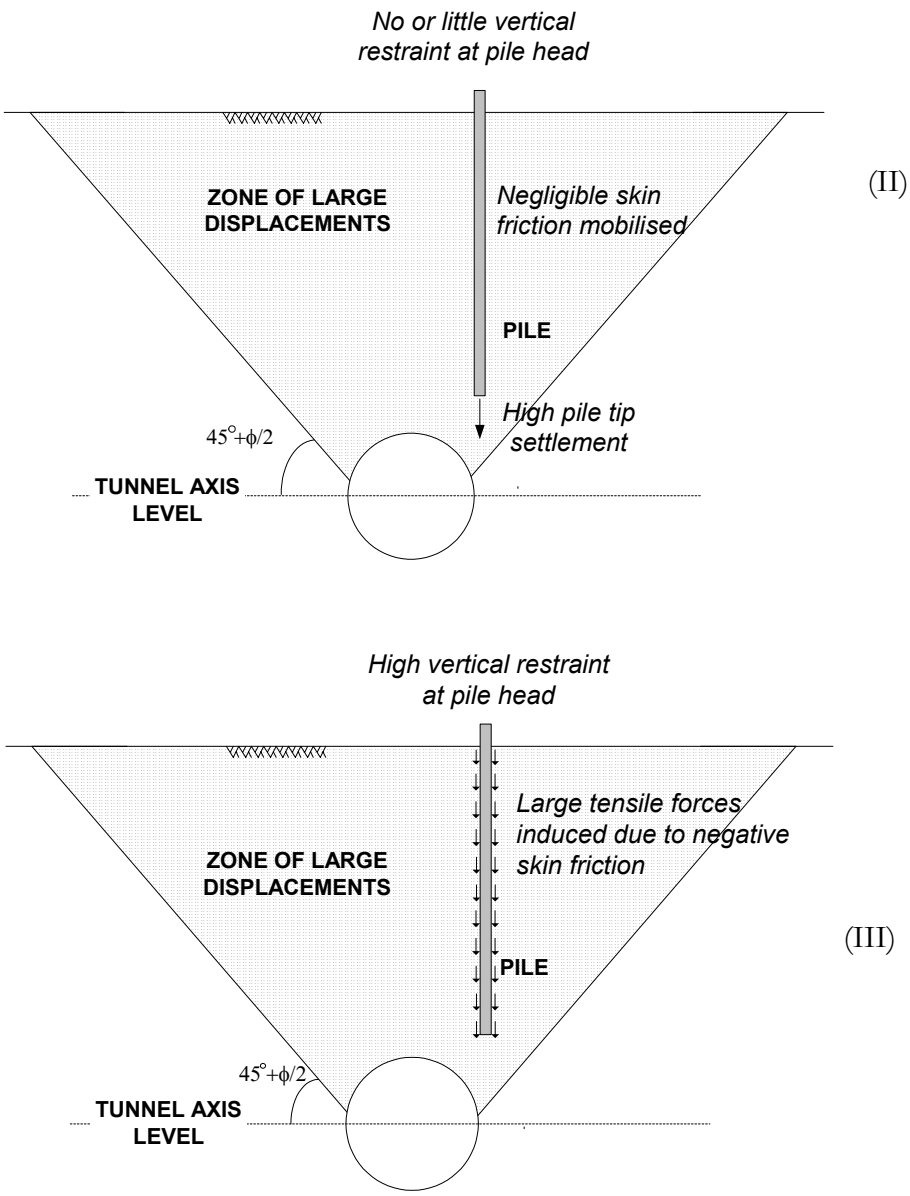

Fig. 2.7. Mechanisms of pile failure due to tunneling induced ground movements

Case I. *Pile tip located below tunnel invert level.*

Structural failure could be induced to the pile by a combination of excessive bending moments due to high lateral soil movements and or compressive strength of pile being exceeded due to negative skin friction. Full skin friction is expected to be mobilized along the pile shaft located in the zone of large

displacements as the downward force is resisted by the remaining shaft length of the pile (positive skin friction) and end bearing capacity thus resulting in high compressive forces. Where high vertical restraint to pile head is encountered, compressive forces are reduced as tensile behaviour develops near the pile head.

Case II. *Pile tip located within zone of large deformation with no or little vertical restraint to pile head*

Serviceability failure could result as pile tip settles together with soil, causing loss in pile bearing capacity and excessive pile head settlement. Negligible skin friction is mobilized as the pile moves downwards together with soil. Example of structures where Case II failure may occur is viaduct or bridge footings where tunnel excavation proceeds beneath the pile tip level, creating a zone of large displacements enveloping the entire foundation system.

Case III. *Pile tip located within zone of large deformation with high vertical restraint to pile head*

Tensile strength of the pile could be exceeded as negative skin friction occurs. Negative skin friction develops as soil attempts to drag the pile downwards but is resisted by the high vertical restraint at the pile head. This failure mechanism could occur for the case of piled raft foundations or smaller pile groups connected by ground beams and slabs where higher vertical restraint conditions are encountered.

While induced pile *P* is predominantly a function of absolute soil displacement magnitudes, induced *BM* is dependant on curvature profiles along the pile length. Thus the shape of soil displacements profiles must be reasonably predicted before accurate assessment of pile *BM* can be performed. Following is the discussion according to the nature of the study; field observation, laboratory testing and predictive methods.

2.3.1 Field Observations

Field data on tunneling induced pile bending moments and axial forces are few as it is difficult to predict when such a situation may arise unless prior planning and arrangements are made to instrument the pile. The North East Line Mass Rapid Transit Project in Singapore represents one such unique case where instrumentation was catered for as the tunnel was excavated within a short time frame after bored piles were constructed to support a 1.9 km vehicle viaduct (Coutts and Wang, 2000). The tunnels with an excavated diameter of 6.4m (northbound and southbound) closely follow the alignment of the viaducts on opposing sides. Tunnel boring proceeded within a close distance of $0.855D_t$ (tunnel to pile centre) to the pile at an average axis depth of 20m. The diameter of instrumented bored piles was 1.2m with lengths ranging from approximately 54 to 60m. Field data show that significant bending moments (59% of design working moment) and axial forces (91% of design working load) could be induced in pile for moderate volume losses of 1 to 2%. This could be due to the stiff weathered granite soil encountered throughout the ground stratigraphy.

Lee et al. (1994) detailed an escalator tunnel excavated using hand tools below a seven storey building with two basement levels founded on piles. Designated piles were only instrumented with inclinometers although the tunnel was excavated within a close distance of $0.7D_t$ from the pile. Computed results from FE analyses provided a conservative prediction of lateral displacements compared to field data as linear elastic soil model was used for analysis. Inclinometer results (Figure 2.8) generally show pile deforming in the same trend as the soil although magnitudes are lower due to the higher relative stiffness of the pile.

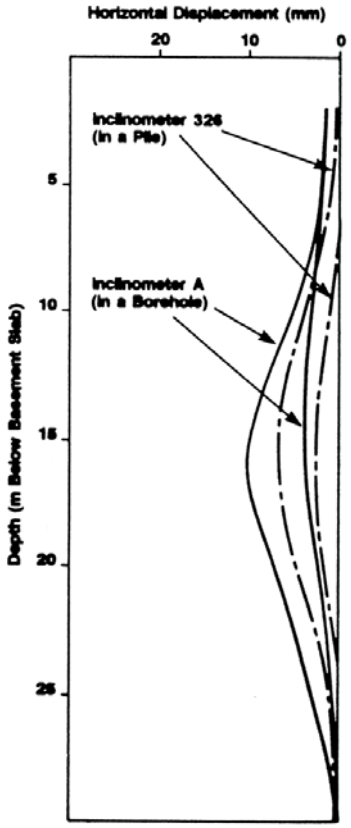

Fig. 2.8. Displacement profile of soil and pile with depth (Lee et al., 1994)

2.3.2 Laboratory Testing

One of the earliest model tests initiated to study the effects of tunneling induced ground movements on piled foundations was by Morton and King (1979). Tests were carried out in a mixture of coarse silt and sand under 1-*g* conditions thus neglecting the effects of confining stress on pile behaviour. Constant pile loads (safety factor of 3) were maintained during the tunneling process while monitoring pile head settlement. It was concluded that a definable critical, triangular boundary exists (Figure 2.9) to which pile experiences high settlements. Although limited in scope and information regarding induced forces on piles, the tests provided useful insight into the settlement behaviour of piles with tip levels above tunnel crown level.

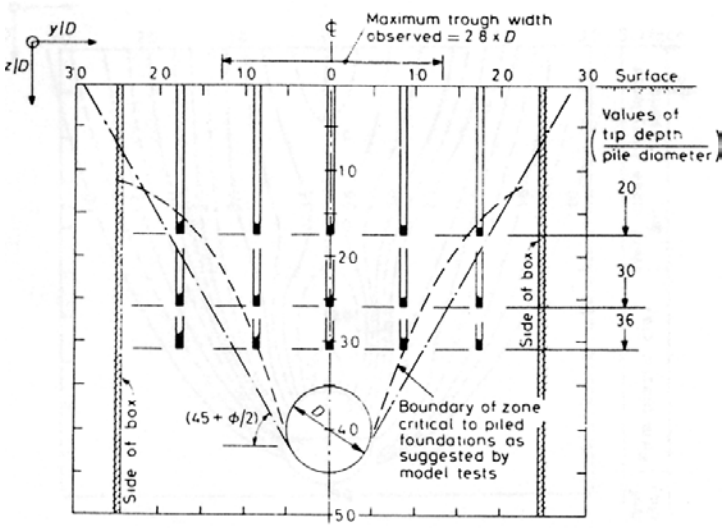

Fig. 2.9. Zone of high pile settlements (Morton and King, 1979)

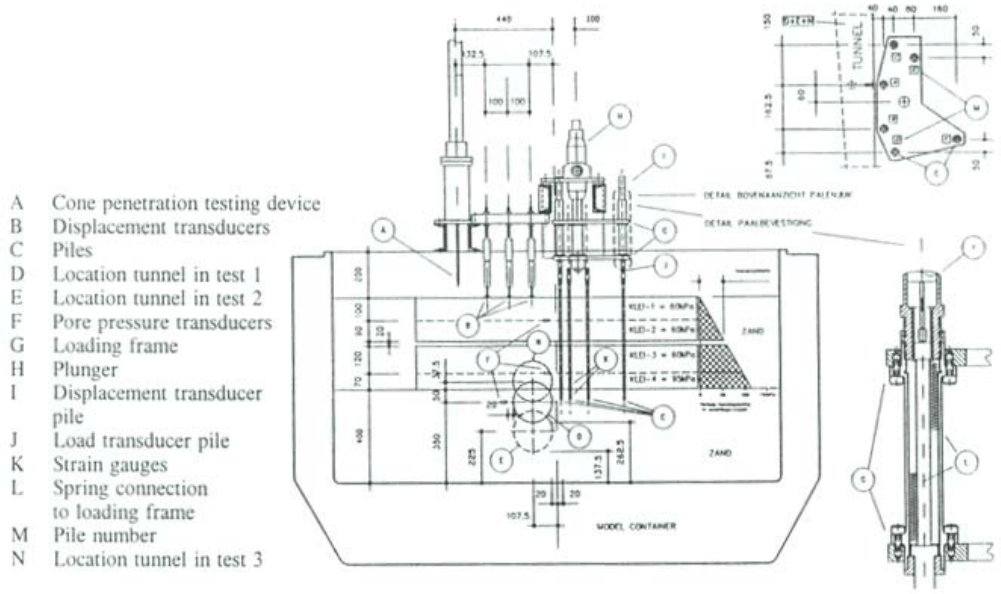

Hegarden et al. (1996) reported model tests carried out at the Delft Geotechnics centrifuge to study the influence of tunneling on end-bearing foundation piles. Tests were carried out at an acceleration of 40-*g* to recreate prototype soil stresses that are typical of field conditions. Tunnel excavation was simulated within soil stratified by clay overlying sand (Figure 2.10) by

a customized instrument able to vary in diameter. Results from Test 3 (pile tip at tunnel invert level) indicate significantly higher pile head settlement and loss of force at pile head for distances of 0.75 D_t and 1D_t from tunnel centerline compared to piles at further distances.

The first efforts to study induced pile bending moments and axial forces due to tunnel excavation in model tests were reported by Loganathan et al. (2000). The scope of study was limited to friction piles (single pile and a 2x2 pile group) in a centrifuge test carried out at an acceleration of 100-*g*. The effect of pile tip level relative to tunnel axis level and volume loss on the displacements and performance of piles was investigated to gain valuable insight into the interaction problem. The relative positions of the pile in various tests with respect to tunnel axis level and zone of large displacements are as shown in Figure 2.11. Maximum bending moments and axial forces obtained for single piles are as presented in Figure 2.12.

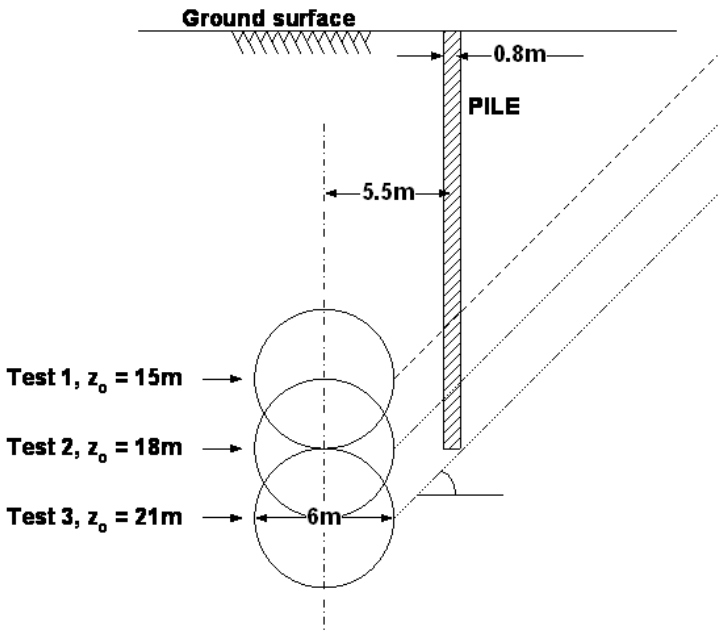

Fig. 2.11. Location of pile relative to tunnel in centrifuge tests by Loganathan et al. (2000)

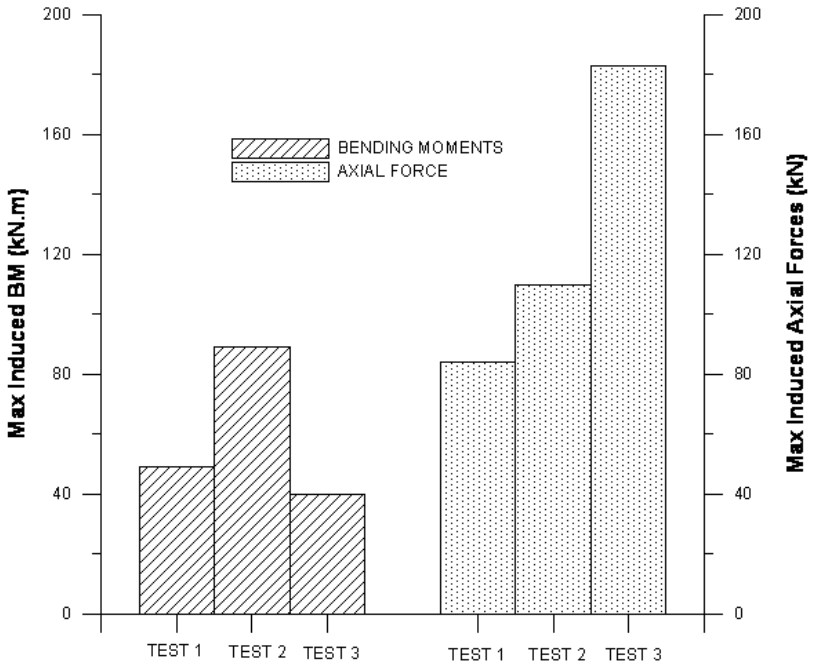

Fig. 2.12. Maximum induced pile bending moment and axial force (Loganathan et al., 2000)

Although individual trends of induced *BM* and *P* along the pile are intuitively reasonable, maximum magnitudes are difficult to interpret and explain when compared across the tests. Maximum induced *BM* would be expected to occur in Test1 where pile tip is below tunnel axis level while minimum induced *P* would be anticipated for the case of Test3 as pile tip is located within the expected zone of large displacements as shown in Fig 2.11. Computed results from parametric studies by Chen et al. (1999) further confirm the inconsistencies observed in the centrifuge test. Presented pile displacement profiles in Loganathan et al. (2000) are also inconsistent with corresponding *BM* distribution. However, the observed increase in maximum induced *BM* with volume loss is reasonable and as would be expected.

Jacobsz et al. (2001) presented centrifuge test data on the effects of tunneling in dry sand, focusing on the axial response of single piles. The experiment was performed at a C/D_t ratio

of 4.25 with a D_t of 4.5m and was spun at an acceleration of 75-*g*. Results show that a triangular zone is formed (Figure 2.13) due to the deforming tunnel which could induce large pile settlements should pile tip be located within this zone and subjected to volume losses exceeding 1.5%.

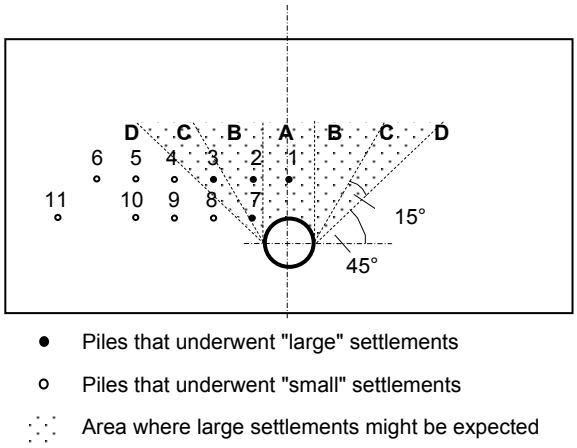

Fig. 2.13. Zone of large pile settlements (Jacobsz, 2001)

2.3.3 Predictive Methods

Chen et al. (1999) presented a simple approach to assess tunneling induced pile responses where a two-stage uncoupled method was introduced. In the proposed method, greenfield tunneling induced ground movements at the pile location is first approximated based on the quasi-analytical method proposed by Loganathan et al. (1998), subsequently applying the movements on soil elements surrounding the pile using separate numerical programs (PALLAS and PIES) to assess the lateral and vertical response. The parametric study provided valuable insight into the various factors affecting pile performance, in particular the variation of maximum induced *BM* and *P* with distance from tunnel centerline and relative position of pile tip to tunnel axis level. In general, maximum *BM* and *P* values decrease to insignificant magnitudes (less than 10% of value at X=1D_t) beyond a respective distance of

$2D_t$ and $5D_t$ from tunnel centerline. At a given horizontal offset from tunnel centerline, pile *BM* is also generally greatest when its tip is below tunnel axis level, decreasing as it moves upwards and above it. However, pile horizontal deflection profiles are almost identical in shape and magnitude to free field soil displacements as shown in Figure 2.14, which appears unrealistic especially near the ground surface where soil stiffness is lowest.

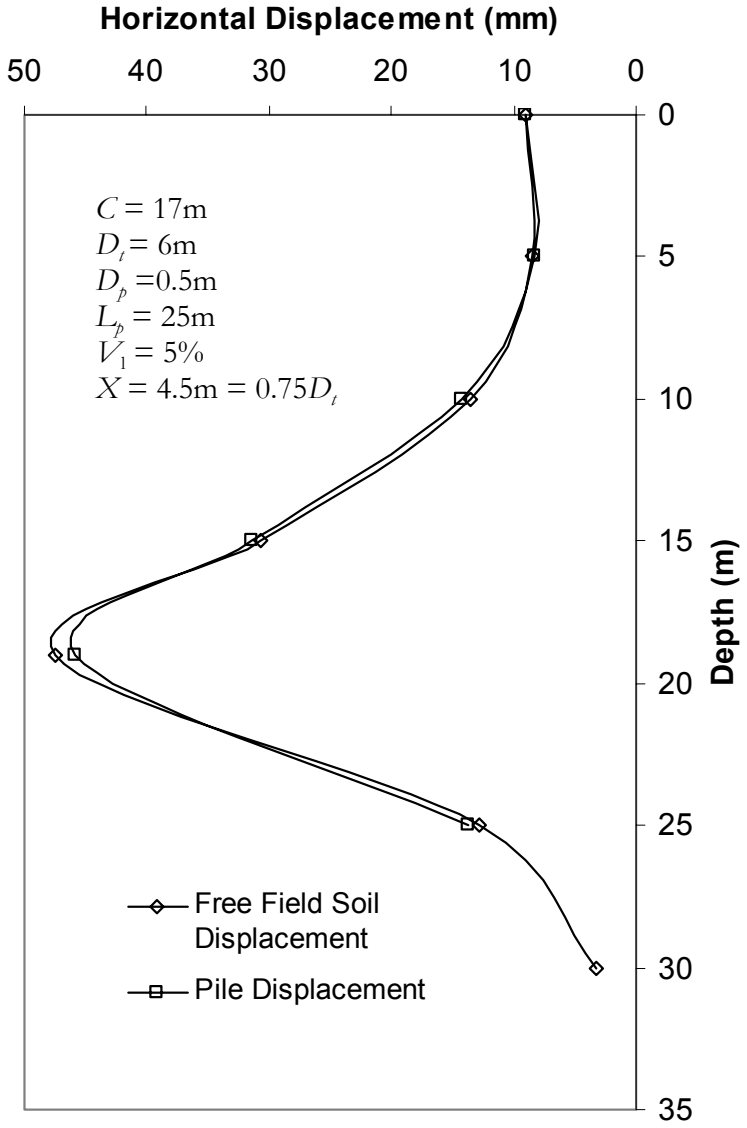

Fig. 2.14. Computed pile horizontal displacement approximately similar in shape and magnitude to imposed free field soil displacement (Chen et al., 1999)

In 3D FE studies by Mroueh and Shahrour (1999), the authors attempted to simulate a sequential shield tunneling process while studying the induced effects on piled foundations. Although three dimensional heading effects are accounted for in this analysis with the inclusion of lining elements, the Convergence-Confinement method (Panet and Guenot, 1982) was used to control soil convergence around the tunnel. The soil elements were modeled as linear elastic with Mohr-Coulomb failure criterion while pile elements are linear elastic with no provision for interface slip between soil and pile. Computed results from the simulation show pile response to vary realistically with advancement of tunnel face as shown in Figures 2.15 (a) and (b) while group effects resulted in significant reductions in internal forces for pile groups. The term x_p/L_p represents length along analysed pile normalized by total pile length.

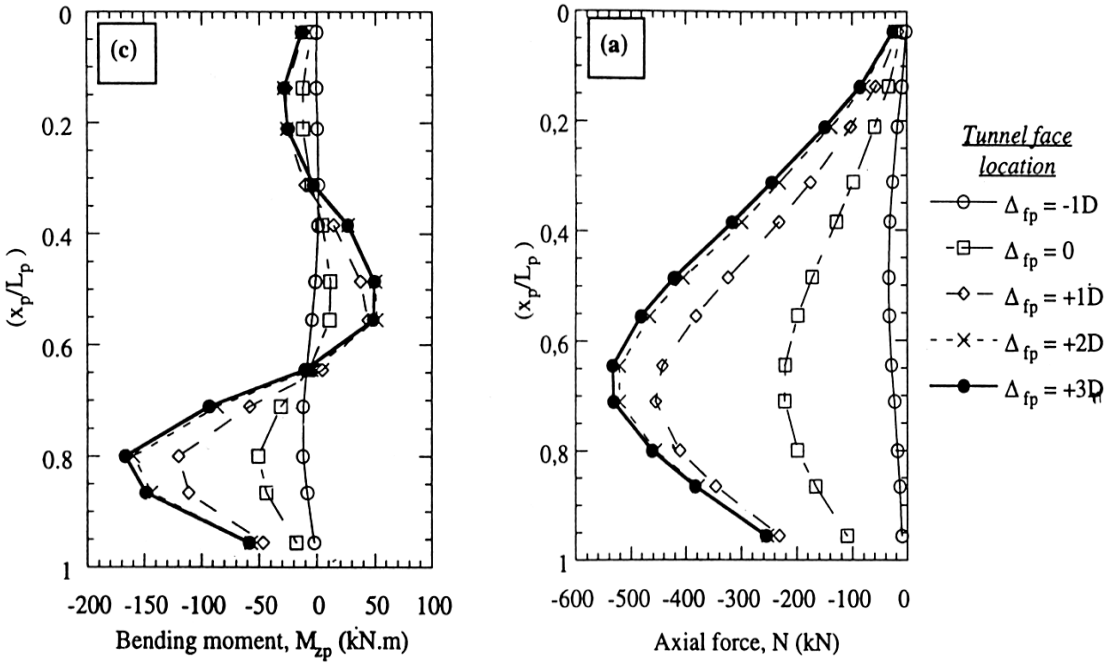

Fig. 2.15. Development of pile bending moment and axial forces with advancement of tunnel face (Mroueh and Shahrour, 1999)

2.4 Summary

Tunnelling induced ground deformation can be approximated to a high degree using empirical or quasi analytical methods. However, these methods are unable to include the effects of construction method, ground conditions and material properties (physical and mechanical). Most important to this study, these methods are unable to directly account for tunnel-soil-structure interaction thus being limited in application to greenfield sites. Therefore, numerical methods are required to perform coupled interaction analysis to accurately assess induced forces on structures such as piles that are dependant on curvature profiles along its length in addition to the absolute magnitudes of ground movement.

Various stress based methods have been proposed by researchers to model tunnel excavation under plane strain condition using numerical methods. These methods rely on sophisticated soil models to obtain improved results of soil displacement profiles around a deforming tunnel. However, computed surface settlement troughs and far field displacements are still generally shallower and higher than those commonly observed in field and centrifuge tests. Hence, the accuracy of subsurface displacement profiles is doubtful due to the incorrect surface settlement trough. These deficiencies would imply that a novel method is required to predict greenfield soil movements to an acceptable degree of accuracy for implementation in tunnel-soil-pile interaction analysis.

To date, research works on the subject of tunnel-soil-pile interaction are generally few with little effort being attempted to explain the possible failure mechanisms. The author has defined three possible cases/situations where failure could be induced from the view of ultimate or serviceability limit states. Even though little is understood in the field of tunnel-

soil-pile interaction, tunnels are being excavated close to piled foundations at centre to centre distances of less than $1D_t$. Efforts from centrifuge works to bridge this gap of knowledge have proved to be useful in providing important insight into the behaviour of piles when a tunnel is excavated along side it.

Recent numerical studies by researchers have resulted in preliminary design charts to assess pile behaviour subjected to tunneling induced ground movements. Greenfield soil movement is approximated from quasi analytical solutions, subsequently being imposed on the pile in a simple numerical program. This approach is uncoupled twofold; (1) when transferring greenfield soil movements to the numerical program and (2) when vertical and horizontal effects are assessed independently using separate programs. The main purpose of this study intends to overcome the above mentioned shortcomings to develop a more reliable means of predicting pile response and to gain a better understanding of the behaviour of piles influenced by tunneling operations.

CHAPTER 3

DISPLACEMENT CONTROLLED MODEL & ITS APPLICATION TO PREDICTION OF TUNNELLING INDUCED GROUND MOVEMENTS

3.1 Introduction

Current approaches to FE modeling of tunnel excavations are stress based in nature where equilibrium conditions around the tunnel boundary are released and allowed to deform freely under self weight. This is performed by removing elements within the tunnel or releasing fixities at the nodes around the tunnel boundary after geostatic equilibrium is achieved. Although the physical process of stress relief due to tunneling is correctly simulated by these methods, profiles and magnitudes of displacement rarely provide a good match with field or test data (Addenbrooke et al., 1997, Dasari et al., 1996).

In this chapter, a novel kinematic approach to model 2D tunneling is proposed to overcome the limitations associated with the conventional stress based methods. The assumptions critical to the development of the method are described along with its implementation in FE analyses of selected case histories.

3.2 Deformation Mechanism

When performing FE analyses of tunnel excavation, emphasis is often placed on obtaining maximum surface settlement and the transverse settlement trough. The computed profiles are usually incorrect when compared with field or test data hence prompting researchers to continually improve on soil constitutive models. Despite the development of numerous

sophisticated soil constitutive models, only marginal improvements have been observed. However, the observation of poor fitting settlement trough profiles common to stress based analyses could be a direct result of the incorrect deformation mechanism around the excavated tunnel.

Uncharacteristically high invert heave is frequently observed in FE analyses (Leca, 1996) when stress based methods are used. Figure 3.1 confirms this observation where high invert heave occurs and is computed to be approximately 40% of crown settlement even using a sophisticated 3-surface kinematic hardening (3-SKH) model (Stallebrass et al. 1996). High invert displacements indicate an approximately uniform convergence profile around the tunnel. The large invert heave provides an avenue for soil below tunnel springline to experience excess stress relief, consequently manifesting itself in the form of higher horizontal deformation. Hence, soil in the far field settles excessively to satisfy volumetric constancy. This shortcoming in stress based techniques as illustrated in Figure 3.2 suggests the need for a different approach to predict 2D tunneling induced ground movements.

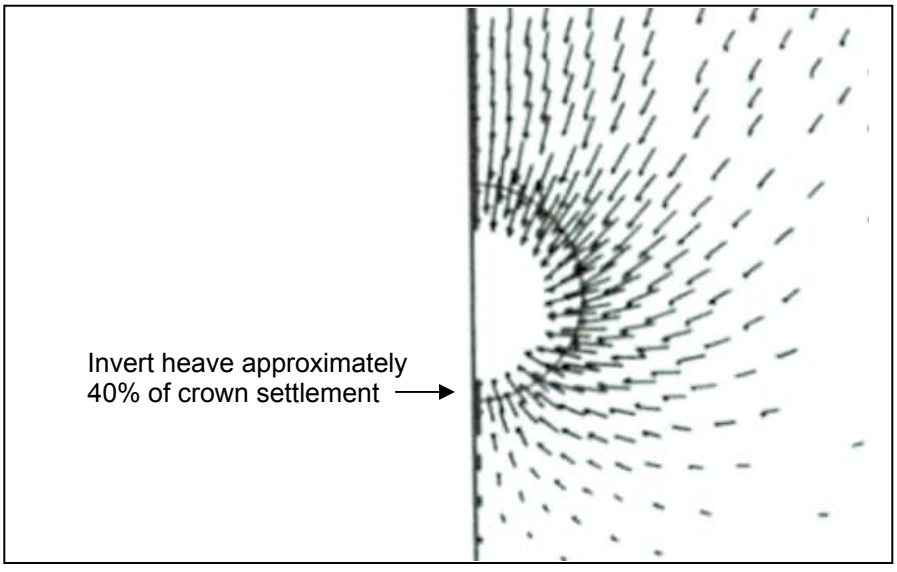

Fig. 3.1. Displacement vector plot around tunnel showing high invert heave in relation to crown settlement (Stallebrass et al., 1996)

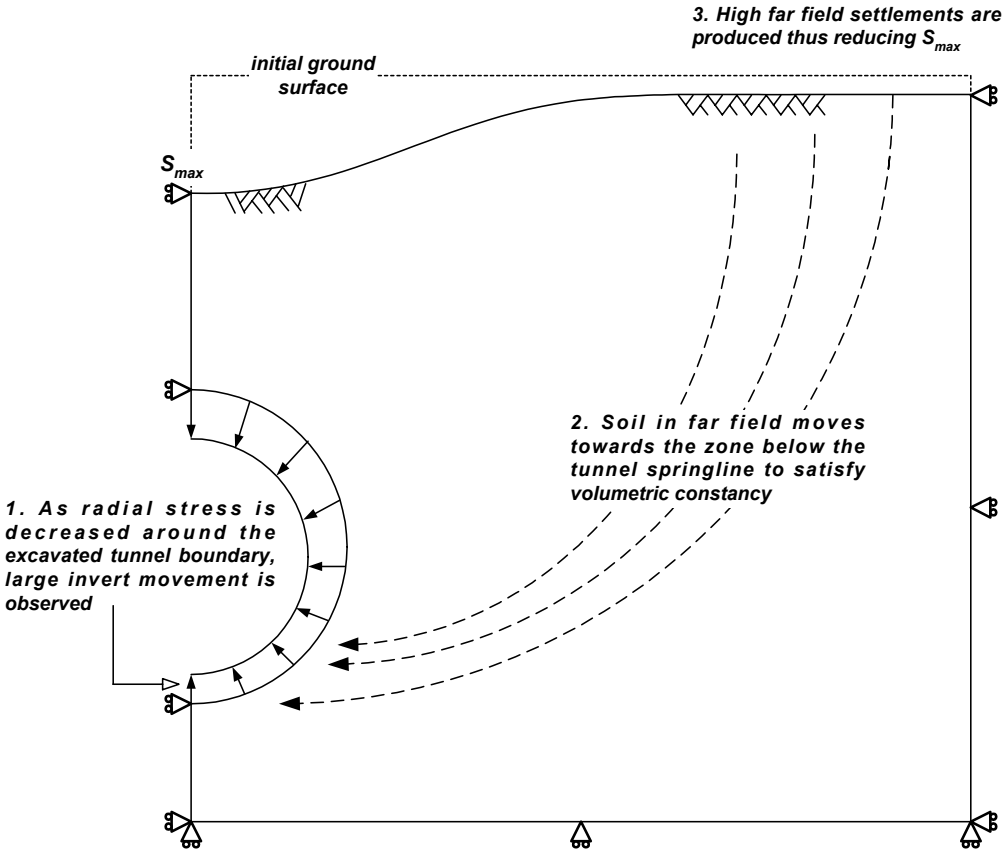

Fig. 3.2. Pitfalls associated with stress based FE analysis of tunnel excavation

3.2.1 Displacement Controlled Method (DCM)

Upon unloading, soil directly around the unsupported tunnel converges inwards in a radial pattern, towards a point on the tunnel centerline. Previously, this pattern of convergence has been ideally assumed to be uniform in the analytical solutions proposed by Sagaseta (1986) and Verrujit and Booker (1996) as a means of simplifying mathematical derivations. However, observations from numerous centrifuge tests and recent studies by Loganathan and Poulos (1998) suggest that this pattern of convergence around the tunnel boundary is highly nonuniform (Figure 3.3).

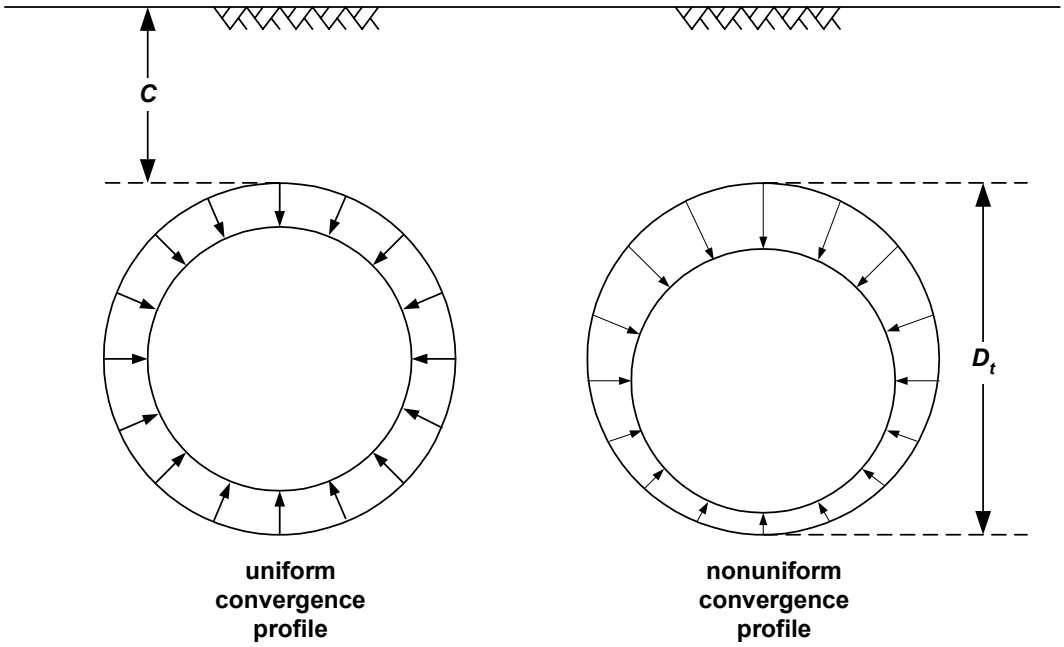

Fig. 3.3. Uniform and nonuniform convergence around excavated tunnel

Figures 3.4 (a) and (b) show undrained displacement vector plots of soil deformation around an excavated tunnel in plane strain centrifuge tests conducted by Mair (1979) and Hagiwara et al (1999).The plot for Mair's test (C/D_t = 1.67) clearly shows the relation between crown to invert displacement whereby significantly higher crown settlement is observed compared to invert heave. Similar behaviour is also observed for the latter experiment which was performed in clay overlain by medium to dense sand giving a total cover of 2.16D_t. This observation provides the basis for the first assumption in the DCM where zero or small heave is assigned to the invert. Although the magnitude of heave is most appropriately determined based on suitable crown to invert displacement ratios, it is however beyond the scope of this study. Thus, all subsequent analyses are performed assuming zero invert displacement.

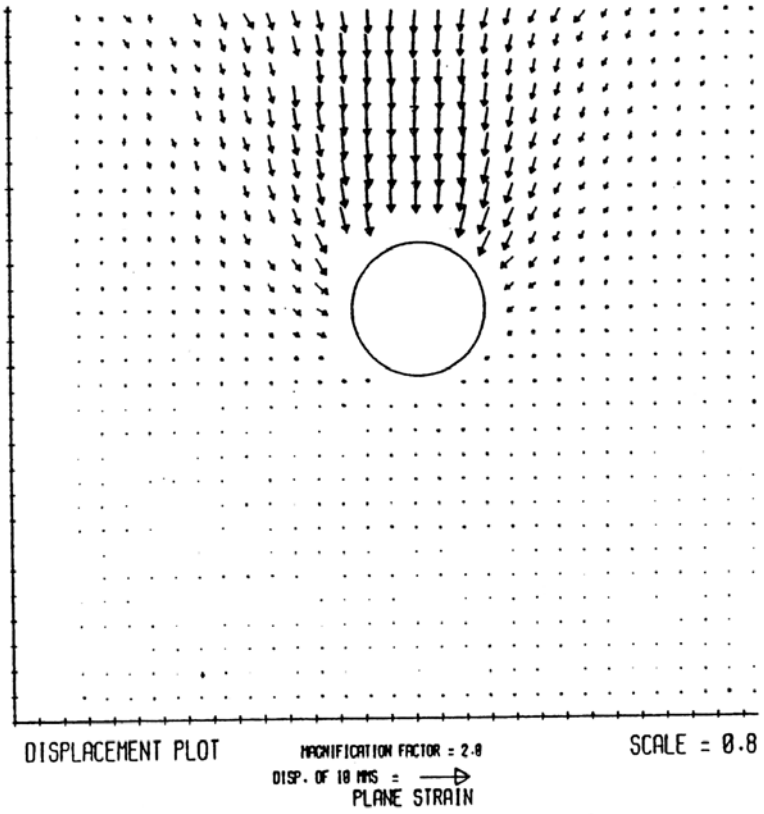

(a)

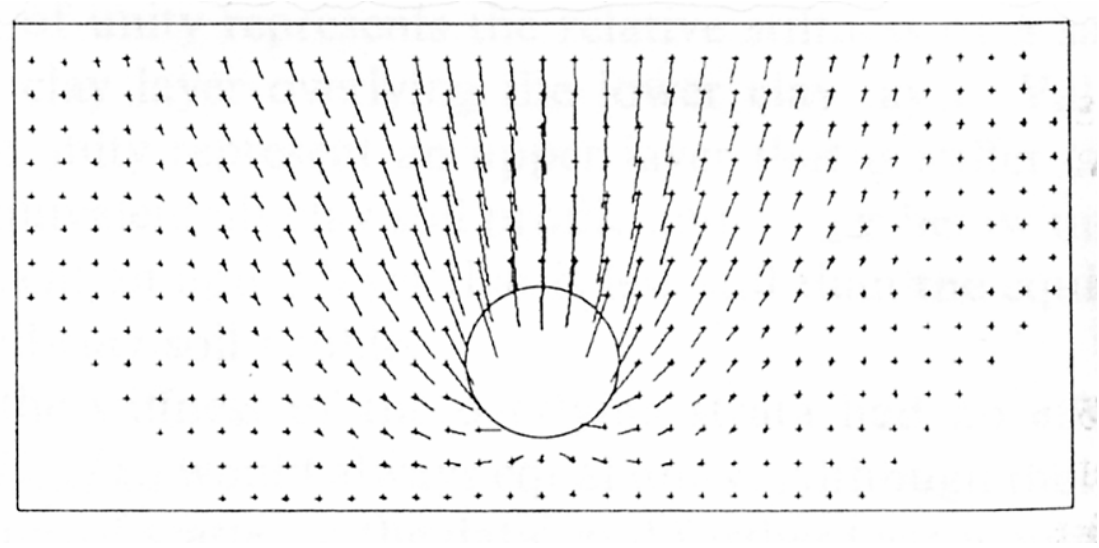

(b)

Fig. 3.4. Displacement vector plots from centrifuge tests (a) Mair (1979) and (b) Hagiwara et al. (1999)

The second assumption necessary in the application of DCM to predict tunneling induced ground movements is for converged tunnel geometry to conform to its excavated shape, ie. circular tunnels remain circular after deformation. This would appear to be reasonable as the converged profile for an open or closed face constructed tunnel, experiencing 1% to 5% volume loss could not possibly deviate too far from the excavated configuration. Moreover, in shield constructed tunnels, lining shape is similar to that of the excavation thus constraining the final soil deformation profile.

With the location of the converged shape set relative to excavated geometry, only the displacement vectors of soil on the tunnel boundary are left to be determined. The third assumption for the proposed kinematic model is that a single point exists on the tunnel centerline to which all nodes on the excavated boundary converge. There have been many proposals that suggest soil converges to the tunnel centre (Attewell, 1978, O'Reilly and New, 1982), $0.175/0.325z_o$ below tunnel axis level (Taylor, 1995) or towards the tunnel invert (Deane and Bassett, 1995). Grant and Taylor (2000) concluded from theoretical studies that, assuming:

- vertical ground settlement profiles are of the Gaussian form
- constant volume conditions apply
- vectors of ground movement at a given horizon above the tunnel focus on a single point on the tunnel centerline,

the focus point lies at the intersection of the tangent to the distribution of i with the tunnel centerline. Centrifuge tests by Grant and Taylor (2000) show that below a depth of approximately $0.5D_t$ above tunnel crown level, the trough width parameter decreases at an

increasing rate with depth as shown in Figure 3.5. This suggests that the point of convergence for soil on the periphery of the excavated tunnel could be simplified to a single point within the bounds of the invert and converged tunnel centre.

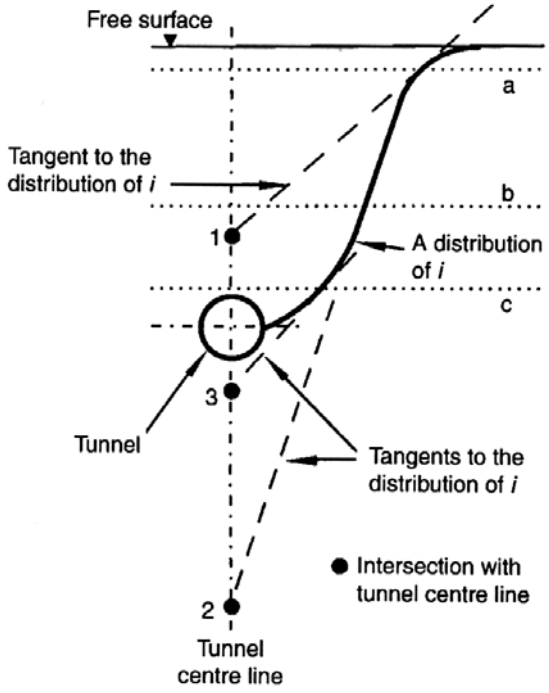

Fig. 3.5. Variation of *i* parameter and focus point with depth (Grant and Taylor, 2000)

The assumption for the convergence point to lie within the above mentioned bounds is justified by the fact that it would be unreasonable for soil below the tunnel springline to focus on a point below the tunnel invert as stress relief occurs in the upwards direction. Taking the ideal case in which a tunnel is excavated in an infinite medium (eg. very deep tunnel), it is logical to assume that the focus point would be at the tunnel centre. As the tunnel is excavated closer towards the surface, (ie. C/D_t ratio decreases) the convergence point is expected to shift downwards within the bounds of the tunnel centre and invert for reasons previously mentioned.

3.2.2 Implementation of DCM in FE analyses

Figure 3.6 illustrates the assumptions necessary in the implementation of DCM to FE analyses. Nodes around the excavated mesh boundary are "pulled" to a final converged profile based on estimated volume loss, location of focus point as well as the heave assumed at the tunnel invert. The area (volume) between excavated and converged tunnel periphery is the volume loss. The selection of volume loss should take into consideration the effects of soil properties, ground conditions, construction method and workmanship quality while the choice of focus point will be presented further on in this study based on results from the backanalysis of case histories. In this study, the focus point is defined by the parameter beta (β) which when multiplied by excavated tunnel radius (*R*) represents the physical distance between the focus point and converged tunnel centre. Derivation of displacements to be applied to nodes on the tunnel boundary is included in Appendix A.

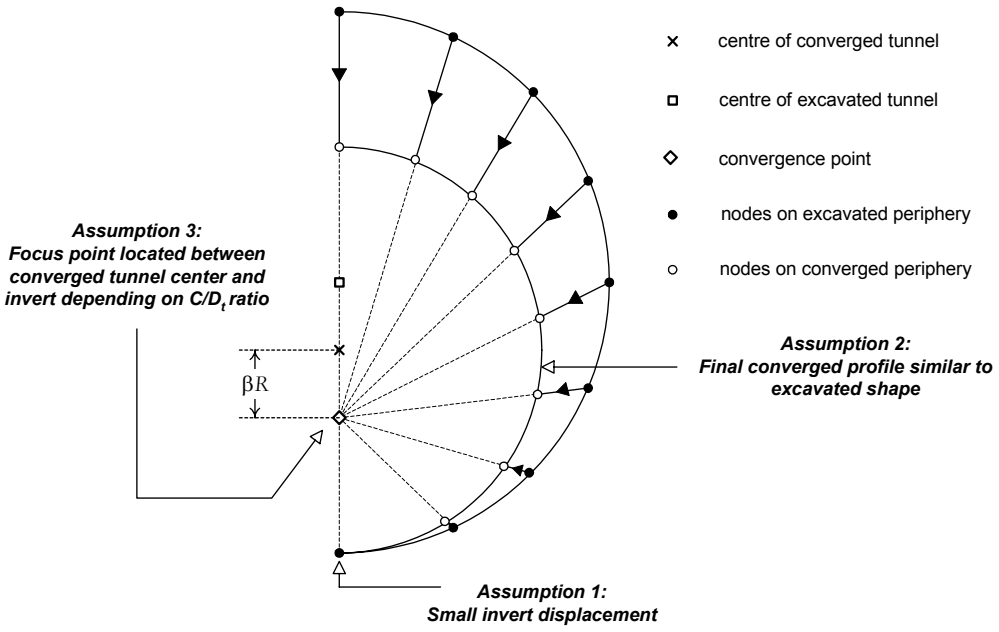

Fig. 3.6. Proposed displacement mechanism around excavated tunnel

3.3 Soil Constitutive Model

Tunnel excavation typically yield shear strains that are less than 1% depending on the volume loss encountered (Mair, 1992). This therefore implies that the effects of stiffness degradation within the small-strain region (ε_q approximately 0.001% to 1%) would have a pronounced effect on the behaviour of soil converging around the excavation. Strains are expected to be concentrated within the region of high stress relief (directly around tunnel), reducing as it moves further away when stiffness decreases with increasing strain levels (Addenbrooke et al.,1997). As a result of the strain localization, settlement trough widths are deeper and narrower compared to FE analysis using isotropic linear elastic perfectly plastic models (Gunn, 1993).

Recognising the importance of modelling the nonlinear behaviour of soils for tunnel problems, a simple power function has been applied to all analyses in this study. To date, the stiffness degradation of soil have been modeled using various forms of proposed power functions. Jardine et al. (1986) proposed an empirical expression for the variation of secant stiffness with strain of the form

$$G_{sec} = A + B\cos\left\{\alpha\left[\ln\left(\frac{\varepsilon_q}{C}\right)\right]^{\gamma}\right\} \tag{3.1}$$

while an alternative equation has been proposed by Dasari (1996) of the form

$$G = Ap'^{N}\, OCR^{M}\, \varepsilon_q{}^{B} \tag{3.2}$$

which accounts for the effects of overconsolidation ratio. In these equations, *A, B, N, M*, α, γ are constants to be determined by curve fitting to lab test data. In this study, a simplified version of Equation 3.2 was used for FE analyses as shown below;

$$G_{tan} = A\varepsilon_q^{\,n} \tag{3.3}$$

where *A* and *n* are constants to be determined. The general variation of tangent shear modulus G_{tan} with deviatoric strain is presented in Figure 3.7. At strain levels less than $\varepsilon_{q(min)}$, stiffness is at a maximum constant value (ie. linear elastic) subsequently decreasing to a minimum at a corresponding deviatoric strain of $\varepsilon_{q(max)}$. Due to the (i) kinematic nature of the DCM and (ii) single material idealization for all analysis, the magnitude of the constant *A* in Equation 3.3 has no bearing on the computed displacement results thus leaving only one constant (*n*) to be determined. Thus, relative magnitudes of stiffness at different strain levels (governed by *n*) are of concern rather than absolute magnitudes (governed by *A*).

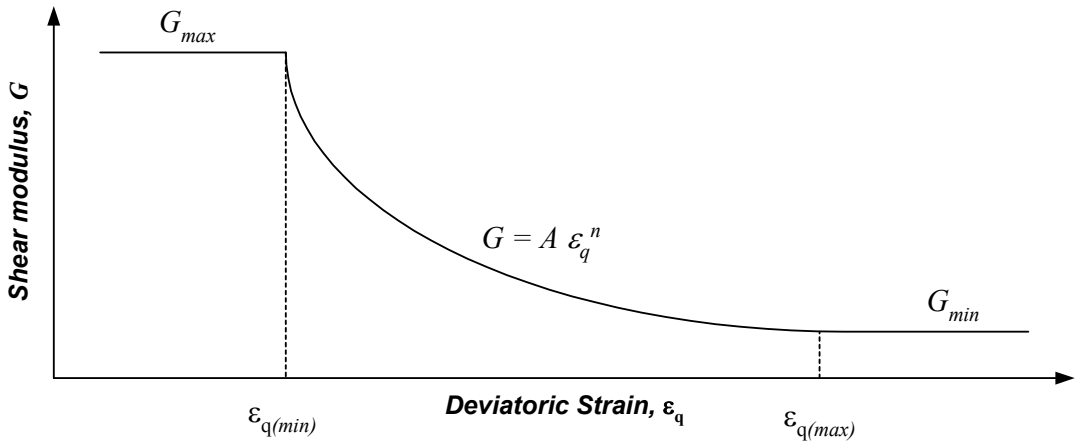

Fig. 3.7. General variation of shear stiffness with deviatoric strain

Table 3.1 and Figure 3.8 as shown below summarise the soil parameters used for the back analysis of the various case histories.

Table 3.1. Parameters to define stiffness variation of various clays

Soil	n	$\varepsilon_{q(min)}$ (%)	$\varepsilon_{q(max)}$ (%)
London Clay (Jardine et al.,1991)	-0.5	0.001	1
Kaolin Clay (Viggiani and Atkinson,, 1995)	-0.6	0.001	1
Mexico City Clay (Diaz-Rodriguez, 1992)	-0.4	1	100
Bangkok Clay (Shibuya and Tamrakar, 2003)	-0.7	0.02	10

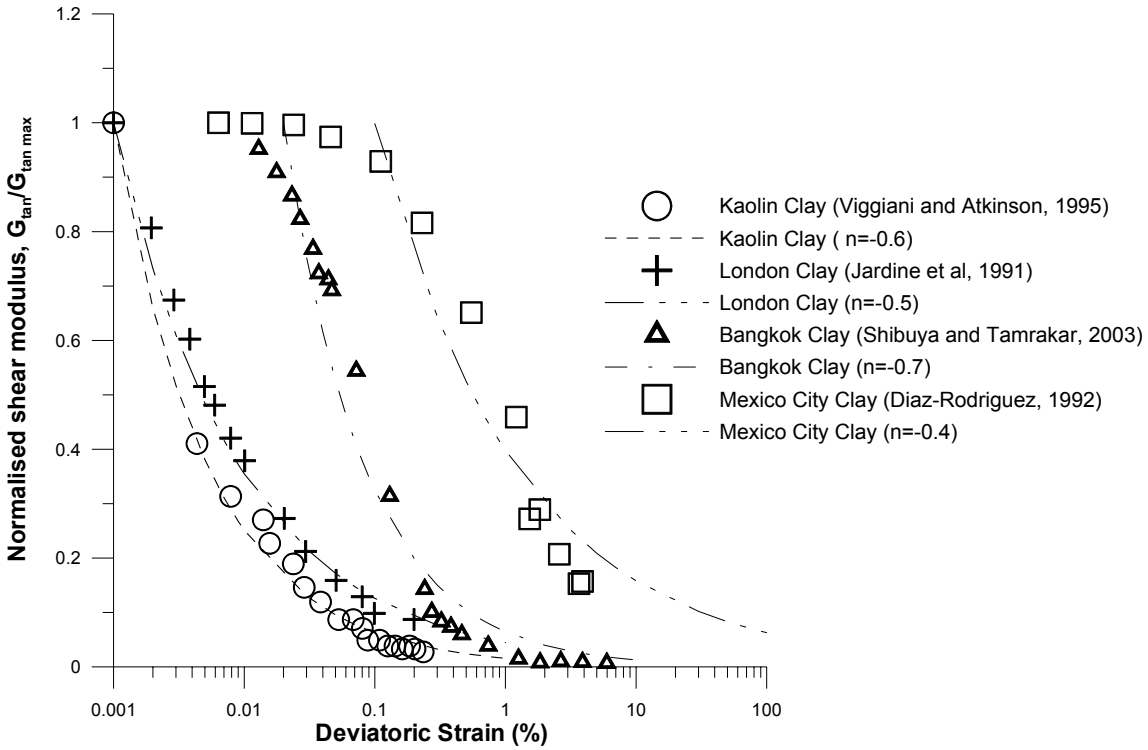

Fig. 3.8. Variation of shear stiffness with deviatoric strain

3.4 Methodology

FE analysis in this study was performed using the commercial software package ABAQUS v.6.3 (Hibbitt, Karlsson & Sorenson, Inc 2002). ABAQUS offers 2D and 3D modelling capabilities with facility to define user constitutive model. Total stress analysis was performed by setting Poisson's ratio to approximately 0.5. Element type employed in all analyses for this chapter is continuum, eight node, second order elements. Zero density was assigned to the elements due to (i) the kinematic nature of the study, (ii) constitutive model used for analysis (non pressure dependant) and (iii) scope of study for this chapter being limited only to displacements.

The symmetry of the problems is exploited by generating a plane strain mesh about the tunnel centerline. Convergence of solutions is ensured in this study by adhering to two simple guidelines based on a typical representative problem:

i) number of elements used for 2D analyses is greater than 400 as preliminary FE studies for a tunnel with dimensions D_t = 6m and z_o = 21m reveal that displacements (Figure 3.9) differ by less than 0.5% from the *constant magnitude* when mesh is sufficiently refined. *Constant magnitude* refers to the converged value of displacement which ceases to change even though mesh is further refined.

ii) mesh is generated in uniform, consistent manner to ensure a common basis for applying guideline (i).

All 2D analyses performed in this chapter have total number of elements greater than 1000.

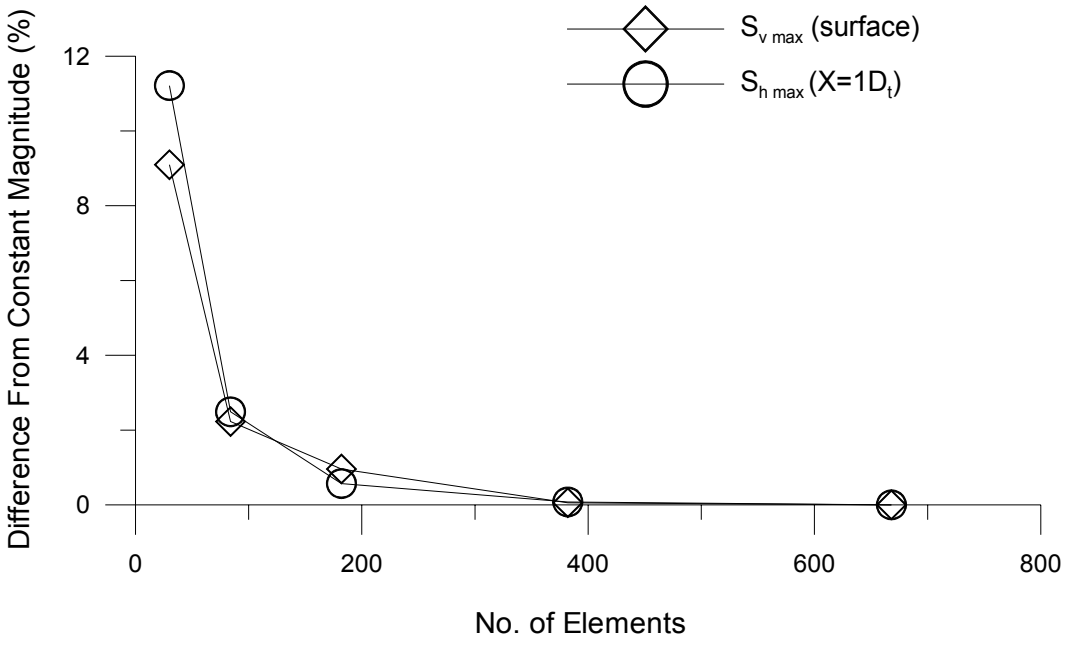

Fig. 3.9. Convergence of solution to constant value based on no. of elements in mesh

3.5 Case Studies

A total of six case histories were back analysed to test the applicability of the proposed kinematic approach to model tunnel excavation. The respective tunnels were excavated in soft to stiff clays with different methods, ranging from shield to NATM constructed tunnels and decreasing tunnel diameter in centrifuge tests. Detailed comparison of the performance of DCM to conventional stress based methods and the necessity of a nonlinear constitutive soil model are demonstrated in the first case history. Tunnel geometry, soil conditions and field data of each case history is presented in Table 3.2. Mesh geometry used for all analyses are included in Appendix A.

Table 3.2. Tunnel geometry, soil and analysis details

Case	Description	Soil Type	D_t (m)	C/D_t	V_l(%)		β
					This Study	Reported	
1	Heathrow Trial Tunnel (Type 2),UK	London Clay	8.74*	1.92	1.06	1.06	0.8
2	Green Park Tunnel, UK	London Clay	4.14	6.60	1.80	1.45	0.4
3	Loganathan's Centrifuge Experiment (Test 1)	Kaolin Clay	6.00	2.00	1.00*	1.00*	0.8
4	Loganathan's Centrifuge Experiment (Test 3)	Kaolin Clay	6.00	3.00	1.00	1.00	0.6
5	Mexico City Sewer Tunnel, Mexico	Mexico City Clay	4.00	2.75	5.00	-	0.6
6	Bangkok Sewer Tunnel, Thailand	Bangkok Clay	2.66	6.45	6.00	6.00	0.4

* Values are obtained by dividing with a factor of 2.35 as actual V_l during experiment is 2.35%

3.5.1 Heathrow Trial Tunnel (Type 2)

Three types of NATM tunnels were constructed in stiff London Clay to assess the sensitivity of ground displacements to excavation sequence in order to minimise effects on major structures. Type 2 construction sequence (excavation of right hand drift after left hand drift) was adopted for construction as it yielded the lowest volume loss and maximum settlement. The beta value (β) of 0.8 (i.e. closer to tunnel invert) was obtained by trial and error, similar to all analysed cases in this chapter. The importance of modelling stiffness nonlinearity is demonstrated through a subsequent linear elastic analysis using a similar β value in Figures 3.15 and 3.16.

The oval tunnel was idealised as a circular excavation with equivalent area of 60 m^2 and cover of 16.8m. The reported undrained volume loss of 1.06% was used for the analysis which translates to an equivalent crown displacement of $\approx$ 46mm. Computed results using a β value of 0.8 for the surface settlement in Figure 3.10 show good agreement with field data in terms of magnitude and profile. Although maximum settlements are slightly under predicted, far field settlements are negligible coupled with a favourable narrow trough width.

Horizontal displacement profiles at different offsets from the tunnel centre (Figure 3.11) also yield a reasonably good fit with field data for soil above the tunnel springline. Maximum computed horizontal movements compare well with field observation and occur slightly above the tunnel springline. Below the tunnel springline, computed displacements are observed to diminish at a rapid rate with depth. This could be due to the idealization of the oval tunnel in the form of a circular excavation thus affecting the horizontal deformation behaviour of soil below the tunnel axis level.

Loganathan's analytical[1] expression yielded settlement magnitudes smaller than field values when using a similar ground loss value. This could be attributed to the expression not satisfying volumetric constancy for undrained cases as have been pointed out earlier. However, horizontal displacements provide a reasonable estimation to field data above the tunnel springline. The decrease in horizontal displacement with depth below the tunnel springline is more gradual when compared with the proposed kinematic method but nevertheless, magnitudes are still lower than that observed in the field.

The computed results are a significant improvement when compared to the 3D FE analysis (Convergence-Confinement method) using an anisotropic elastic soil model by Tang et al. (2000). An undrained volume loss of 1.5% is required to approximately match maximum settlements. Far field settlements remain noticeably high in the stress-based analysis thus producing a relatively flat settlement profile. Meanwhile maximum horizontal displacements are significantly overpredicted (≈ 55% overpredicted for x = 9m) thus demonstrating the inaccuracy related to the method of simulating tunnel convergence.

[1] For convenience of discussion, Loganathan's proposed quasi-analytical equations are termed as analytical

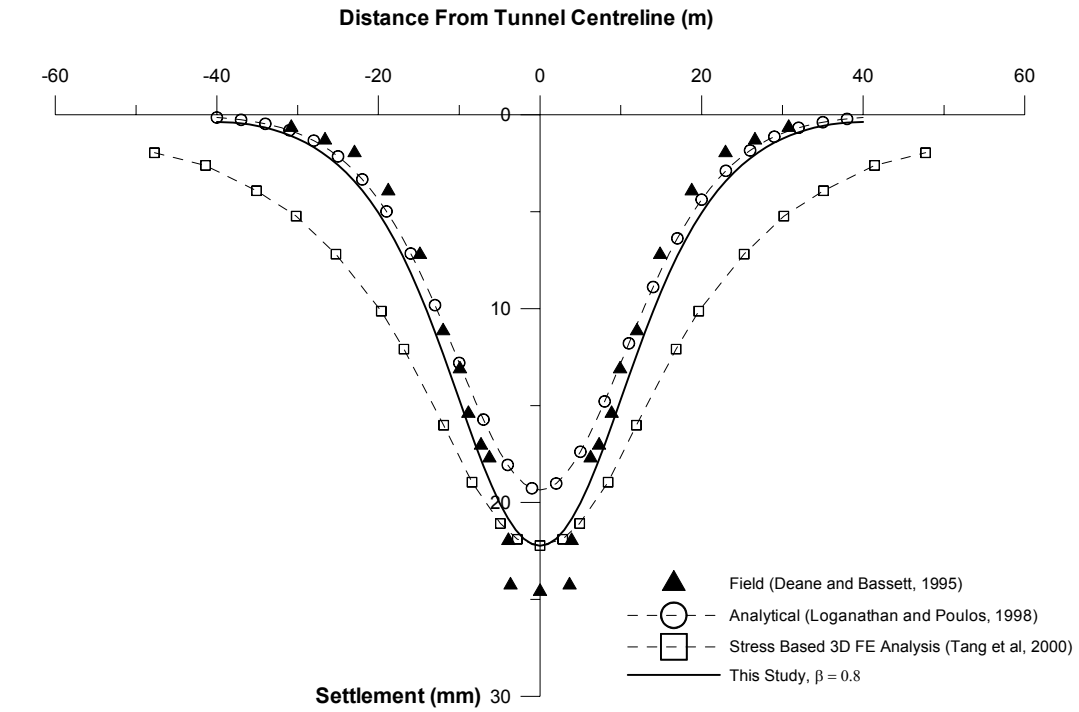

Fig. 3.10. Comparison of surface settlement troughs

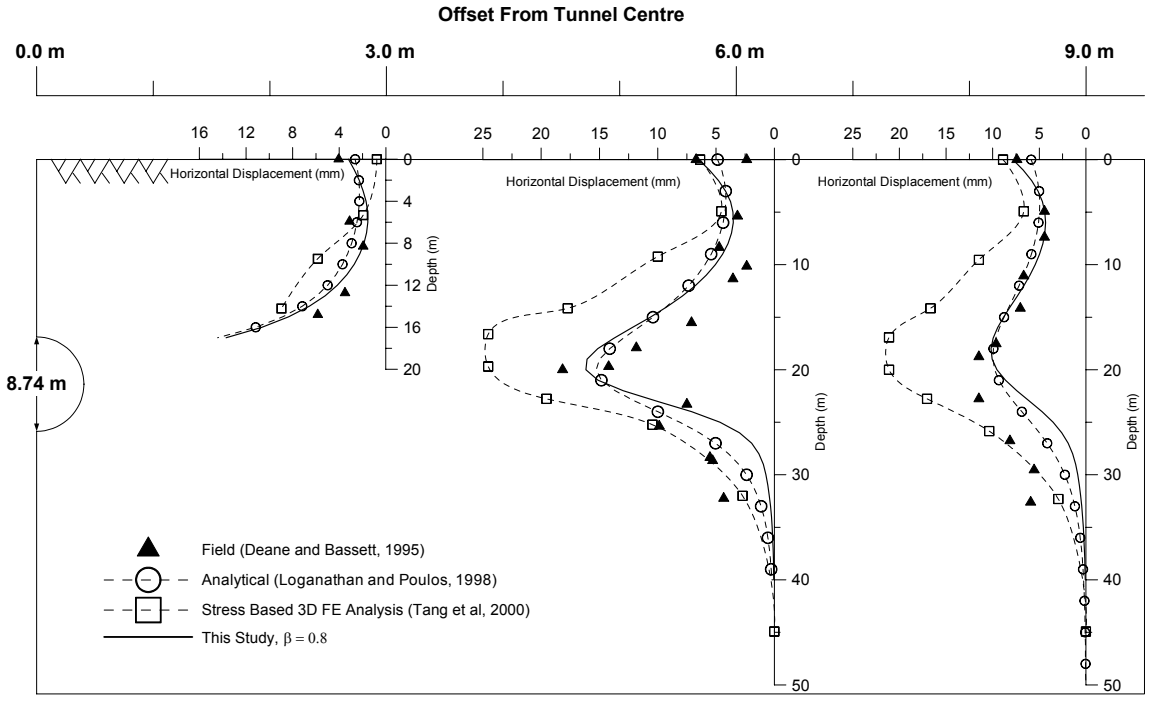

Fig. 3.11. Comparison of horizontal displacements at various offsets from tunnel centre

A comparative study between stress based analysis (Convergence-Confinerment and Volume Loss method) and the current proposed method was also performed using a common mesh and soil model. London Clay was assigned a K_o value of 1.5, bulk density of 18kN/m^3 and a G_{max} value of 100MPa calculated at tunnel axis level. The G_{max} value is obtained assuming an approximate G_{max}/p' ratio of 400 (Jardine et al., 1991) and the water table located 5m below the ground surface. The Convergence-Confinement method yielded high far field settlements when S_{max} is similar to the field value. When volume loss is matched, computed maximum settlements as shown in Figure 3.12 are grossly under predicted (≈50%) coupled with high far field settlements (≈ 5mm) even with the aid of a nonlinear soil model. Although horizontal displacements at a horizontal offset of 6.3m from the tunnel axis (Figure 3.13) appear to be in good agreement with field data for the Volume Loss method, it does not provide an overall consistent solution for the displacement field around a deforming tunnel. The localizing effect caused by DCM and high invert heave typical of stress based methods are obvious when the contour plot of displacement magnitudes as shown in Figure 3.14 are observed.

The importance of modelling stiffness nonlinearity in the constitutive models for the proposed method is demonstrated in Figure 3.15 whereby results from an analysis using a linear elastic soil model with similar β value is presented. The surface settlement trough shows heave of about 2mm in the far field together with a wider settlement trough when compared to the analysis using nonlinear elasticity. Horizontal displacements (Figure 3.16) also suffer from a similar problem whereby soil below the springline is being 'pushed' away from the tunnel instead of converging towards it. This behaviour is counterintuitive, as soil vectors should progress inwards towards the tunnel from stress relief.

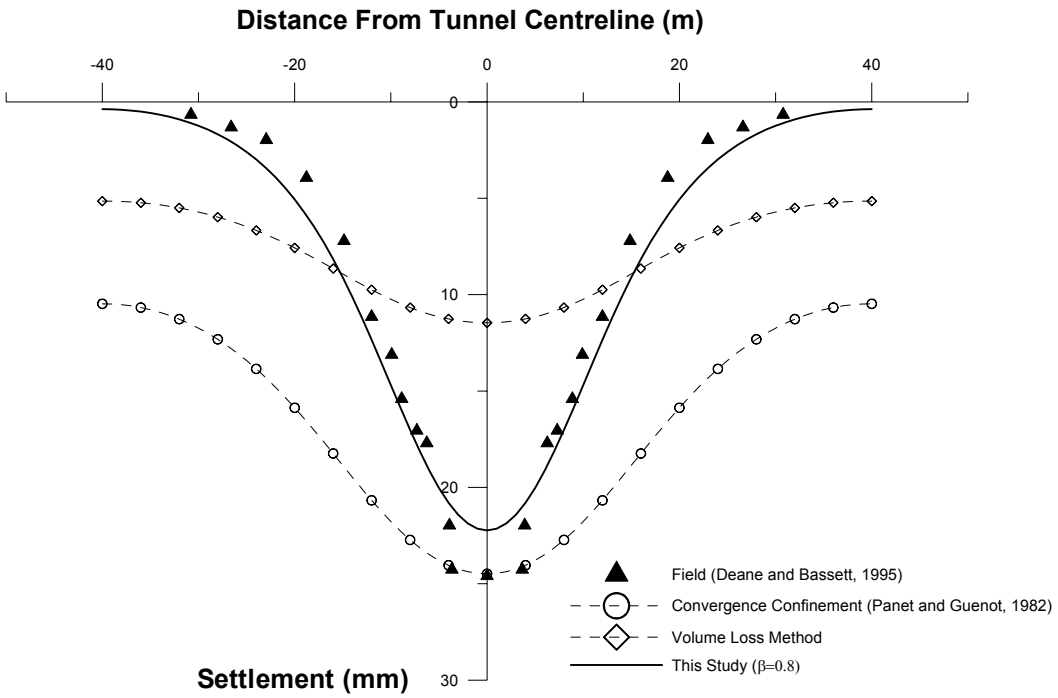

Fig. 3.12. Comparison of surface settlement troughs using stress and displacement based methods

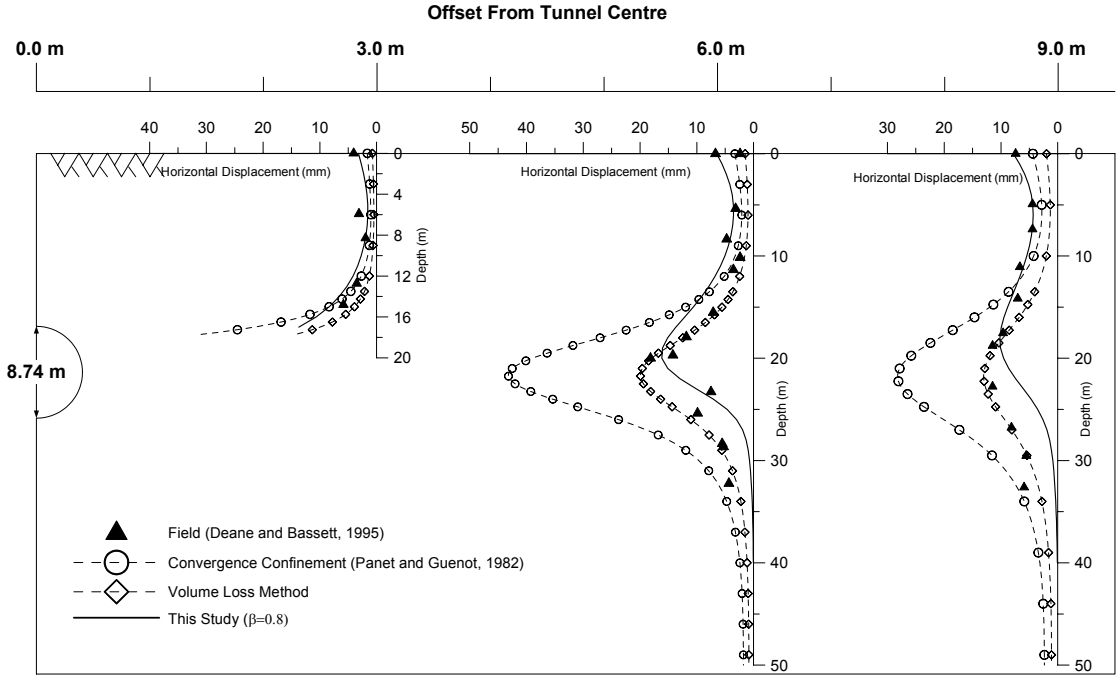

Fig. 3.13. Comparison of horizontal displacements at various offsets from tunnel centre using stress and displacement based methods

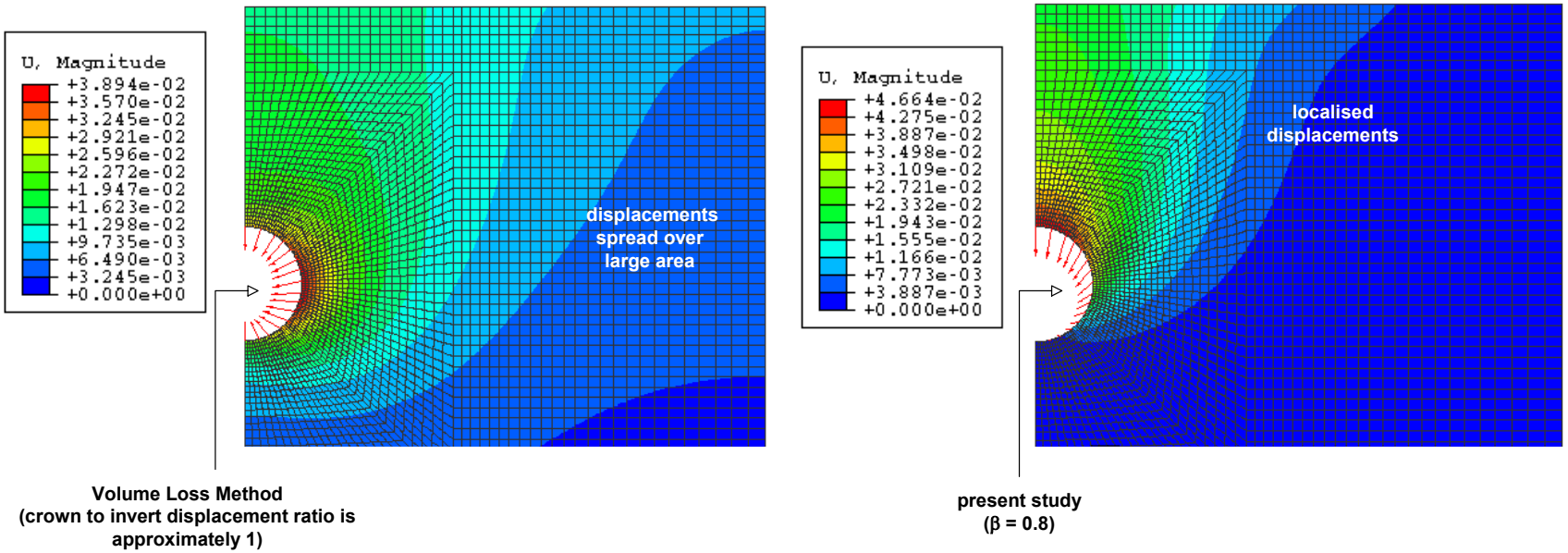

Fig. 3.14. **Localising effect (displacements) of kinematic method compared to stress based methods**

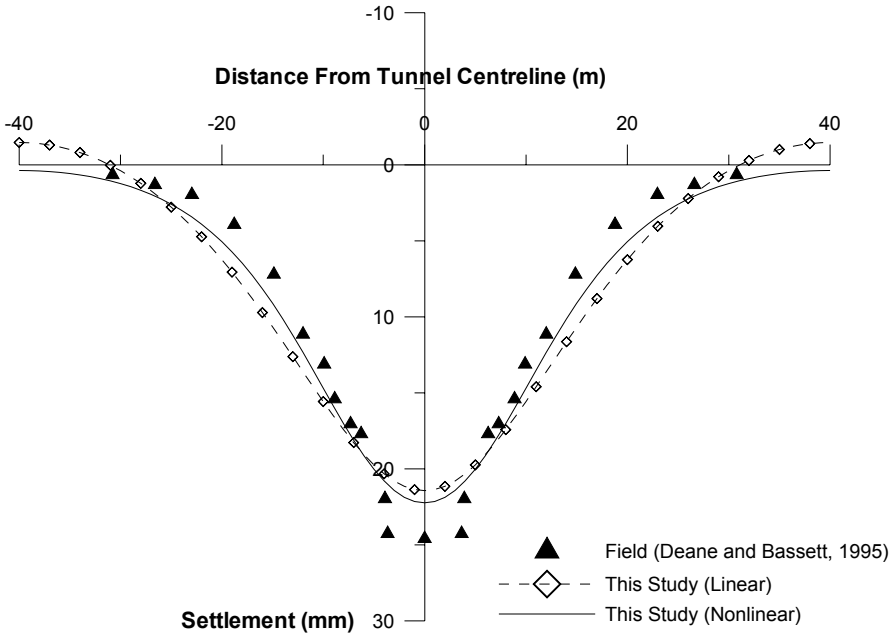

Fig. 3.15. Necessity of stiffness nonlinearity to obtain realistic predictions of settlement trough

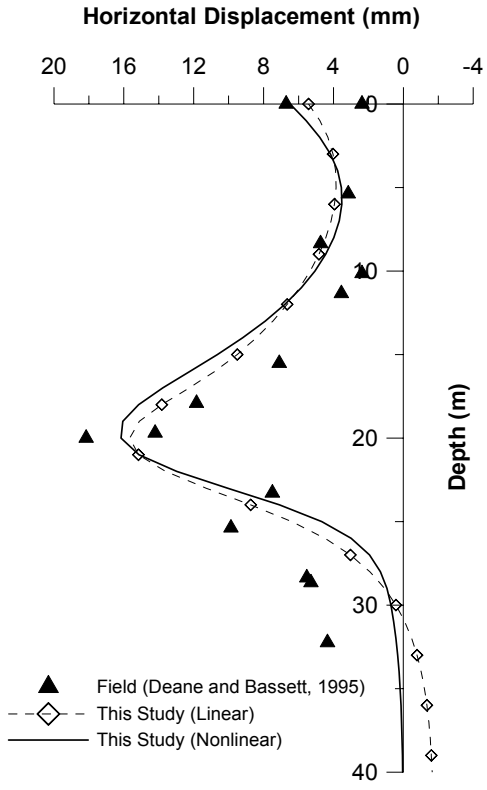

Fig. 3.16. Necessity of stiffness nonlinearity to obtain realistic predictions of horizontal displacements (x = 6.3m)

3.5.2 Loganathan's Centrifuge Experiment

To date, only three published experiments (Morton and King, 1979, Hergarden et al. 1996, Loganathan and Poulos, 2000) have been reported to investigate the effects of tunnelling induced ground deformation on existing piles. The latter centrifuge experiment represented an ideal case to test the proposed displacement based FE method of analysis in this study as comprehensive surface as well as subsurface data are available for comparison. Moreover, three tests at various C/D_t ratios were performed to investigate the performance of piles whose tips are located at different positions relative to the tunnel axis level. FE analyses for a C/D_t ratio of 2 (Test 1) and 3 (Test 3) was performed for this study.

The tunnels were deformed in a plane strain mode and have a diameter of 6m. Tests were conducted in heavily over consolidated kaolin clay (OCR at tunnel axis approximately 5.2) and spun at an acceleration of 100*g*. The authors obtained results for Test 1 by linearly interpolating between an undrained V_l of 0% and 2.35% as the intended value of 1% was overshot due to equipment problems. Computed results for Test 1 were obtained assuming a V_l of 2.35% and subsequently dividing by a factor of 2.35 to simulate actual test conditions.

The computed transverse surface settlement trough provided a good match to experimental data for Test 1 and Test 3 despite displaying a slightly wider trough width (Figure 3.17(a) and (b)) Both analyses were carried out assuming a volume loss of 1%. However, Test 1 required a lower convergence point ($\beta = 0.8$) to reasonably match test data as compared to the deeper tunnel level in Test 3 where a β value of 0.6 was chosen. This proves to be consistent with the proposed deformation mechanism in which the point of convergence shifts downwards moving away from the tunnel centre with decreasing C/D_t ratio. A chart of C/D_t ratio with β

value is presented later on to further validate the proposed deformation mechanism. Undrained surface settlements are under predicted when employing Loganathan's analytical expression to quantify the corresponding displacements for both tests.

Horizontal displacements were obtained at an offset of 5.5m from the tunnel centre as the single piles were located at a similar distance. The expected trend in which horizontal displacements decrease with depth from the ground surface down to a certain depth and then increase to a maximum approximately at tunnel axis level was reproduced for both analyses as shown in Figure 3.18. Computed test results provided a reasonably good match with field data for Test 3 but magnitudes from the analyses of Test 1 were over predicted by as much as 70% slightly above the tunnel axis level. Experimental data from Test 1 indicate that the zone of influence for tunnelling induced horizontal ground movements do not extend below the invert level as opposed to the previous Heathrow Trial Tunnel case where corresponding displacements only diminish to negligible magnitudes beyond a depth of $1D_t$ below tunnel invert level. FE results indicate that horizontal displacements are negligible beyond a depth of 1 tunnel diameter ($1D_t$) below the invert level, agreeing with field data from the Heathrow Trial Tunnel, as compared to Test 1 centrifuge data.

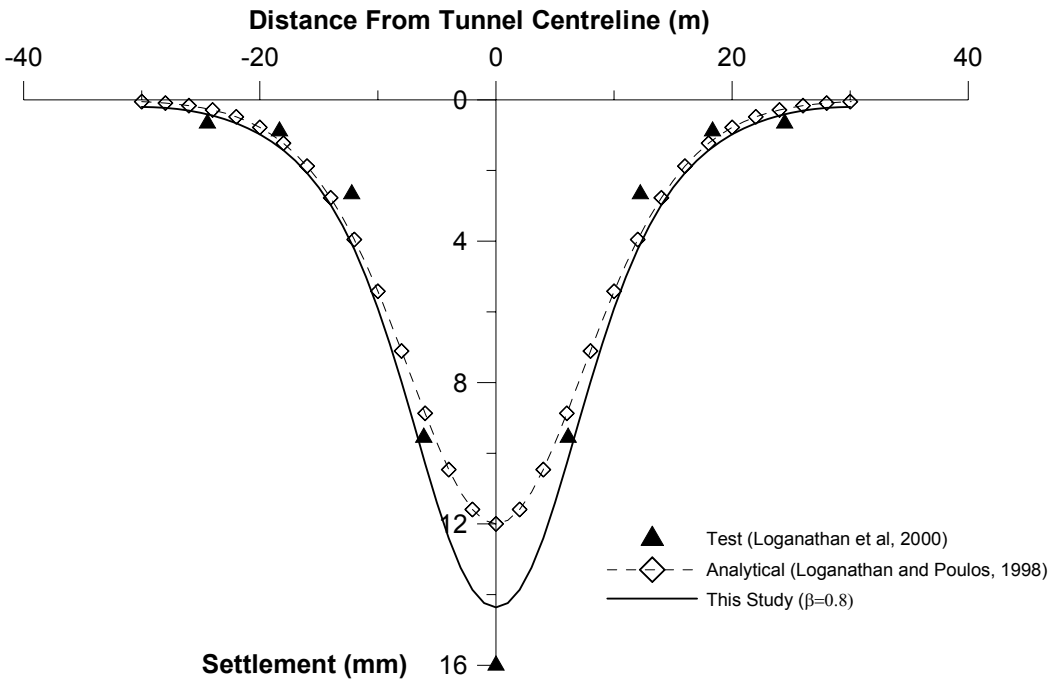

(a)

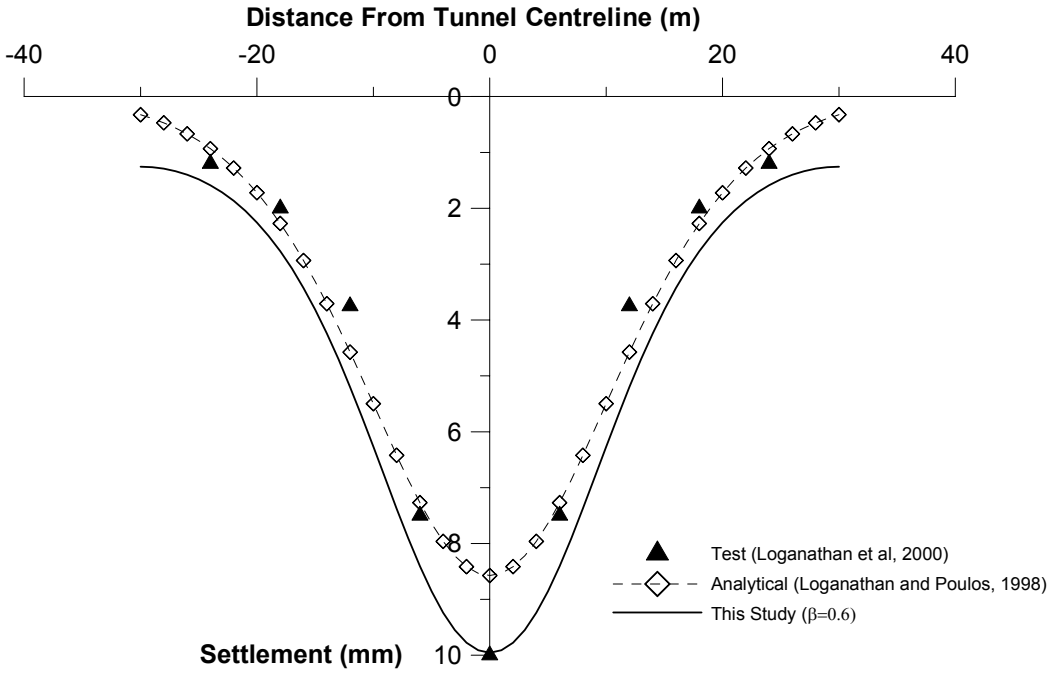

(b)

Fig. 3.17. Transverse settlement troughs for (a) Test 1 and (b) Test 3.

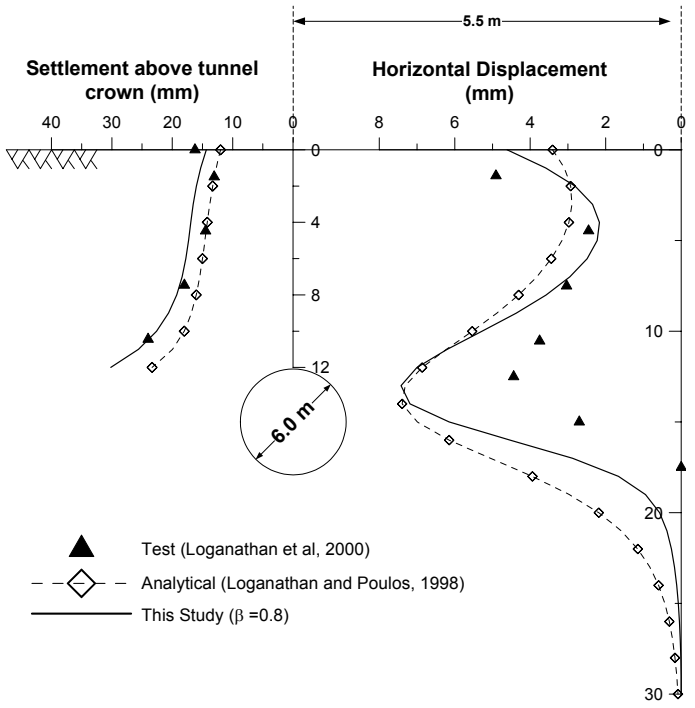

(a)

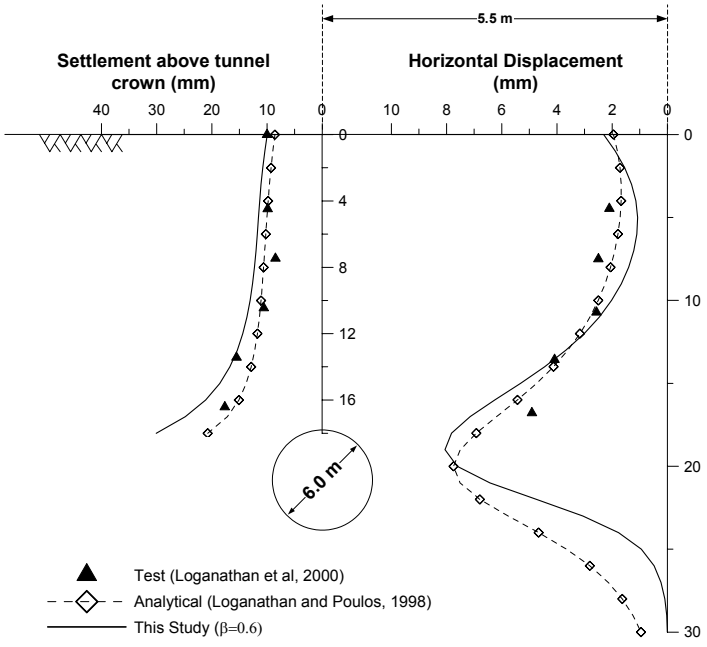

(b)

Fig. 3.18. Horizontal displacements (x = 5.5m) and settlements above tunnel crown for (a) Test 1 and (b) Test 3

Predictions from Loganathan's expression yielded displacements profiles that have a more gradual change in curvature as compared to FE predictions. This would imply a less conservative approximation of the stresses and bending moment that would be induced on vertically embedded structural or service members such as pipes and piles. The localisation of horizontal displacements within the bounds of the invert and crown level due to the effects of small-strain nonlinearity is obvious when compared with the displacement profile produced using the analytical expression. Maximum displacements were over predicted by approximately the same magnitude as in the FE results.

Computed results from Test 1 and 3 also shown in Figure 3.18 reproduced settlement magnitudes above the tunnel crown to a satisfactory degree of accuracy. The approximate agreement in crown settlement magnitudes between FE and experimental results provide an indirect validation of the assumption that invert heave is negligible compared to crown settlement.

3.5.3 Green Park Tunnel

A tunnel of approximately 4.14m diameter was hand excavated through stiff heavily overconsolidated London Clay to create the Green Park Tunnel. Depth to tunnel axis level was 29.3m thus producing a C/D_t ratio of 6.6. Information covering instrumentation, construction details and field data was reported by Attewell and Farmer, 1974. Horizontal displacements are not reported in this analysis due to insufficient field data.

Figure 3.19 shows the transverse surface settlement profile obtained from FE analysis and the field. The displacement based FE method produced negligible far field settlements

coupled with a narrow trough width which is in good agreement with field data. Based on the Gaussian settlement profile (Peck, 1969) and *i* parameter to be 50% of z_o for soft or stiff clays (O'Reilly and New), settlements are expected to be negligible beyond 45m and this is observed in the computed curve. However, a V_l of 1.8% was required to reproduce the settlement profiles compared to the reported 1.4% V_l. A possible explanation for the under prediction of the volume loss could be the non-existence of settlement data beyond 20m thus requiring inaccurate extrapolation of the settlement curve. A β value of 0.4 (closer to tunnel centre) was required to reproduce the surface and subsurface settlement magnitudes.

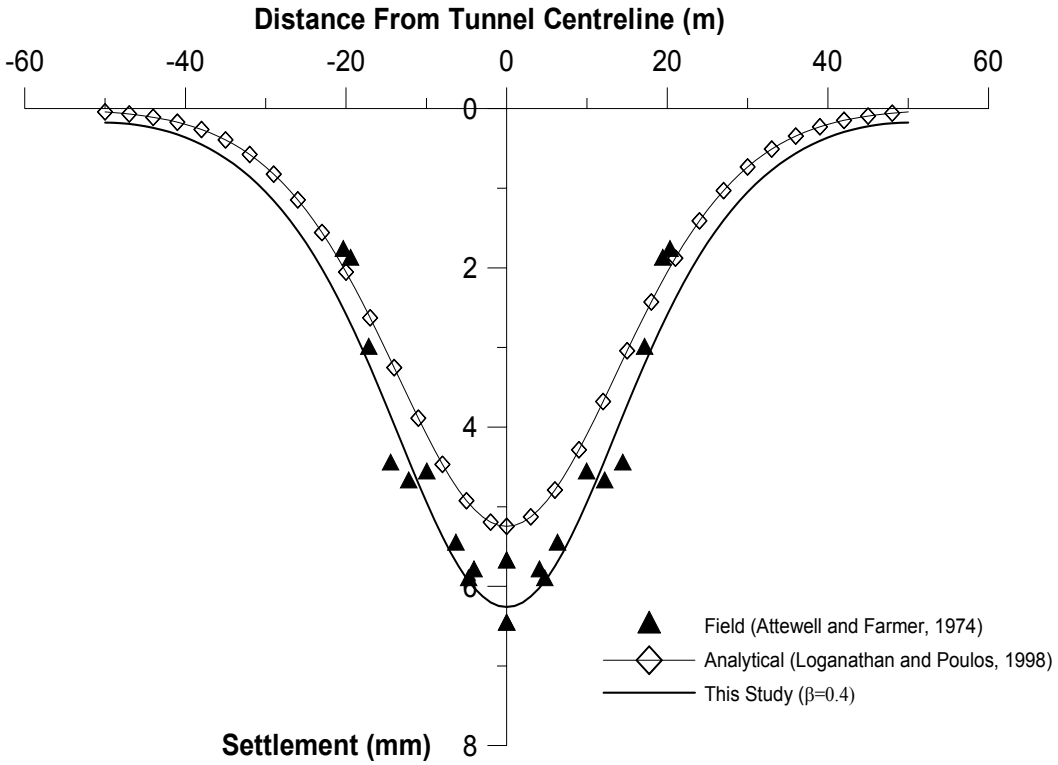

Fig. 3.19. Observed and predicted surface settlement for Green Park Tunnel

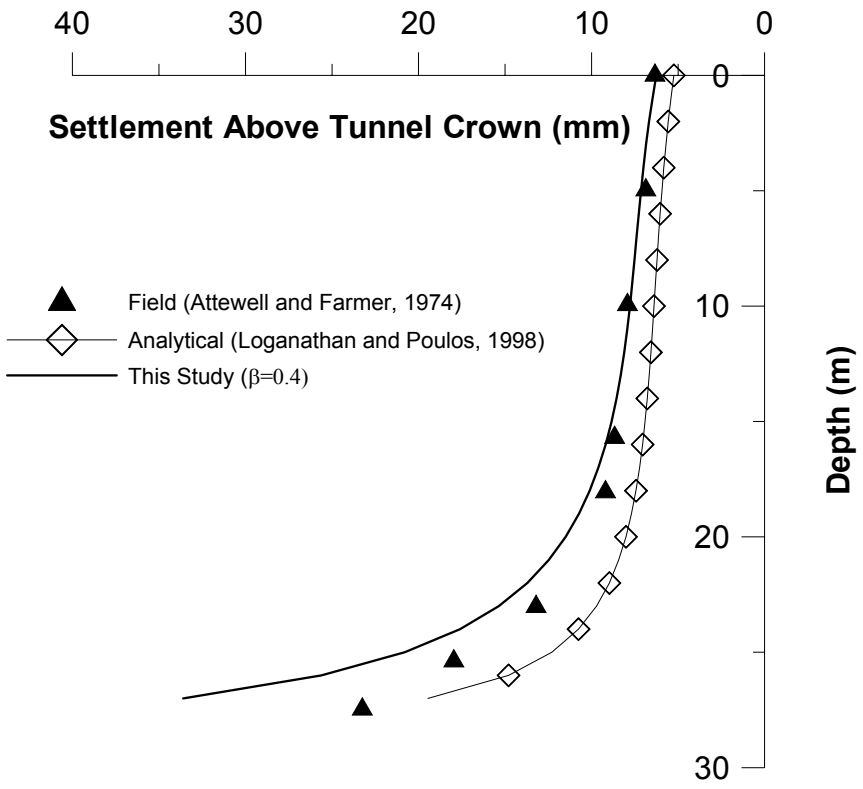

Fig. 3.20. Observed and predicted settlement above tunnel crown for Green Park Tunnel

Referring to Figure 3.20, good agreement between field and computed results were observed down to a depth of about 18m. The prescribed crown displacement in FE analysis appears to be significantly higher than that recorded in the field.

3.5.4 Mexico City Sewer Tunnel

A tunnel was bored through the soft lacustrine clays in the south-east Mexico City zone as part of a sewerage system using a pressurized slurry shield. The tunnel had an average axis depth of 13m and an excavated diameter of 4m, passing through clay with unusually high friction angles up to 43° (Diaz-Rodriguez et al.,1992). Instrumentation, field measurements and soil parameter details are as documented by Romo (1997). No reported volume loss

values were presented for the tunneling project, thus a value of 5% was used in the analysis based on a best fit Gaussian curve to field data obtained from instrumentation at Line A.

Figure 3.21 shows the computed transverse surface settlement profile against field data. Although maximum settlement is under predicted by approximately 12%, settlement profiles are in good agreement with field data. Far field settlements are negligible beyond a distance of 25m while horizontal displacements at an offset of $1.125D_t$ from tunnel centerline as shown in Fig 3.22 are predicted to a reasonable degree of accuracy. Horizontal displacements above tunnel axis level are slightly over predicted but the depth to which $S_{h\,max}$ occurs corresponds with field data.

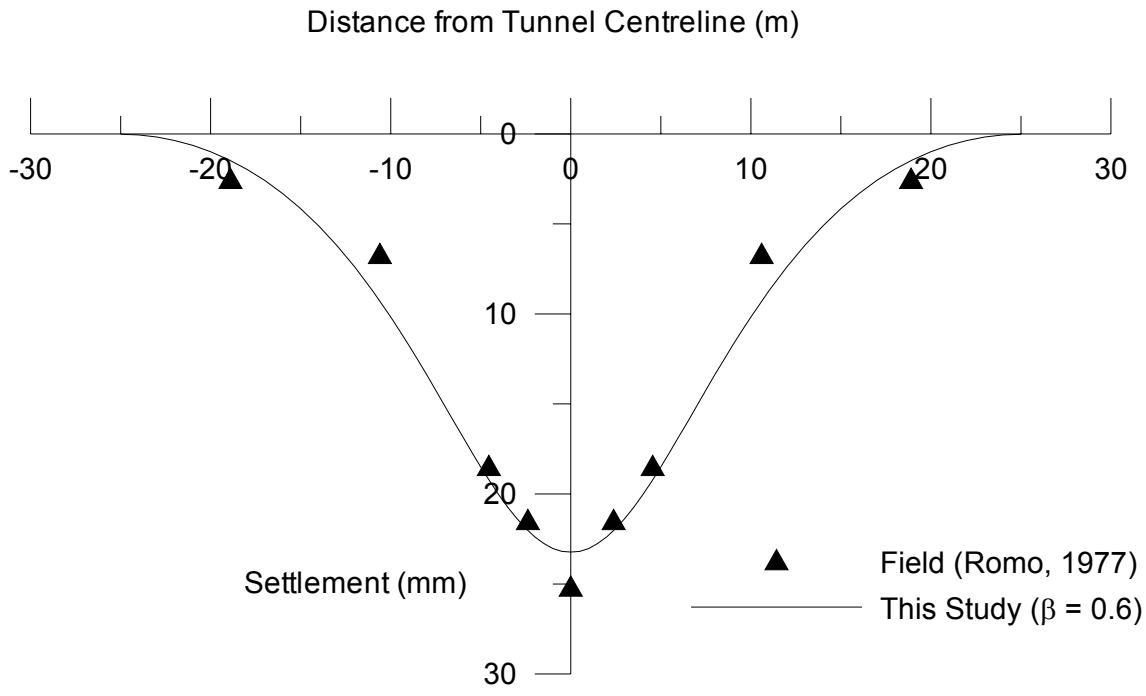

Fig. 3.21. Observed and predicted settlement troughs for Mexico City Sewer Tunnel

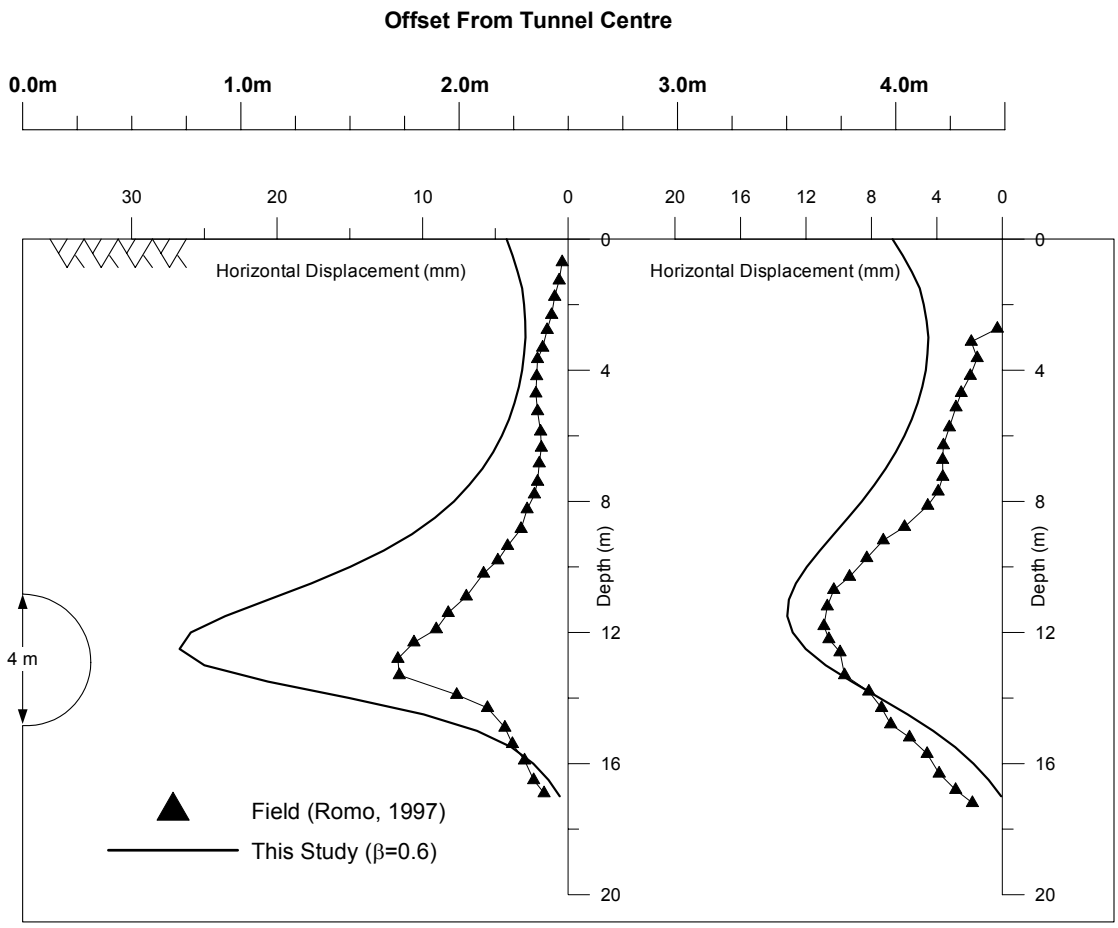

Fig. 3.22. Observed and predicted horizontal displacements at an offset of 2.5m and 4.5m from tunnel centreline

Horizontal displacements at a nearer offset of $0.625D_t$ from tunnel centerline are over predicted by more than two times as shown in Figure 3.22. However, it has to be pointed out that field horizontal displacements at $0.625D_t$ and $1.125D_t$ are approximately similar in magnitude thus raising some doubt as to the accuracy of the field data. A beta value of 0.4 provided an overall best fit to field data.

3.5.5 Bangkok Sewer Tunnel

The Bangkok Sewer Tunnel was constructed as part of a water transmission project undertaken by the Bangkok Metropolitant Water Works Authority. The tunnel runs for 2.2km from Ratchadaphisek to Phahonyothin with an excavated diameter of 2.66m at the instrumented section. A semi-mechanical backhoe and hand mining method was adopted to excavate the tunnel which resulted in a moderately high volume loss of 6%. Information regarding soil parameters, tunnel dimensions and field measurements are published by Phienwej (1997) and Ramasamy (1992).

A beta value of 0.4 was most suitable in representing surface and subsurface soil behaviour for this analysis. Using an input volume loss of 6%, the surface settlement profile as shown in Figure 3.23 provides a reasonably good match to field data despite being slightly wider. Settlements along tunnel centerline as shown in Fig 3.24 are also well predicted when compared with field data.

However, computed horizontal displacements at an offset of 4m ($x \approx 1.5D_0$) from tunnel centerline (Figure 3.24) were significantly larger than field data (≈ 2.7 times) due to unconfirmed reasons. One possible explanation for such observation is that tunnel lining diameter increases horizontally while decreasing in the vertical direction due to the difference in stresses in the corresponding directions. Lee (2002) reported horizontal "squeezing" of tunnel lining up to 5mm (excluding compensation grouting) for a 5.85m tunnel with lining thickness of 250mm excavated through London soils (Appendix A). The author explained that it could be possibly due to the over consolidated nature of London soils where horizontal stress is greater than vertical stress. Hence, the same explanation

could be extended to the current case where vertical stresses are generally larger than horizontal stresses for Bangkok clays. OCR values of Bangkok clays at three different sites in Bangkok (Nong Ngoo Hao, Outer Bangkok Ring Road and Asian Institute of Technology) range from 1.0-1.5 (Shibuya, 2002), neglecting the upper 5m of soil, thus indicating low K_o values. Maximum horizontal displacements occur at a level slightly above tunnel crown which coincides with field data.

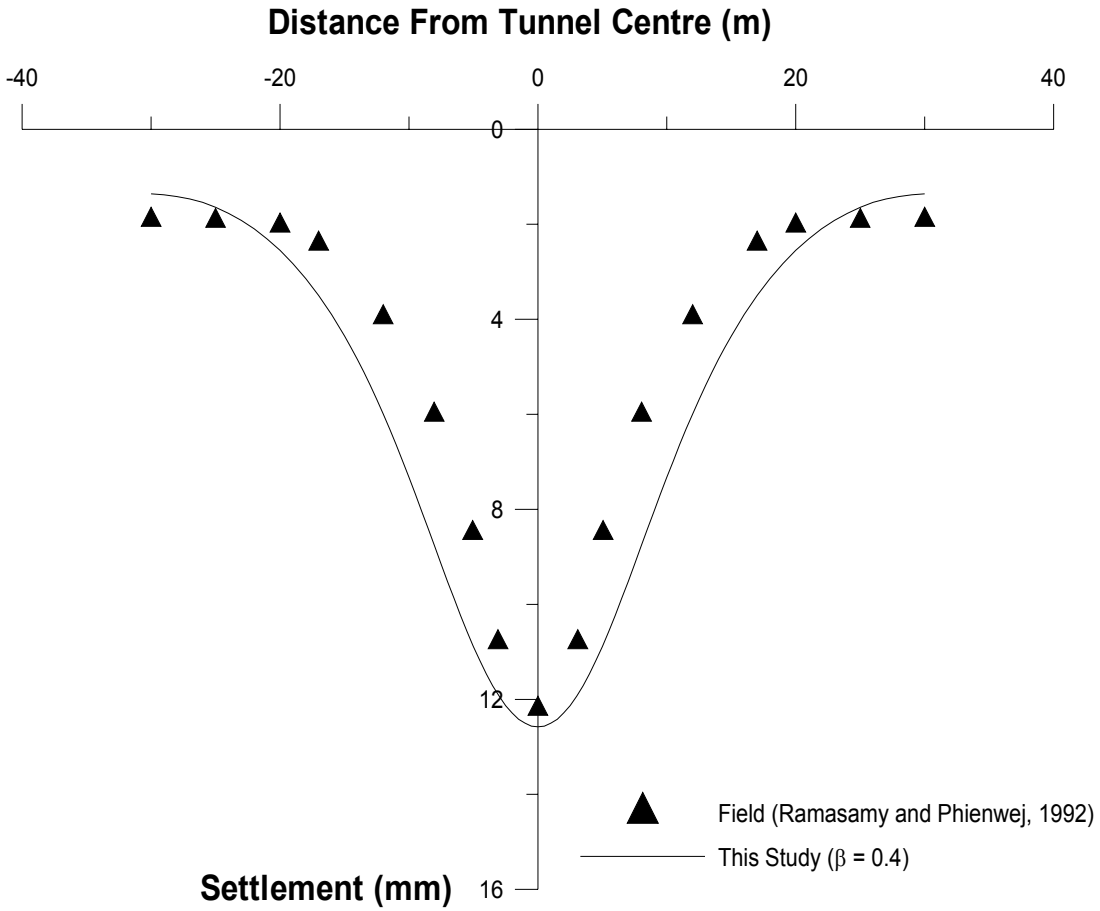

Fig. 3.23. Observed and predicted settlement trough for Bangkok Sewer Tunnel

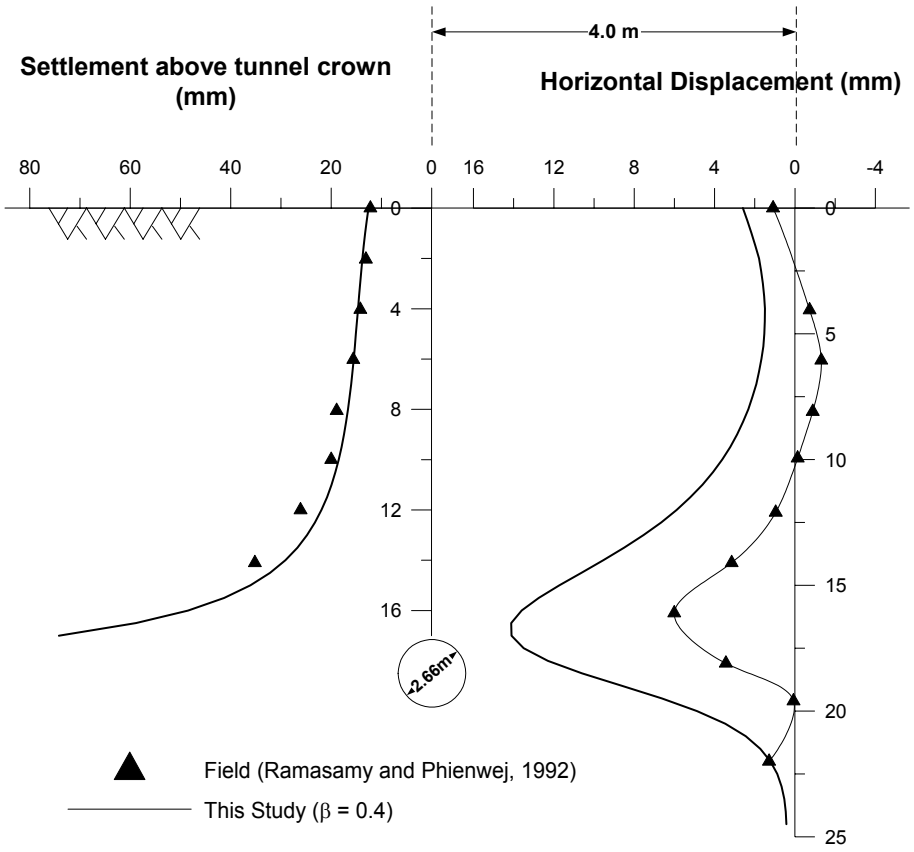

Fig. 3.24. Observed and predicted horizontal displacement (x = 4m) and vertical settlement above tunnel crown for Bangkok Sewer Tunnel

3.6 Discussion

Results from the six analysed case histories yielded transverse surface settlement profiles that are in close agreement with field or test data. Far field settlements were relatively small compared to maximum settlements (S_{max}) simultaneously producing a narrow settlement trough width. Despite this, far field settlements are still noticeably large as observed in Figures 3.17(b) and 3.23. A possible explanation for the settlements is that the vertical boundary of the mesh is not located sufficiently far away from the tunnel. However, the effect of mesh boundaries on tunnel excavation analysis is not addressed in this study.

To further investigate the validity of the proposed method, computed results were compared with subsurface data and it is found that the results are generally in good agreement, both trend and magnitude. Horizontal displacement magnitudes were over predicted for Test 1 of Loganathan's centrifuge experiment. Experimental data shows zero horizontal displacement at the invert level thus raising some doubt as to the accuracy of the data acquired. Field data from the Thunderbay Tunnel (Ng et al., 1986) and Heathrow Trial Tunnel (Deane and Bassett, 1995) show that horizontal displacements only diminish to a negligible magnitude beyond a distance of $2D_t$ below the tunnel invert.

Changes in tunnel lining vertical/horizontal diameter could occur from the difference in stresses as proposed by Lee (2002). Thus tunnel lining is expected to "squeeze" horizontally in heavily over consolidated soils with the opposite occurring for normally and lightly over consolidated soils as shown in Figure 3.25. This phenomenon could be a possible factor in the overestimation of computed horizontal displacements (compared with field data) for the Bangkok Sewer Tunnel as Bangkok Clays are typically normally to lightly consolidated.

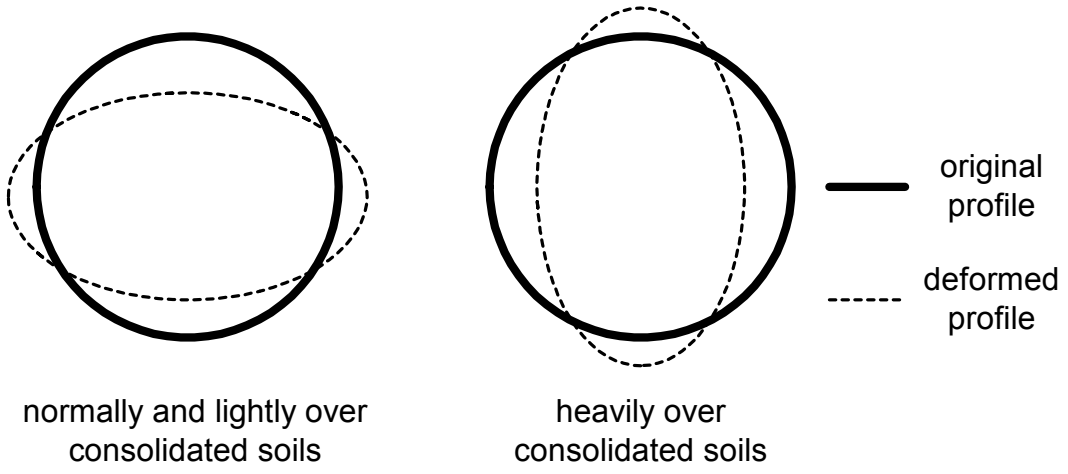

Fig. 3.25. "Squeezing" of tunnel lining in different soils

Figure 3.26 summarises the relationship between convergence point of soil displacement vectors (β) around the excavated tunnel boundary and C/D_t ratio. Based on the six case histories, the fitted linear curve validates the intuition that the excavation of a deeper tunnel in clay result in displacement vectors converging closer to the tunnel centre.

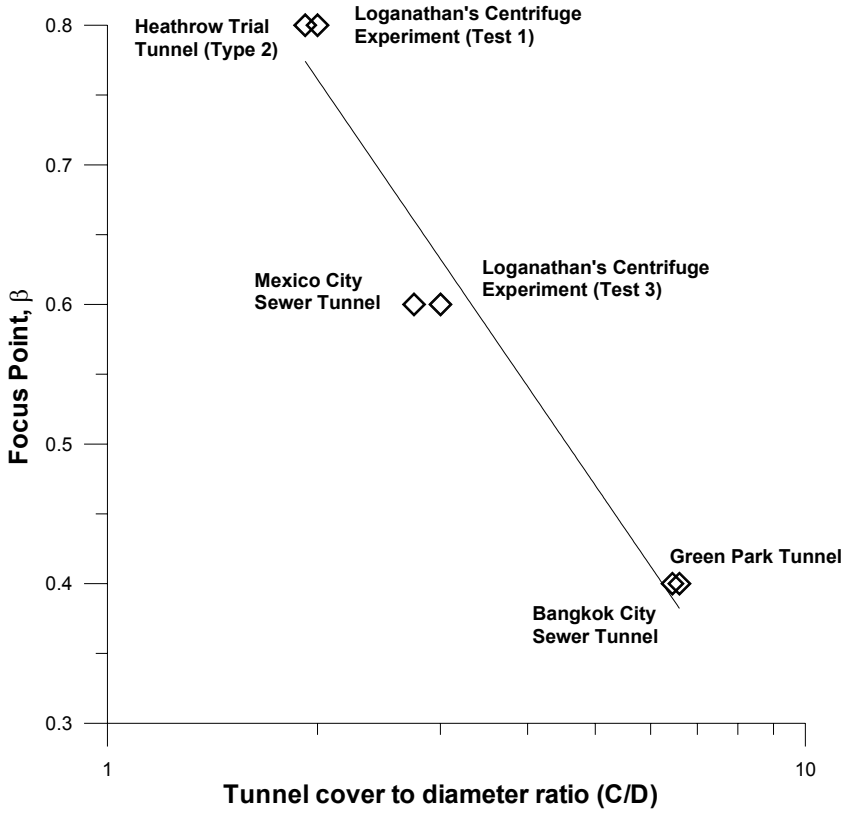

Fig. 3.26. Variation of Focus Point with C/D_t ratio

CHAPTER 4

TUNNEL SOIL PILE INTERACTION STUDIES

4.1 Introduction

Accurate assessment of pile performance subjected to tunneling induced ground movements is not only dependant on correct predictions of maximum displacement magnitudes (to satisfy serviceability requirements) but also displacement profile. Realistic deformed profiles of piles are necessary as bending moments are dependant on shape rather than magnitude. The induced stresses on the pile are typically derived from a combination of axial (tensile or compressive) and bending response to the soil movement that could be damaging in effect.

This chapter focuses on the prediction of single pile performance in clays subject to tunneling induced soil movements. In these predictions, tunnel heading is assumed to have advanced past the pile section, i.e. uniform soil movements along the tunnel boundary in the longitudinal direction. These soil movements are referred to as uniform convergence for the convenience of subsequent discussion. Uniform soil convergence due to tunneling is simulated by the displacement control method, DCM, developed in the previous chapter. Parametric studies using the software ABAQUS are performed to assess the influence of (i) pile tip position relative to tunnel axis level, (ii) relative soil-pile stiffness effects, (iii) ground loss value, (iv) horizontal offset between tunnel and pile centre and (v) pile head fixity conditions.

A summary of the significant findings in this tunnel-soil-pile interaction study are presented at the end of the chapter.

4.2 FE Analysis

Three dimensional total stress analysis was performed for all cases in this chapter using the software package ABAQUS. The choice of total over effective stress analysis is justified by a preliminary study which indicates that induced pile bending moment and axial force for a given set of material properties are approximately similar for both types of analysis (Appendix A). Hence, computational time is reduced without significantly compromising the accuracy of results. Insitu effective stress (p') was obtained for the pressure dependant soil constitutive model by multiplying total stress (p) with a conversion factor as shown in Appendix A. Element type employed to model the soil and pile are continuum, twenty node quadratic elements. Zero thickness slip elements were used to model the soil-pile interface behaviour to allow for relative movement. Unlike the previous chapter, elements are prescribed with self weight (i.e. influence of gravity accounted for) to:

i) enable soil stiffness to vary with depth as a strain and pressure dependant constitutive model was necessary to produce realistic results of pile response.

ii) enable limiting shear stress (τ_{lim}) at which plastic sliding between the soil and pile surface is mobilised to increase with depth

Analysis was carried out in two steps as described below:

Step 1 - Attain geostatic equilibrium for element stresses under gravitational force

Step 2 - Excavated tunnel boundary displaced using DCM to simulate stress relief

Bored piles are assumed for the analyses and changes in the soil insitu stress state and stiffness due to the installation of the pile are ignored in this study. Construction sequence is not modeled in all analyses as uniform displacements around the tunnel in the longitudinal

direction is prescribed, simulating the case in which tunnel heading has advanced past the pile section.

4.2.1 Mesh Dimensions and Properties

A typical mesh used for the parametric study is as shown in Figure 4.1. The symmetry of the problem is exploited by creating a half mesh about the vertical centerline of the tunnel (longitudinal axis) and along the pile centerline (transverse axis). Tunnel cover and diameter as well as pile diameter are kept constant for all analyses in the parametric study while a tunnel length of 10m was assigned to ensure that soil displacement fields at the far end of the mesh is not affected by the presence of the pile (Appendix A). Table 4.1 shows the constant mesh dimensions used in the parametric study.

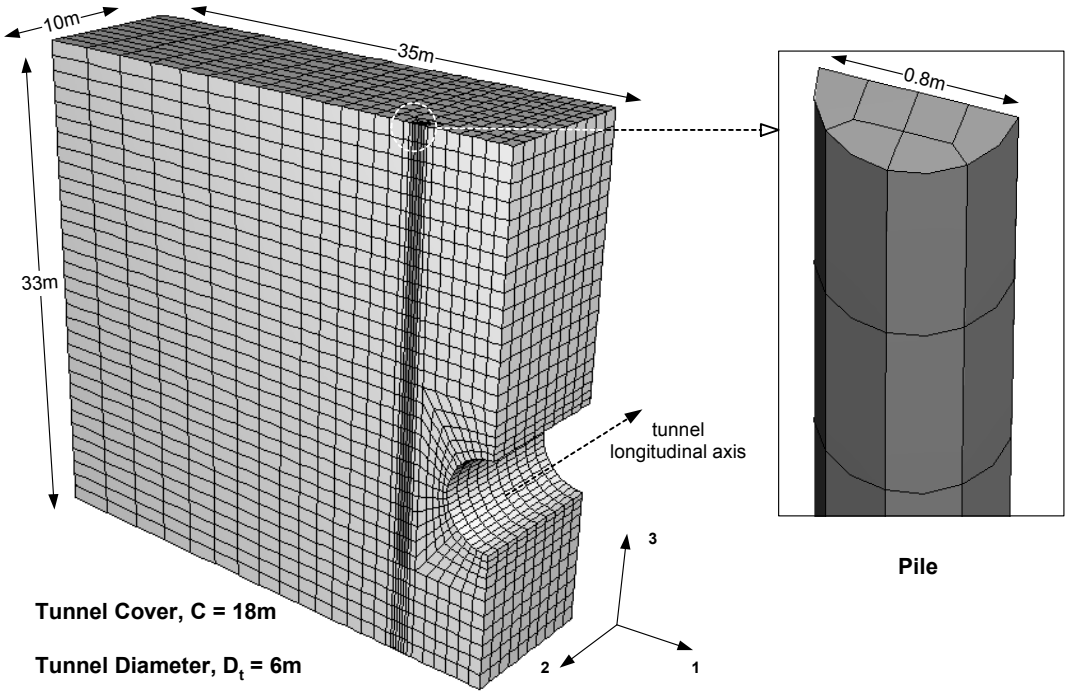

Fig. 4.1. Typical mesh used for parametric study

Table 4.1. List of constant mesh dimensions for parametric study

Tunnel Cover, C	18m
Tunnel Diameter, D_t	6m
Tunnel Length	10m
Pile Diameter, D_p	0.8m

Piles of three different lengths (15m, 21m, 27m) were considered to study the influence of relative location of pile tip to tunnel axis level. The relative positions are denoted by Y_p whereby a positive value would indicate pile tip located above tunnel axis level and vice versa. The corresponding Y_p values for the piles are -1D_t (27m), 0D_t (21m) and +1D_t (15m).

4.2.2 Boundary Conditions

The free surfaces of the mesh (except for ground surface) as shown in Figure 4.1 are assigned with roller type boundary conditions, restraining movement in the direction normal to the free surface.

In this parametric study, two pile head boundary conditions are considered. The first case would correspond to the pile head being totally free of restraint in the form of displacements and rotation while the second is completely fixed. Zero rotation was indirectly maintained for the second case by imposing zero displacement (vertical and horizontal) to all nodes on the pile head. The two extreme fixity conditions assigned to the pile head are expected to provide a bound to the response of single piles in the field while providing detailed insight in to its behaviour along the length of the pile.

4.3 Soil and Pile Properties

The soil constitutive model used for tunnel-soil-pile interaction studies is with a strain and pressure dependency as shown in Figure 4.2. Stiffness variation with strain is modeled similar to Equation 3.3 with the invariant pressure term (ie. effective stress) included as shown in Equation 4.1. An *n* value of -0.5 was prescribed for all analyses in the parametric study, decreasing the stiffness from a $\varepsilon_{q(min)}$ of 0.001% to $\varepsilon_{q(max)}$ of 1%. The *n* value of -0.5 was chosen as an approximate average based on the range of -0.4 to -0.7 for various soils as presented in Table 3.1.

$$\frac{G}{p'} = A\varepsilon_q^{\ n} \tag{4.1}$$

The inclusion of pressure dependency (as compared to the previous chapter) is aimed at increasing soil stiffness with depth to obtain more realistic predictions of pile vertical and lateral response. The effects of three soil stiffness values (Table 4.2) on the performance of piles subjected to tunneling induced ground movements were studied. The soils range from stiff to very soft clays that would typically be encountered in the field. Soil density was assumed to be 18kN/m^3 with a coefficient of pressure at rest (K_o) of 1.0.

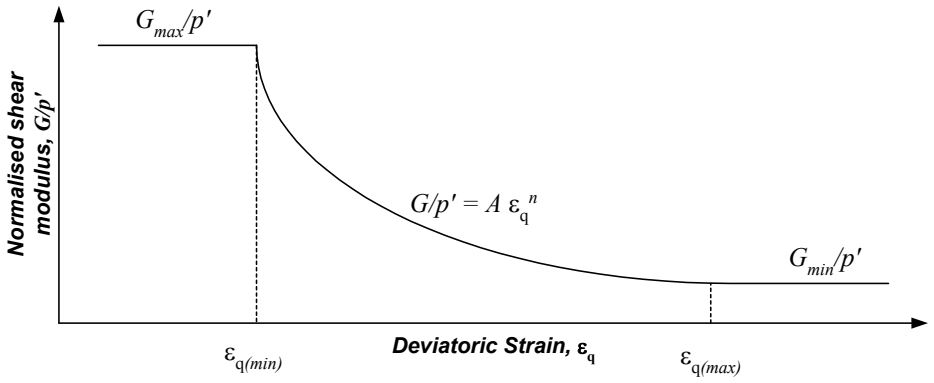

Fig. 4.2. Soil constitutive model used for tunnel-soil-pile interaction studies

By making the shear modulus a function of mean effective stress, the principle of energy conservation (i.e. non zero work for a closed cycle of soil unloading-reloading) has been violated as permanent shear deformation is obtained at the end of the closed cycle (Zytynski et al. 1978). This inadequacy in the soil constitutive model could result in inaccurate prediction of stresses but as Zytynski has pointed out, it is difficult to find a conservative model that matches the observed behaviour of soil throughout the range of elasticity.

The pile elements were assigned a typical concrete Young's modulus, E_p, of 30GPa (linear elastic behaviour). Concrete is assigned a density of 24kN/m^3.

Table 4.2. Soil stiffness values used for parametric study

Soil Type	G_{max}/p'	n	$\varepsilon_{q(max)}$	$\varepsilon_{q(max)}$	Typical Soils	Source
Stiff	400	-0.5	0.001%	1%	London Clay	Hight (2002)
Soft	200	-0.5	0.001%	1%	Bangkok Clay	Shibuya and Tamrakar (2003)
Very Soft	100	-0.5	0.001%	1%	Normally Consolidated Clay	-

Table 4.3. Summary of soil and pile properties

Material	K_o	Bulk Density (kN/m^3)	ν
Soil	1.0	18	0.499
Pile	-	24	0.25

4.4 Interface Constitutive Model

Numerical analysis of pile downdrag due to consolidating soil or construction induced soil movements typically result in exaggerated induced pile movements and stresses. This is predominantly due to the non-allowance for relative movement or slip between soil and pile surface. Numerous authors (Kuwabara and Poulos, 1989, Chow et al., 1990, Teh and Wong, 1995 and Lee et al.,2002) have reported the importance of simulating the effect of soil slip at the pile-soil interface to obtain realistic predictions of skin friction that are closer to field

behaviour. Recognising this importance, slip between pile and soil surface is modeled for all subsequent tunnel-soil-pile analyses.

The contact sliding behaviour was simulated by the ABAQUS interface modeling technique where duplicate nodes are created to form an interface of zero thickness. ABAQUS uses the Coulomb frictional law criterion to determine the onset of plastic sliding between pile and soil. As shown in Figure 4.3, the equivalent shear stress (τ_{equi}) increases linearly with slip displacement until limiting shear stress (τ_{lim}) is reached. An allowable elastic slip or limiting displacement (γ_{lim}) is specified for the relative displacement that may occur before surfaces actually begin to slip.

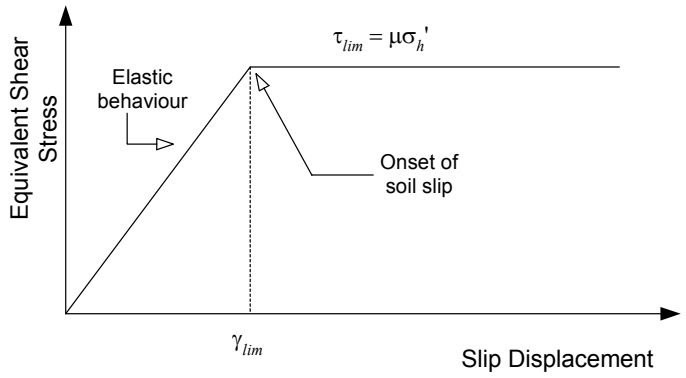

Fig. 4.3. Skin friction behaviour between pile and soil interface

A conservative limiting displacement of 1mm was assumed for all analyses in the parametric study to achieve full mobilization of skin friction. Although this value is at the low end of typical field measurements of 1-10mm reported by Broms (1979), it is observed in simple shear lab tests between steel and normally consolidated clays (Tsubakihara and Kishida, 1993) that limiting shear stress, τ_{lim}, occurs at slip displacement magnitudes less than or equal to 1mm (Figure 4.4). In addition, although interface studies between clay and various

construction materials (Subba Rao et al.,2000) performed using the more popular shear box test tend to yield limiting displacements typically greater than that of simple shear tests, the mode of shearing of the soil around the pile bears greater similarity to that of the latter test (Randolph and Wroth, 1981).

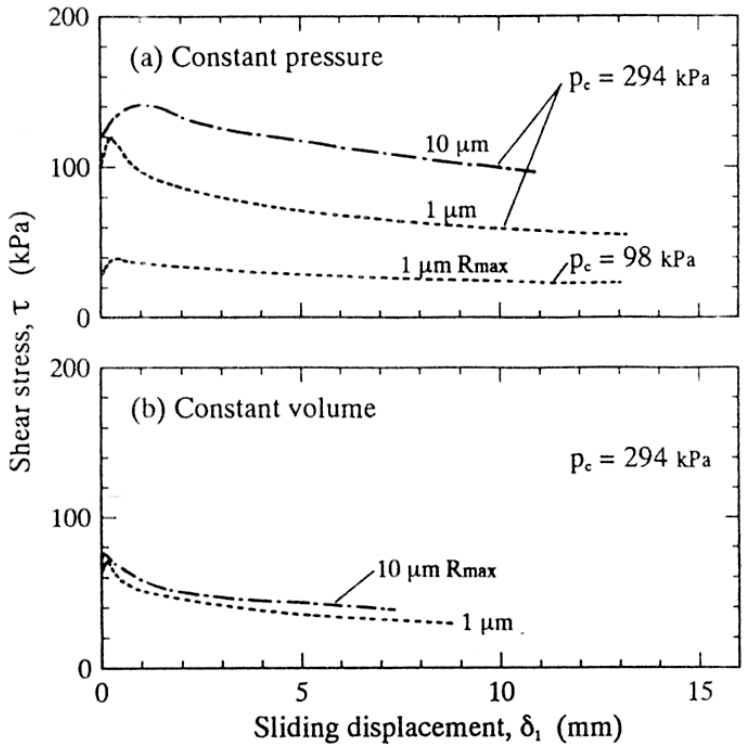

Fig. 4.4. Plot of sliding displacement with shear stress (Tsubakihara and Kishida, 1993)

The limiting shear stress, τ_{lim}, increases linearly with depth as it is governed by the product of lateral effective stress, σ'_h, and the interface coefficient of friction, μ, as shown in Equation 4.2

$$\tau_{lim} = \mu\sigma'_h \qquad (4.2)$$

If the shear stress applied along the surfaces is less than $\mu\sigma'_h$ (ie. slip displacement less than γ_{lim}), the surfaces would stick. A coefficient of friction of 0.4 was used for this parametric

study simulating the case whereby soil with a friction angle of approximately 22° fails at the soil-pile interface. Soil is assumed to have reconsolidated back to equilibrium conditions thus warranting the use of a high coefficient of friction. A comparison of pile responses with and without allowance for relative movement between soil and pile is reported in Appendix A.

4.5 Displacements and Calculation of BM and P

Computed far field soil displacements are plotted together with pile displacements (horizontal and vertical) to provide a better understanding of soil-pile interaction. In this chapter, far field soil displacements are taken as the soil movements at the far end of the mesh, away from the influence of the pile. This assumption is reasonable as preliminary analysis without the pile (ie. pile not modeled in analysis) shows that surface settlements are approximately similar to the corresponding settlements with the pile included (Appendix A).

Induced pile bending moments are obtained using a central finite difference representation of the bending equation for an Euler-Bernoulli beam. The governing equations are as shown below:

$$M = EI \frac{d^2 u_1}{dz^2} \tag{4.3}$$

$$M = EI\left(\frac{u_{1(i-1)} - 2u_{1(i)} + u_{1(i+1)}}{\Delta z^2} \right) \tag{4.4}$$

where u_1 is the pile displacement in the transverse tunnel direction and z denoting the vertical axis. Similarly, induced pile axial forces are obtained using a backward finite difference scheme as shown below:

$$P = AE\frac{du_3}{dz} \tag{4.5}$$

$$P = AE\left(\frac{u_{3(i)} - u_{3(i-1)}}{\Delta z}\right) \tag{4.6}$$

where u_3 is the displacement in the vertical direction. Subscripts 1,2 and 3 for displacements (u) correspond to the same axis directions as shown in Figure 4.5.

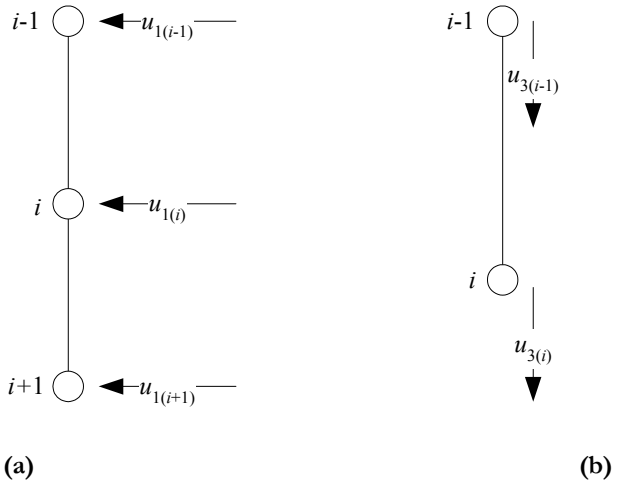

Fig. 4.5. Notations used in finite difference equations for (a) bending moment and (b) axial force

Displacements (u_1, u_3) are selected at the centre of the pile to obtain an average behaviour of induced pile bending moments and axial forces. Whenever possible, pile performance is quoted relative to cracking moment (M_{cr}), ultimate moment (M_{ult}) and limiting tensile force (P_{ult}) with the corresponding calculations shown in Appendix A. Positive pile displacement in this study would indicate movement towards the tunnel while positive axial force would indicate pile in compression. Five parameters affecting pile performance are studied in detail in the subsequent sections. Each parameter is varied under a fixed set of conditions to ensure a common basis for comparison. Table 4.4 lists the numerous parameters that are varied and kept constant to facilitate easy interpretation of subsequent results.

Table 4.4. List of factors varied and kept constant

Section	Variable	Constant
4.5.1	Y_p	G_{max}/p'=400, X=1D_t, V_l=1%, Free head
4.5.2	G_{max}/p'	X=1D_t, V_l=1%, Free head
4.5.3	V_l	X=1D_t, Free head
4.5.4	X	G_{max}/p'=400, Free head
4.5.5	Pile head fixity	G_{max}/p'=400, X=1D_t, V_l=1%

4.5.1 Pile Performance at Different Relative Pile Tip to Tunnel Axis Levels (Y_p)

Figures 4.6 (a) and (b) shows the respective pile horizontal displacements and induced BM for various relative positions of pile tip to tunnel axis levels subjected to 1% volume loss. Horizontal displacements generally conform to the far field (undisturbed) soil displacement profile due to the low bending stiffness (EI) of the pile along its length. Despite this, pile displacement is computed to be less than soil displacement at tunnel axis level. The restraint in movement can be attributed to the higher strains and thus lower soil stiffness encountered directly around the converging tunnel.

Bending moments as presented in Figure 4.6(b) is maximum ($0.25M_{ult}$) for the case where pile tip is located below tunnel axis level (Y_p = -1D_t) as the change in curvature is most pronounced slightly above tunnel axis level. Lowest bending moment magnitudes are observed for the case where pile tip is above tunnel axis level (Y_p = +1D_t). Pile bending behaviour changes from triple to predominantly single curvature as the pile tip moves from 1D_t below to 1D_t above tunnel axis level.

In Figure 4.7(a), the high axial stiffness of the pile is evident as the pile settles approximately uniformly along its length. The pile experiences significant compression at levels closer to

tunnel axis level due to the effects of negative skin friction. As is intuitively expected, induced pile axial force is largest for the case in which pile tip is below tunnel axis level as shown in Figure 4.7(b). This is explained by the fact that it has greater surface area to develop larger negative skin friction and also due to the pile tip being located far below and away from the zone of large displacements. The length of pile outside the zone of large displacements provides the reaction force to oppose the downward force by developing positive skin friction and end bearing reaction.

When the pile tip is located within the zone of large displacements, the pile is expected to settle in manner closer to a rigid body translation (ie. no or little relative displacement between soil and pile) as bearing capacity reaction is not able to fully develop. This phenomenon is verified in Figure 4.7(a) where the pile tip is observed to settle at an approximately similar magnitude to the far field soil displacements.

Approximating the soil settlement directly around the pile location to be similar to the far field soil settlement, the level of maximum induced axial force for a Y_p of -1D_t and 0D_t is coincident with the intersection level of the soil and pile settlement profile. This is correct as positive skin friction develops below the point of intersection to resist the induced downward drag.

Additional studies with a relative Y_p level of -2D_t and -3D_t were performed to investigate the pile response below a relative Y_p level of -1D_t. Figure 4.8 shows that maximum magnitudes remain constant below a critical relative pile position of one tunnel diameter below tunnel axis level. This indicates that a relative pile tip level of 1D_t below tunnel axis level is

sufficient to bend the pile to maximum curvature which occurs at a level slightly above tunnel axis level.

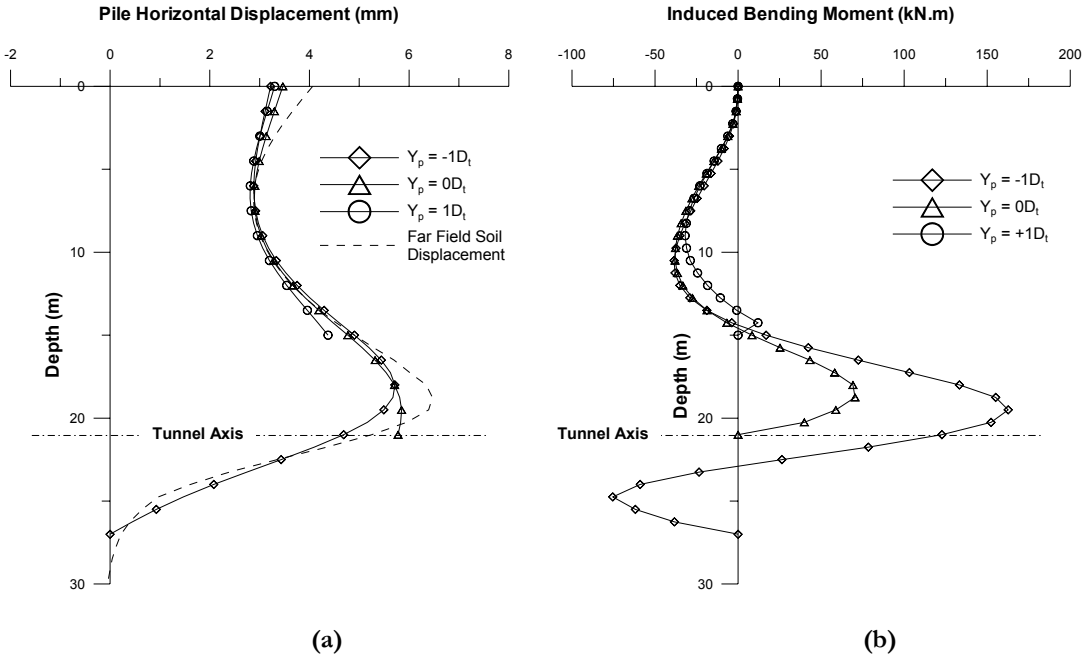

Fig. 4.6. Horizontal displacement (a) and bending moment (b) profiles along pile length

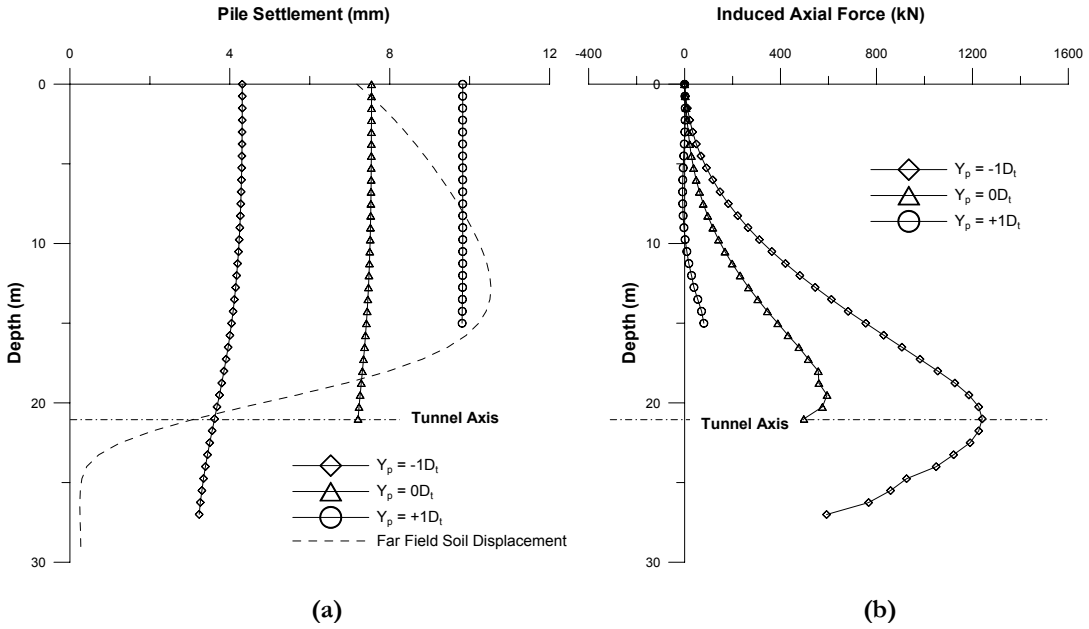

Fig. 4.7. Settlement (a) and axial force (b) profile along pile length

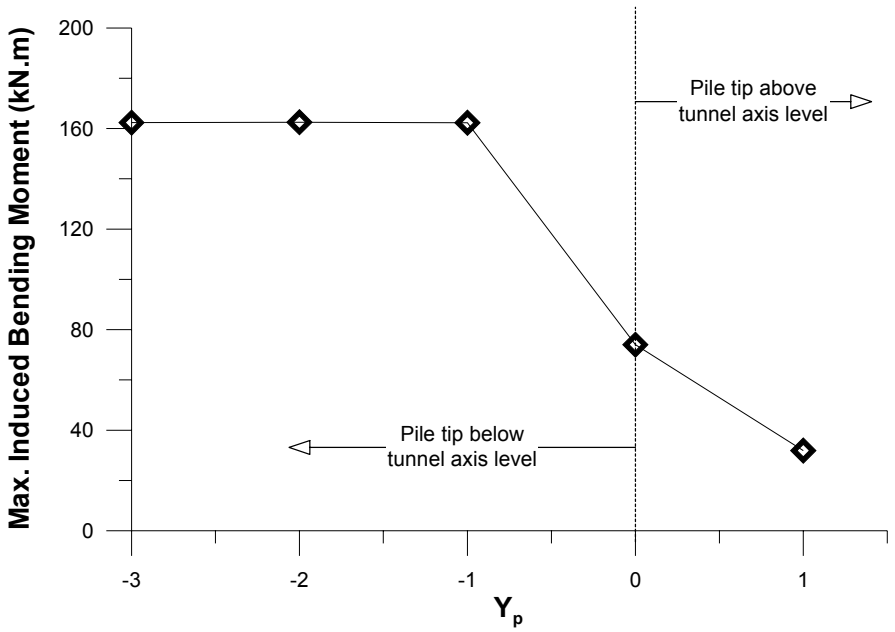

Fig. 4.8. Variation of maximum induced bending moment with relative Y_P levels

4.5.2 Pile Performance at Different Soil Stiffness (G_{max}/p')

Figures 4.9 to 4.14 show the lateral (displacement and BM) and vertical (settlement and P) pile responses to tunneling induced ground movements for relative Y_p levels of -1D_t, 0D_t and +1D_t. The computed results of pile behaviour/performance at a volume loss of 1% and horizontal offset from tunnel centre, X, of 1D_t are as expected for most of the cases. The general observations are:

i) Pile head displacements decrease as pile to soil stiffness ratios increase.

ii) Pile settlement profile along its length is approximately constant with marginally larger settlement for the case in which soil is least stiff relative to the pile. Pile tip settlement for the case where Y_p is +1D_t is observed to be similar to soil settlement at the corresponding level (Figure 4.14 (a)).

iii) Maximum induced bending moments on the pile increase as pile to soil stiffness ratios decrease for a given volume loss. Assuming a commonly encountered tunnel volume loss of 2% under working conditions for two different soils (soft and stiff), induced bending moments are expected to be higher for the pile in stiff soil as its deformed shape conforms closer to the far field soil displacement profile than for a pile installed in soft clay.

iv) For the case in which pile tip is located outside the zone of large displacements (Y_p position $-1D_t$ and $0D_t$), maximum induced compressive axial forces increase with decreasing pile to soil stiffness ratios for a given volume loss. This observation is explained by the fact that a softer soil would experience less shear stress around the pile at a given volume loss hence inducing less relative displacement. Therefore, a smaller percentage of the pile length is experiencing limiting shear stress thus inducing smaller axial forces. Pile did not experience tensile forces for these cases.

v) When pile tip is located within zone of large displacements (Y_p position $+1D_t$), maximum induced compressive force is approximately similar for all three soil stiffness values used. However, some tensile forces developed for the case where soil is stiffest as the pile settled more relative to the soil without developing significant end bearing reaction.

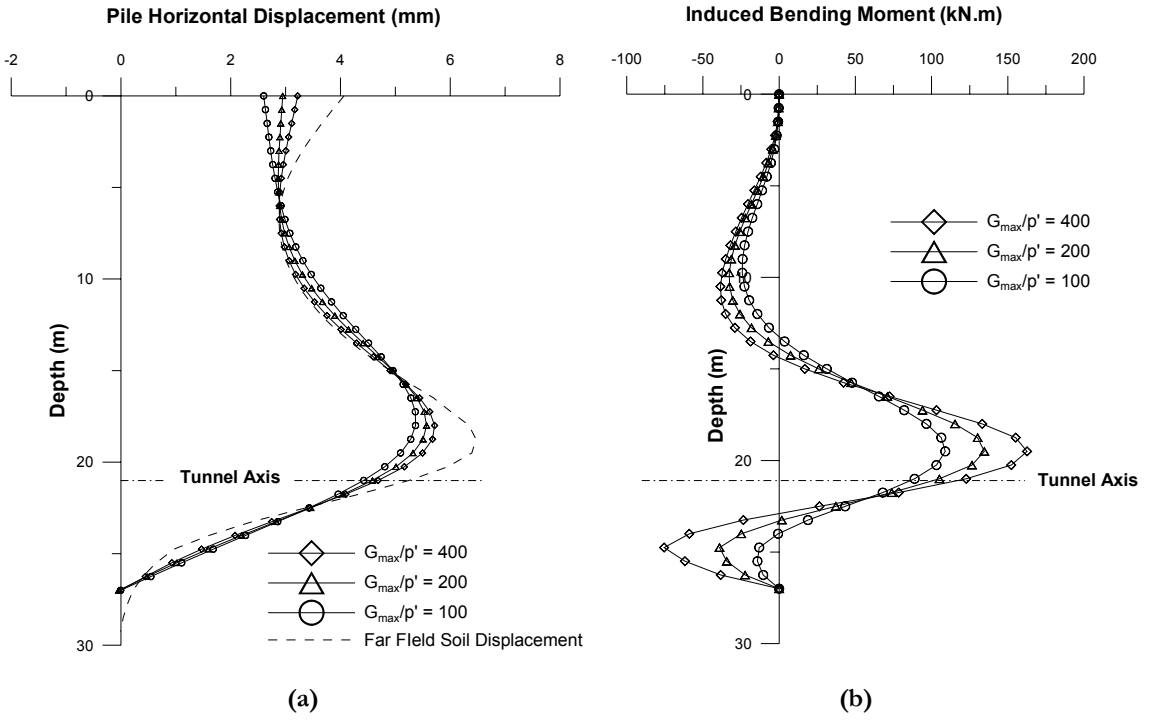

Fig. 4.9. Pile (a) horizontal displacement and (b) bending moment profile for Y_p of -1D_t

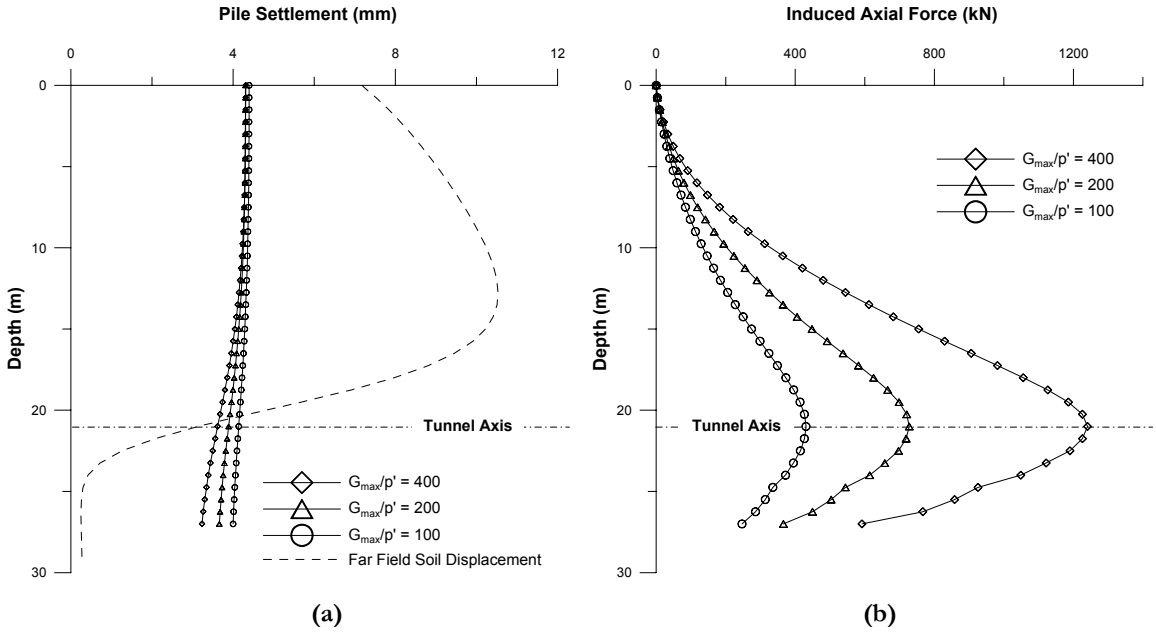

Fig. 4.10. Pile (a) settlement and (b) axial force profile for Y_p of -1D_t

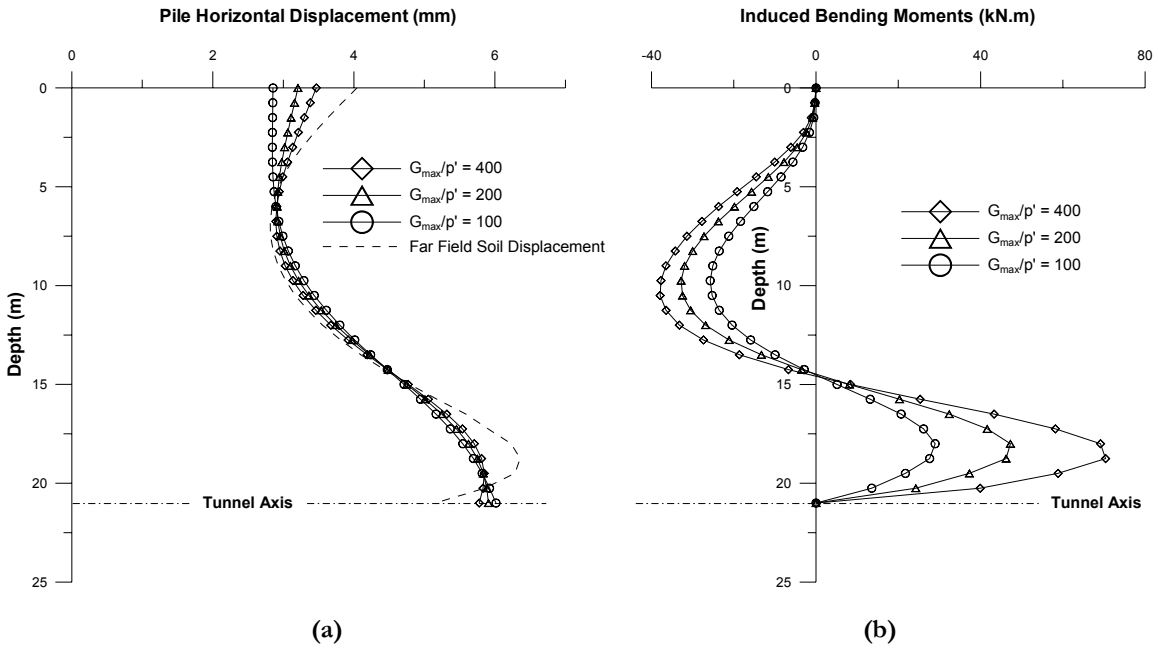

Fig. 4.11. Pile (a) horizontal displacement and (b) bending moment profile for Y_p of $0D_t$

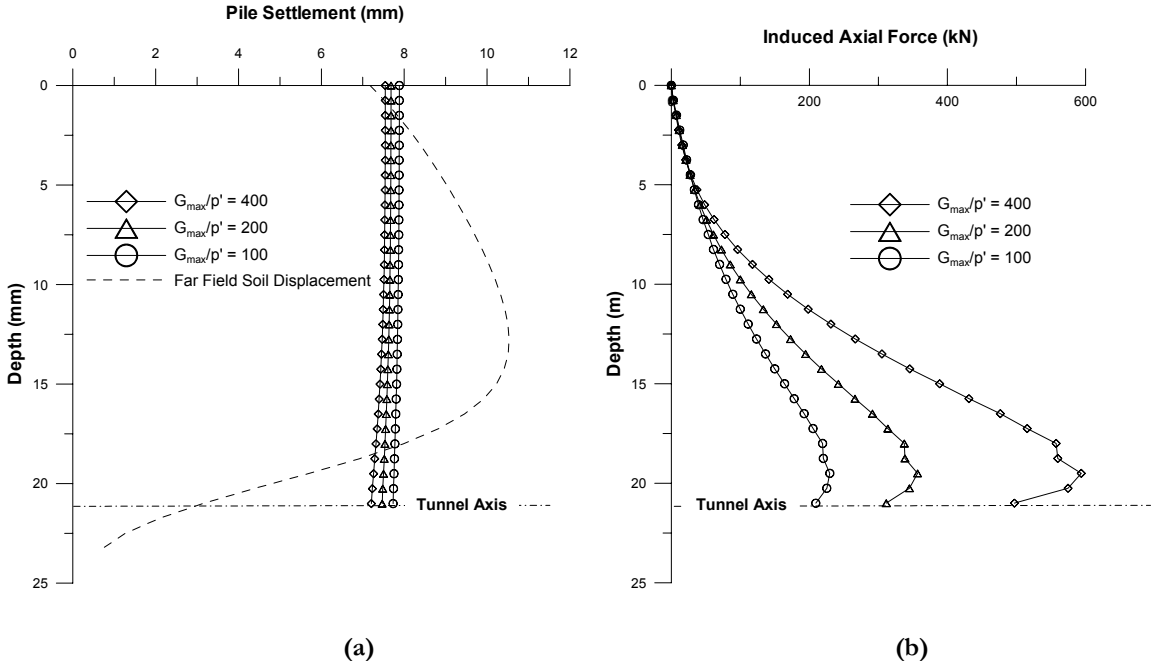

Fig. 4.12. Pile (a) settlement and (b) axial force profile for Y_p of $0D_t$

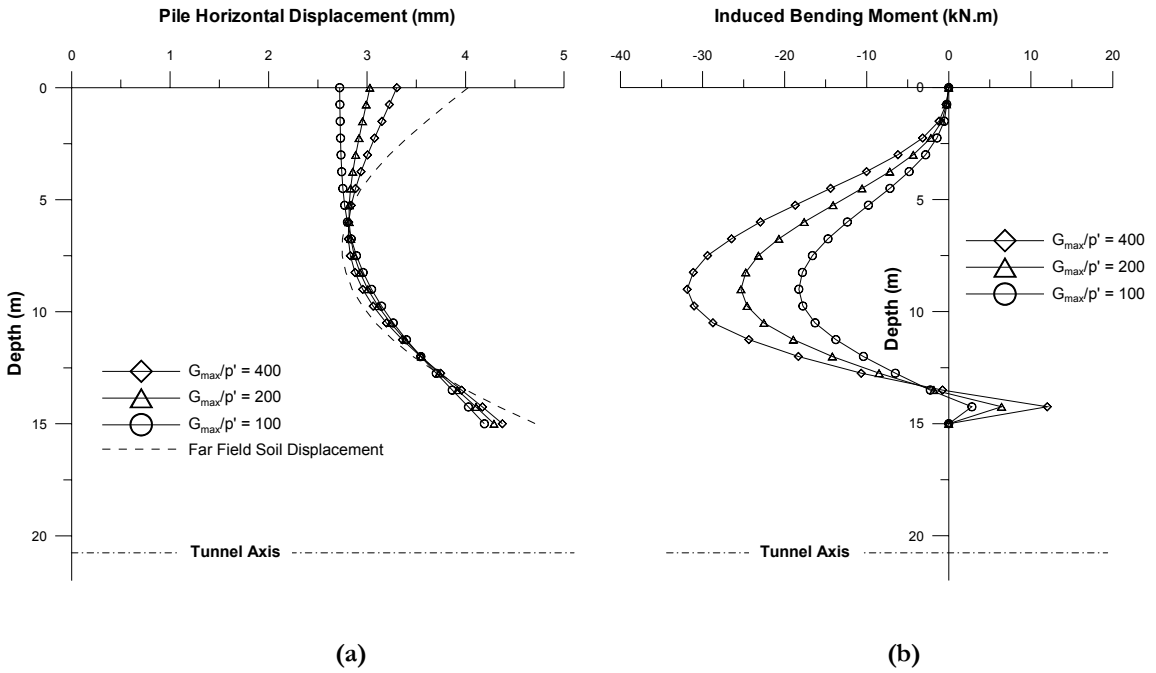

Fig. 4.13. Pile (a) horizontal displacement and (b) bending moment profile for Y_p of $+1D_t$

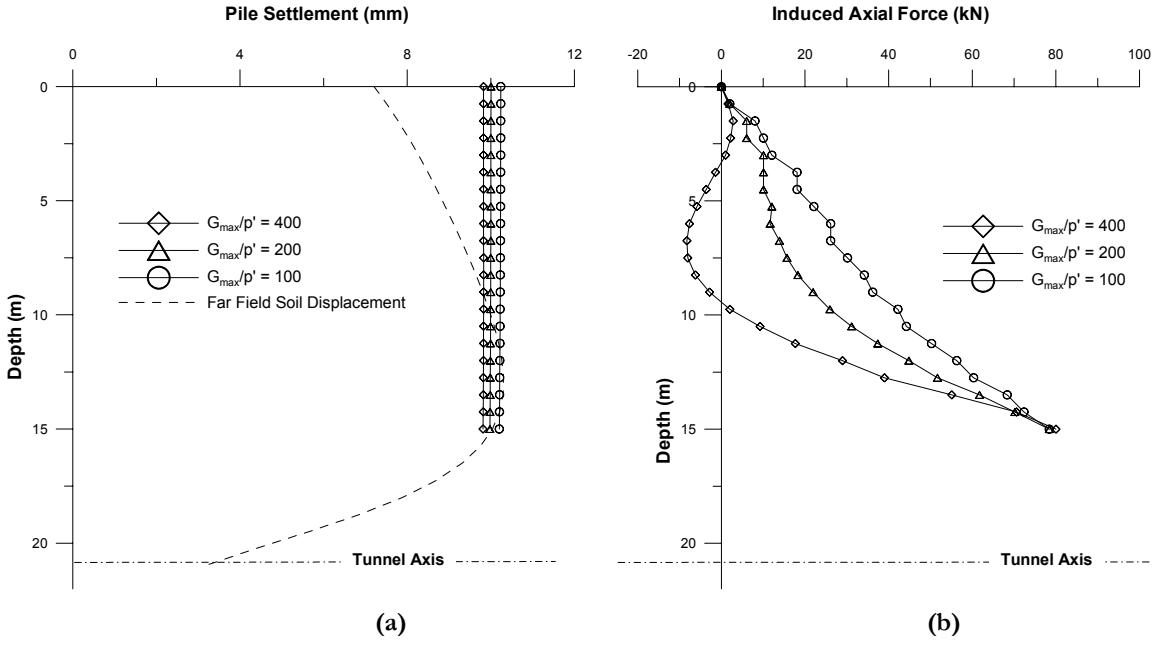

Fig. 4.14. Pile (a) settlement and (b) axial force profile for Y_p of $+1D_t$

4.5.3 Pile Performance at Different Volume Loss Magnitudes (V_l)

Volume losses were varied from 1% to 3% in this study to simulate values that are typically encountered in field conditions under reasonably good tunnel construction technique and workmanship. The results from Figures 4.15(a), 4.16(a) and 4.17(a) show that maximum induced bending moments respond in an approximately linear behaviour when volume losses are greater than 1%. Below a volume loss of 1%, the rate of increase in maximum induced bending moments with volume loss is greater than the corresponding gradient beyond 1%. This can be explained by the nonlinear variation of soil stiffness where initial soil shear modulus is high due to the small induced deviatoric strains directly around the pile at tunnel axis level.

For the case in which pile tip is $1D_t$ below tunnel axis level, cracking moment (M_{cr}) is exceeded beyond a volume loss of approximately 1.0-1.5% for all values of soil stiffness as shown in Figure 4.15 (a). This could be detrimental to the structural integrity of the pile as it is projected that ultimate bending moments (M_{ult}) is exceeded for a pile in soft to stiff clay beyond a volume loss of approximately 5%. Although a volume loss of 5% is not commonly encountered in the field, the probability of it occurring is sufficiently high for it to be considered in the design of the pile. Maximum induced bending moments for the case where Y_p is $0D_t$ and $-1D_t$ is not expected to cause any structural concern for the pile.

Maximum induced compressive force for the pile generally increases with tunnel volume loss for the case in which pile tip is at and below tunnel axis level as shown in Figures 4.15(b), 4.16(b). Although increasing in magnitude, the rate of increase decreases significantly after a volume loss of only 1%. This observation is explained by the fact that full skin friction has

been mobilized at significant lengths of the pile at a volume loss of 1% (Figure 4.21). Maximum induced pile axial force for the case in which pile tip is $1D_t$ above tunnel axis level shown in Figure 4.17(b) is relatively constant beyond a volume loss of 1% for reasons previously mentioned.

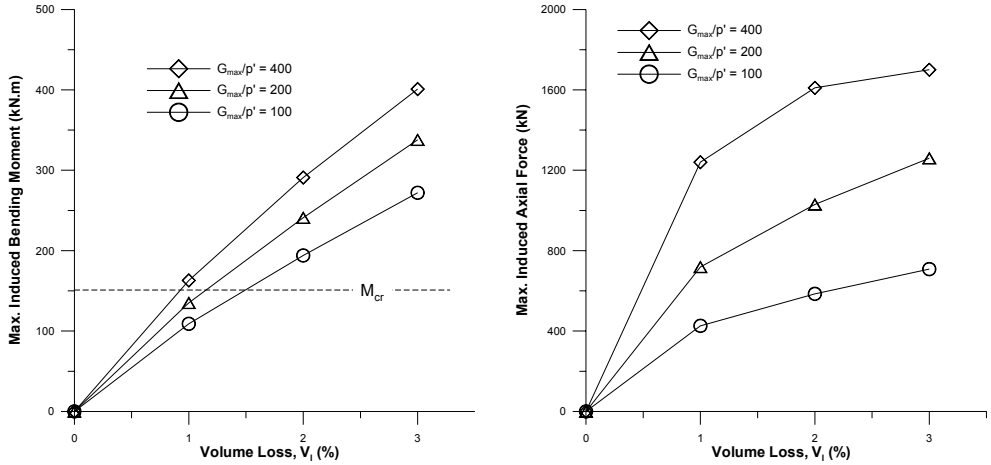

(a) **(b)**

Fig. 4.15. Variation of (a) maximum induced bending moment and (b) axial forces with tunnel volume loss for $Y_p = -1D_t$

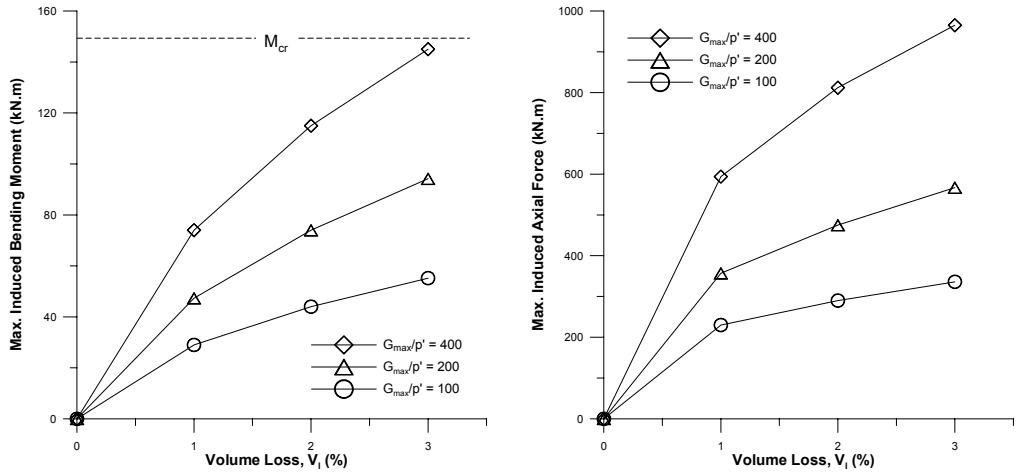

(a) **(b)**

Fig. 4.16. Variation of (a) maximum induced bending moment and (b) axial forces with tunnel volume loss for $Y_p = 0D_t$

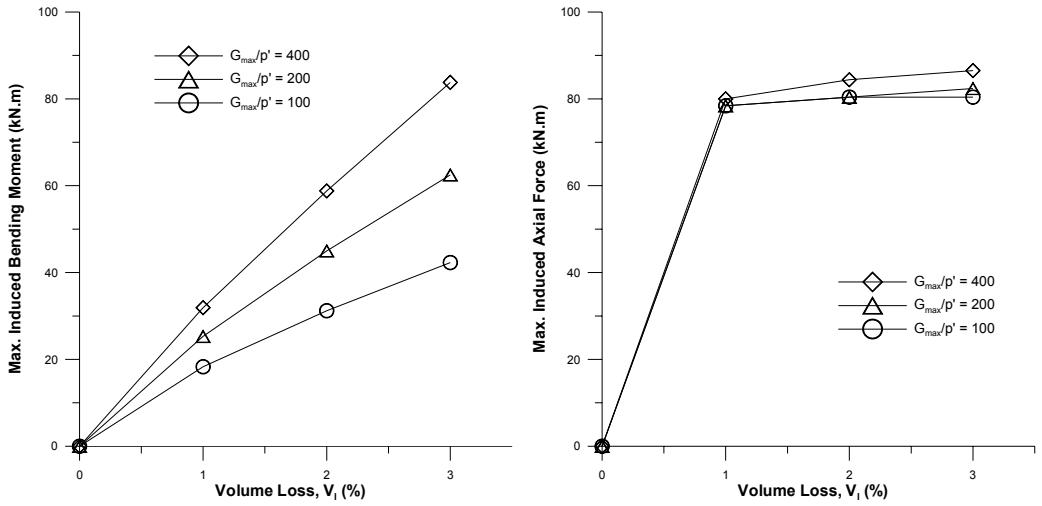

(a) **(b)**

Fig. 4.17. Variation of (a) maximum induced bending moment and (b) axial forces with tunnel volume loss for $Y_p = +1D_t$

4.5.4 Pile Performance at Different Horizontal Offset From Tunnel Centre (X)

The horizontal and vertical component of soil displacement at a horizontal offset from tunnel axis (X) of $1D_t$ and $2D_t$ is presented in Figure 4.18(a). For the case in which X is $2D_t$, pile horizontal displacement profiles (i.e. shape) along its length are dissimilar to the corresponding profile when X is $1D_t$. Horizontal displacements decrease steadily with depth (X=$2D_t$) thus producing mild changes in curvature with maximum values occurring at the soil surface. This change in displacement profile at a further distance from tunnel centre is expected to result in significantly smaller induced pile bending moment.

A similar steady decrease in soil vertical settlement with depth at an X distance of $2D_t$ is observed in Figure 4.18(b). However, magnitudes of soil settlement at all levels are less than that at an offset of $1D_t$. The smaller magnitudes of soil settlement is expected to induce less negative skin friction for the case in which pile tip is below or at tunnel axis level.

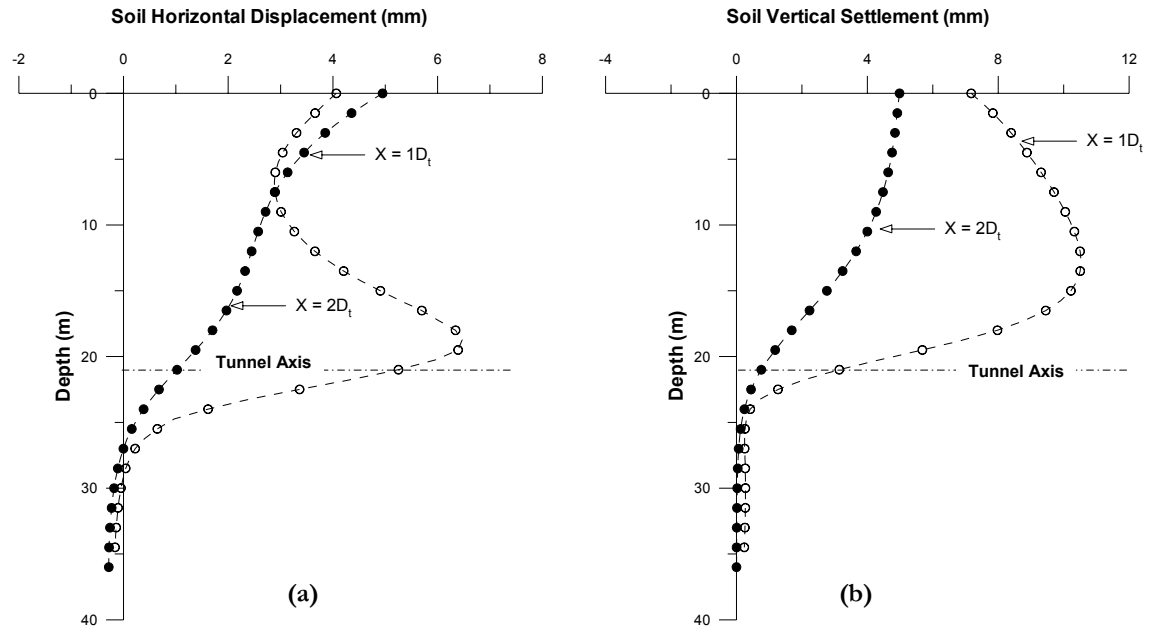

Fig. 4.18. Comparison of (a) horizontal and (b) vertical soil displacement profiles at $1D_t$ and $2D_t$ from tunnel centre.

Figure 4.19 shows the variation of maximum induced bending moment with pile horizontal distance from tunnel centre for a soil with G_{max}/p' of 400. The maximum induced bending moments generally decrease, as expected with increasing horizontal distance, X, from tunnel centre as observed in Figures 4.19(a), (b), and (c) for a pile in stiff clay. Hence, it would be reasonable and safe to assume that induced bending moments are generally negligible beyond a horizontal offset of $2D_t$ from tunnel centre as magnitudes are less than 50kN.m or 33% of cracking moment (M_{cr}) even at a tunnel volume loss of 3%. This reduction in maximum induced bending moment with X distance is different for piles located at different levels with respect to tunnel axis level. The average ratio (for all soil stiffness) of maximum induced bending moments at a X distance of $1D_t$ to $2D_t$ decreases as pile tip moves upwards from a Y_p level of $-1D_t$ to $+1D_t$. This is explained by the decreasing degree of curvature a pile is subjected to as pile tip changes from below to above tunnel axis level.

Maximum induced pile axial forces are observed to decrease with increase in X distance from the tunnel centre. This is simply explained by a shorter portion of the total pile length which undergoes full mobilization of skin friction as the pile moves away from the zone of large displacements as shown in Figure 4.21. The slight deviation in trend for the case where Y_p is -1D_t and V_l is 3% is explained by the fact that the variation of maximum induced axial force for the pile at a X distance of 1D_t with volume loss (Figure 4.15(b)) is leveling off as it is reaching a constant value.

As is mentioned earlier in Section 4.5.1, the development of axial force in a pile depends not only on relative location of pile tip to tunnel axis level, but also on whether pile tip is located within the zone of large displacements due to tunnel excavation. This is observed in Figure 4.20(c) where maximum induced pile axial force increases as the pile is further away from tunnel centre. Pile tip is located within the zone of large displacements at a X distance of 1D_t but moves outside of it when located at a X distance of 2D_t as shown in Figure 4.22.

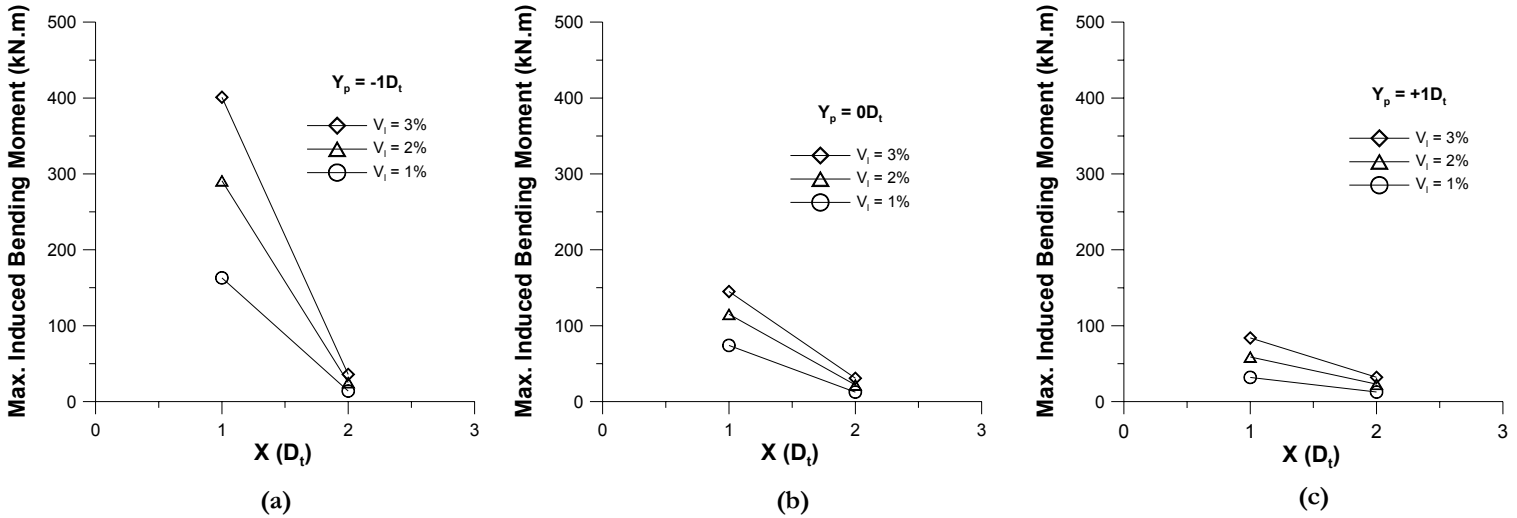

Fig. 4.19. Variation of maximum induced bending moment with horizontal distance from tunnel centre

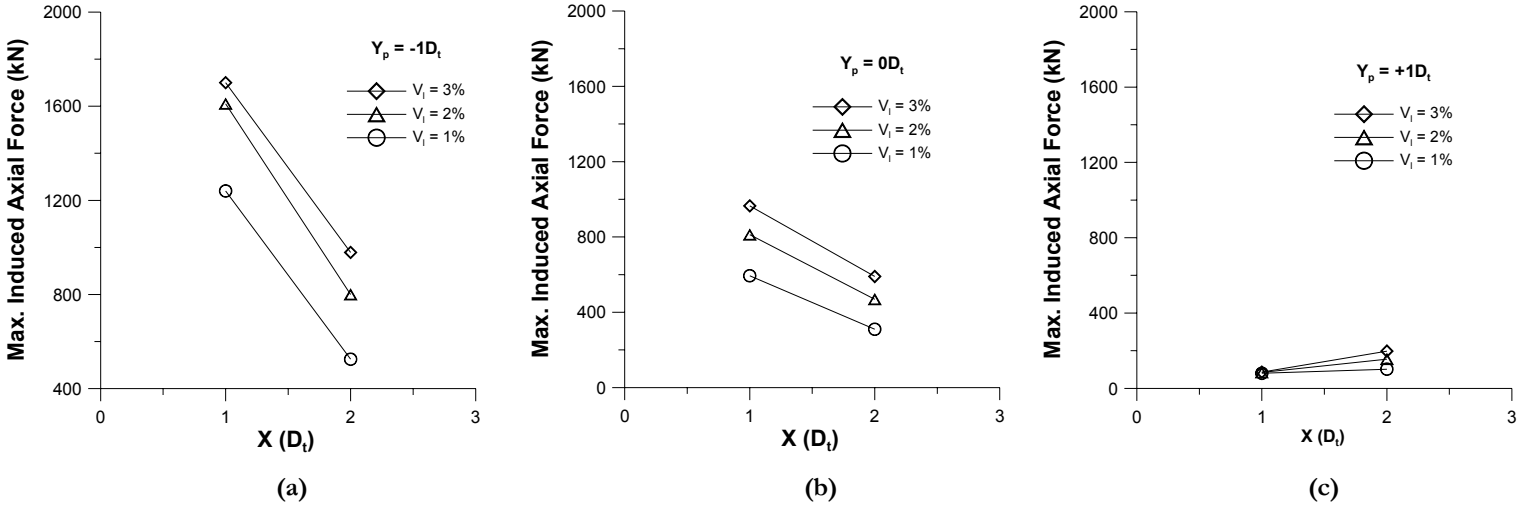

Fig. 4.20. Variation of maximum induced axial force with horizontal distance from tunnel centre

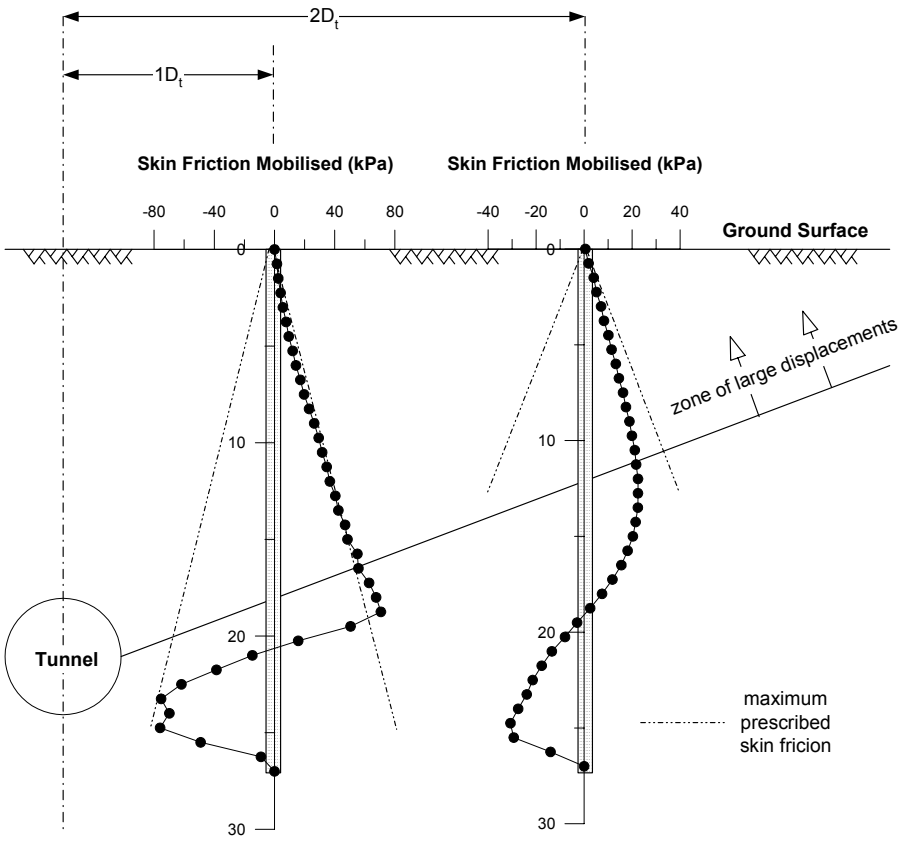

Fig. 4.21. Varying degrees of skin friction being mobilized

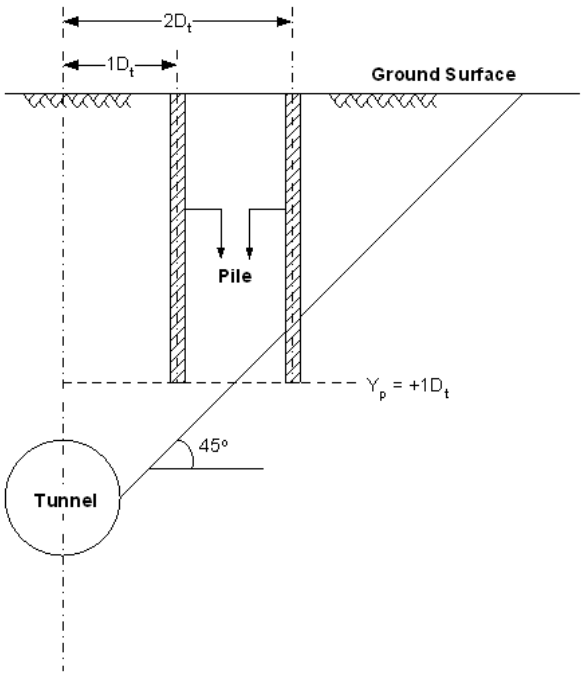

Fig. 4.22. Relative position of pile tip to zone of large displacements for pile ($Y_p = +1D_t$)

4.5.5 Pile Performance with Different Pile Head Fixity Conditions

Nine analyses were performed at an X distance of $2D_t$ while varying relative Y_p levels (-1D_t, 0D_t and +1D_t) and volume loss (1%, 2% and 3%). Results corresponding to 1% tunnel volume loss are presented in this section while others are included in Appendix A.

As shown in Figures 4.23(a), computed pile bending response is markedly different when the pile head is fixed against rotation and displacement. Maximum induced bending moment occurs at the pile head for all studied cases (Appendix A). The maximum magnitudes are observed to be approximately similar for all three cases thus demonstrating the slender behaviour of the pile in conforming to soil movements near the pile head. Cracking moments, M_{cr}, is exceeded for all three cases.

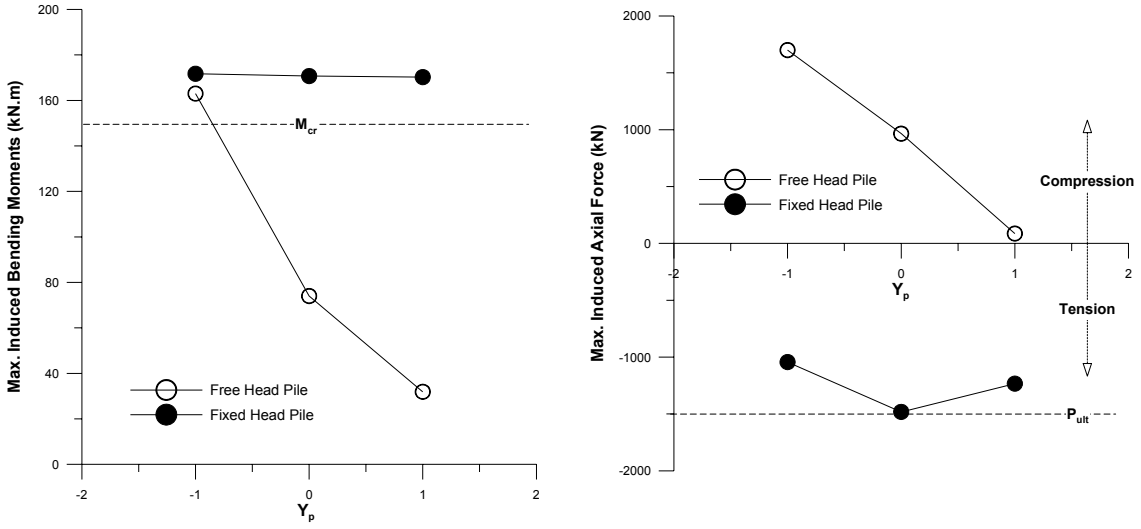

Fig. 4.23. Comparison of pile maximum (a) induced bending moment and (b) axial force for fixed and free pile head case

Significant tensile forces developed for the fixed head pile when compared to the predominantly compressive behaviour of the free head pile as shown in Figure 4.23(b). The

maximum induced forces are critically close to the ultimate tensile force able to develop in the pile based on a concrete tensile strength that is assumed to be one tenth of its compressive strength. Skin friction is fully mobilized along significant lengths of the pile for the case where Y_p is $0D_t$ and $-1D_t$ even though volume loss magnitude is small (1%).

4.6 Summary

Although the computed responses of pile behaviour subjected to tunneling induced ground movements are as expected based on reference to relevant literature and simple engineering judgment, several new interesting observations and important insight has been gained from this study. It has to be noted that the following findings of induced bending moment and axial force magnitudes are unique to the tunnel-pile configurations chosen for this study but general trends in behaviour are applicable to all cases.

1. For a given pile horizontal offset (X) of $1D_t$, largest induced bending moment is achieved at a relative Y_p location of $-1D_t$. Similar magnitudes are obtained for Y_p of $-2D_t$ and $-3D_t$.

2. For the case in which pile tip is less than or equal to a relative Y_p level of $-1D_t$, pile cracking moment is easily exceeded beyond a tunnel volume loss magnitude of 1.5% even when the pile is installed in soft soil conditions. Ultimate bending moments are exceeded at a volume loss of 5% for a pile in soft to stiff soil.

3. When the pile tip is situated within the zone of large displacements, end bearing reaction cannot fully develop as soil directly below the pile tip settles by

approximately the same amount as the pile tip. Consequently, induced pile axial forces are minimal as skin friction is not able to fully mobilize.

4. Maximum induced pile bending moments are generally negligible (less than M_{cr} even at V_l of 3%) beyond a horizontal offset of $2D_t$ from the tunnel centre. Although the reduction in compressive axial force is not as significant as is observed for bending moments, the overall magnitudes are generally not critical for all cases.

5. For the extreme case where pile head is completely fixed against rotation and displacement, maximum bending moment is induced at the pile head. This maximum value is a constant for all three relative Y_p levels studied thus demonstrating the slender behaviour of the pile. The axial behaviour of the pile changes from a compressive to a predominantly tensile response. Maximum tensile forces are similarly induced at the pile head which are critically close to the ultimate tensile force of concrete.

6. The application of the displacement control method (DCM) to simulate tunnel-soil-pile interaction is able to reproduce reasonable and realistic predictions of pile response when compared with centrifuge test results. Successful simulation of tunnel-soil-pile interaction problems are heavily dependant on correct input of soil and soil-pile interface properties.

CHAPTER 5

CASE STUDIES OF TUNNEL-SOIL-PILE INTERACTION

Two case histories were back analysed to demonstrate the ability of DCM to predict pile responses due to tunneling induced ground movement. Loganathan's centrifuge experiment (Test3) was used as the first case history while the field data from the Singapore North East Line (NEL) twin tunnel project provided the second case history.

5.1 Analysis of Loganathan et al. (2000) Test 3

5.1.1 Details of Analysis

The relative tunnel-pile geometry and summary of the centrifuge test has been described in Chapter 2. Tunnel-soil-pile interaction in Test 3 (relative Y_p of $+0.5D_t$) was simulated by adopting the same procedure in the parametric case studies. Exact container and soil height dimensions shown in Figure 5.1 were meshed to accurately model the problem. The problem was approximated to be symmetrical about the tunnel and single pile centerline.

The pile was installed in heavily overconsolidated kaolin clay (OCR at tunnel axis level ≈ 5.2) with a bulk unit weight of 16.5kN/m^3. Based on extensive experimental work on the small strain characteristics of kaolin clay by Viggiani and Atkinson (1995), an average G_{max}/p' ratio of 550 obtained at tunnel axis level (calculations shown in Appendix A) was assigned to the clay elements. This ratio was observed to decrease when higher confining stresses were applied in the lab tests. An n value of -0.6 was adopted to represent the degradation of stiffness with deviatoric strain.

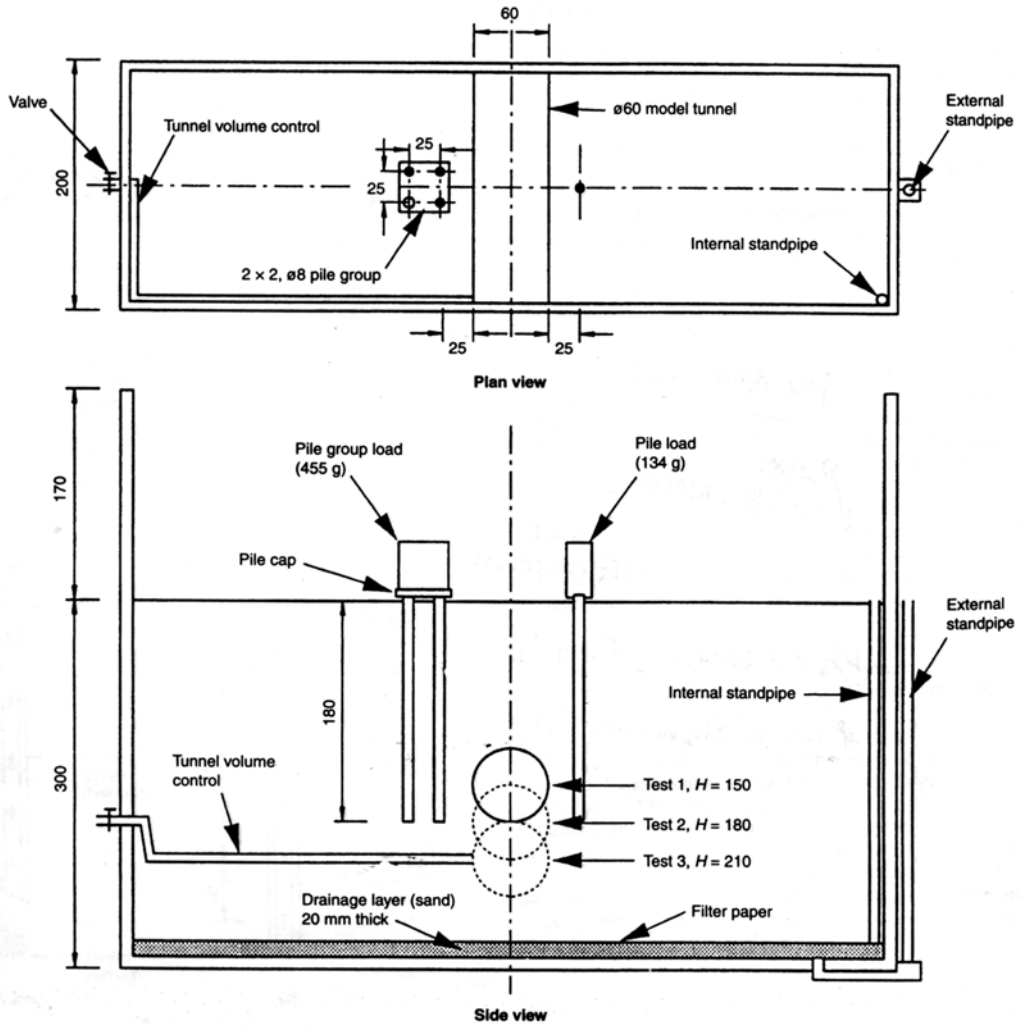

Fig. 5.1. Configuration of centrifuge model set up.

As the pile was coated with epoxy resin to waterproof the strain gauges, its effective diameter (D_p) is chosen to be 0.9m in the simulation although the brass pile had an outer diameter of 0.8m in prototype scale. Since the finishing details of the epoxy coating are not detailed, the soil-pile interface is chosen to slip at a friction angle ($\mu = 0.4$) close to that of the soil (ϕ'=23° (Stewart, 1992)) thus simulating a rough finishing surface. Pile elements were assigned a bending stiffness, E_pI, of 662 MNm^2 based on a brass Young's modulus of 100GPa and pile inner and outer radius of 0.362m and 0.4m at prototype scale. Table 5.1 summarises the physical and mechanical properties of the soil, pile and soil-pile interface.

Table 5.1. Summary of properties assigned to soil, pile and soil-pile interface

Material	Bulk Density (kN/m^3)	E (GPa)	G_{max}/p'	n	μ	γ_{lim} (mm)
Soil	16.5	-	550	-0.6	-	-
Pile	24.0	20.5	-	-	-	-
Soil-Pile Interface	-	-	-	-	0.4	4

5.1.2 Results and Discussion

Pile and soil displacements are compared in Figure 5.2(a) and (b). The pile is observed to approximately assume the shape of the far field horizontal soil displacement with smaller movements near the ground surface (Figure 5.2(a)). In Figure 5.2(b), soil is observed to settle with a lower magnitude than the pile for the top 8m of soil. Below this level, pile settles more than the soil.

Figure 5.3(a) shows the comparison of computed induced bending moment to experimental data. The pile bends in predominantly single curvature similar to that observed from the centrifuge test. However, the pile depth at which maximum magnitudes are observed is shallower in the numerical simulation compared to test data. Nevertheless, maximum magnitudes as shown in Figure 5.4 are reasonably well predicted.

The variation of induced pile axial force along its length (Fig. 5.3(b)) deviates from test results for regions closer to the ground surface, achieving similar magnitudes at the pile tip. As the pile tip is located within the zone of large displacements (Figure 2.11), the region of the pile close to the ground surface should settle by a larger magnitude than the corresponding soil around the pile. This would imply that low compressive forces or even tensile forces should develop as compared to the pile behaviour observed in the centrifuge test. This is verified by the pile and soil (far field) settlement profile as shown in Figure

5.2(b) where soil settles less than the pile near the ground surface. Despite this deviation in trend, maximum magnitudes are well predicted as is shown in Figure 5.4.

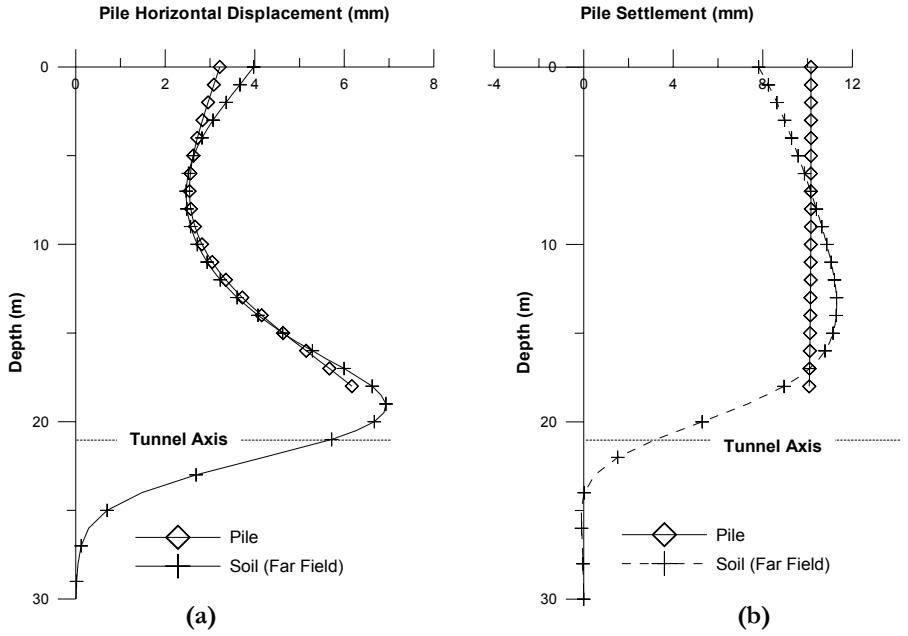

Fig. 5.2. Computed pile and soil (far field) (a) horizontal and (b) vertical displacements

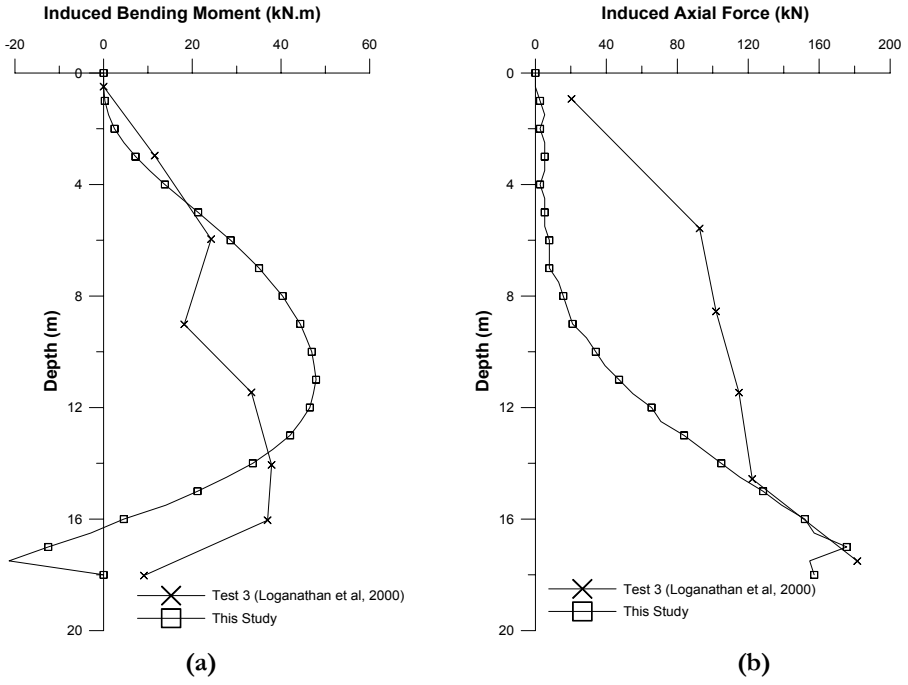

Fig. 5.3. Variation of induced pile (a) bending moment and (b) axial force for Test 3

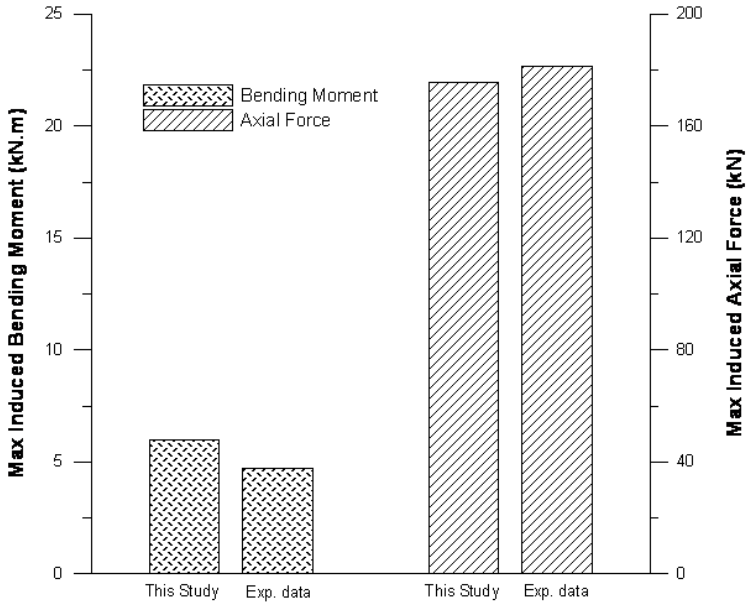

Fig. 5.4. Comparison of maximum induced bending moment and axial force for pile in Test 3 (Loganathan et al.,2000)

5.2 Analysis of North East Line (NEL) Mass Rapid Transit (MRT) Project

5.2.1 Background

The NEL tunnels were constructed to extend the existing rail system in Singapore by an additional 20km to meet increasing public transportation demands. The twin lines run completely underground with 16 stations, linking the World Trade Centre to Punggol. Eleven contracts (Contract 701-711) were awarded for the construction of the project.

Contract 704 encompassed the construction of the tunnels from Serangoon to Woodleigh and a 1.9km long, 2 way 3 lane vehicle viaduct supported by piled foundations. The North Bound (NB) and South Bound (SB) tunnels run on opposite sides of the viaduct thus having similar alignment. The tunnels were excavated after the construction of the viaduct using

Earth Pressure Balance (EPB) tunnel boring machines, producing an excavated diameter of approximately 6.4m. Figure 5.5 shows the relative layout of the viaduct pier, pile and tunnel lines.

The piles supporting the viaduct are generally 1.2m in diameter with concrete strength of 30 to 40MPa. A series of 2x2 and 3x2 pile groups were designed to support the viaduct depending on soil conditions encountered along the viaduct passage. Soil types encountered by the EPB machines were predominantly residual soils of granitic (Bukit Timah Granite) origin. These soils are classified locally as G4 and G3 materials based on characterization works by Dames and Moore (1983). G4 and G3 soils have weathering grades of V-VI and III-IV respectively.

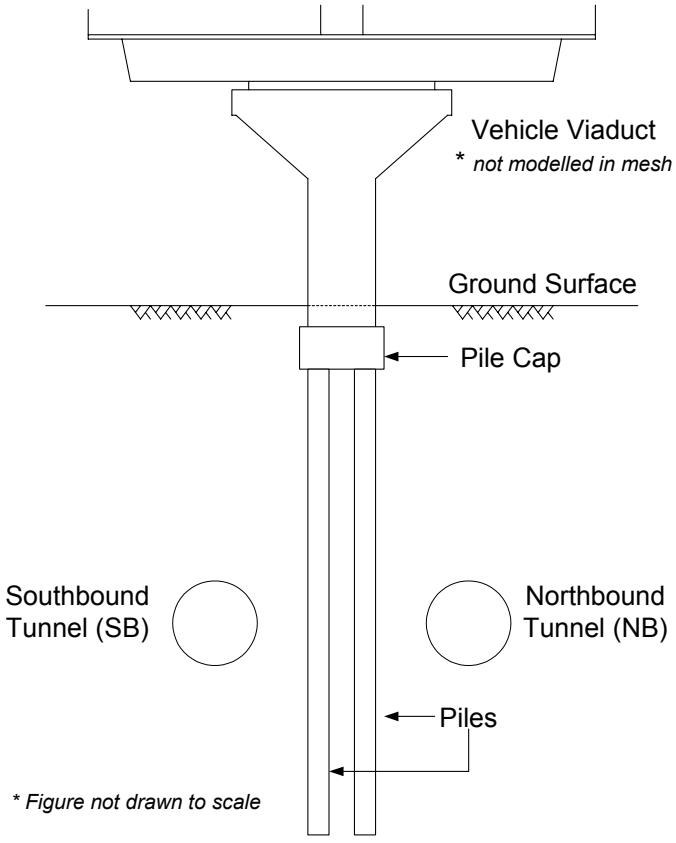

Fig. 5.5. Viaduct pier, pile and tunnel layout

5.2.2 Details of Analysis

5.2.2.1. Mesh Dimensions

A 2x2 piled foundation supporting Pier 14 and the vehicle viaduct was backanalysed as field data was available for comparison. The piles were spaced at centre to centre distances of approximately 3.6m connected by a square pile cap of 6m length as shown in Figure 5.6. The geometry of the pile cap was assumed by the author as no details were available for reference. The generated mesh assumes symmetry about the transverse section of the pile group (resulting in a half mesh) as soil displacements along the longitudinal axis of the twin tunnels are prescribed with constant and uniform displacements (i.e. uniform soil convergence similar to Chapter 4). The influence of the pier and viaduct are neglected in this study as focus is placed on studying induced stresses within the pile due to the component of tunnel excavation. The mesh dimensions are as shown in Figure 5.7.

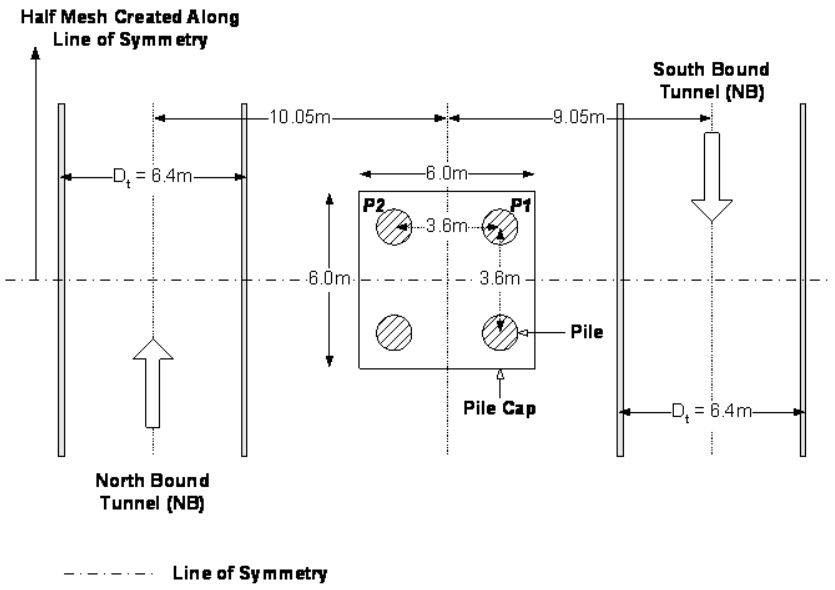

Fig. 5.6. Plan view of relative pile-tunnel location drawn to scale

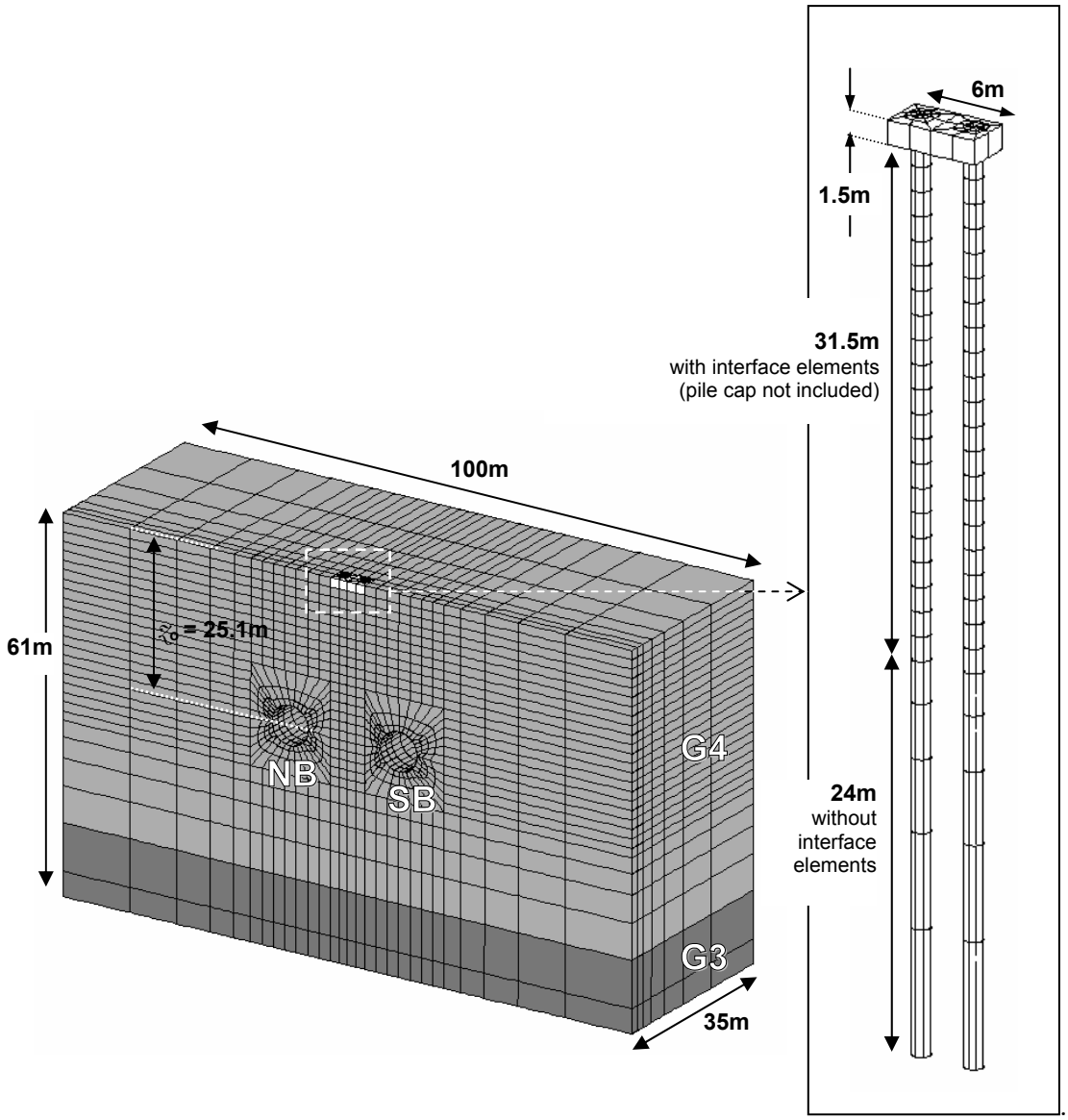

Fig. 5.7. Mesh and pile geometry with soil strata

In this study, the piles directly alongside (nearest) to the SB and NB tunnels are referred to as pile P1 and P2 (Figure 5.6) respectively as the SB tunnel is excavated past Pier 14 before the NB tunnel. Pile P1 is located at a horizontal offset of 7.25m (X_{SB}=1.13D_t) from the centre of the SB tunnel while pile P2 is at a horizontal offset of 8.25m (X_{NB}=1.29D_t) from the centre of the NB tunnel. An average pile length of 57m was assumed for all piles as constructed lengths ranged from 54.6m to 58.8m. As soil movements below tunnel invert

level (28.3m below ground level (BGL)) are not expected to be significant, zero thickness interface elements were only provided along the pile shaft down to a depth of 33m BGL to model soil-pile interface behaviour. The NB and SB tunnels are located at a depth (z_o) of 25.1m thus giving a C/D_t of approximately 3.4.

5.2.2.2. Material Properties

The twin tunnels at Pier 14 are bored through 49m thick of G4 soil (SPT N<100) which is underlain by G3 soil (SPT N> 100). Residual soils of G4 classification in Singapore typically exhibit highly variable properties as the soil can be generally described as silty clay or clayey silt with varying percentages of fines (≈ 0%-80%) as reported by Dames and Moore (1983). In this analysis, G4 and G3 material is assigned with a bulk density of 20kN/m^3 and 22kN/m^3 respectively. Both soils are prescribed with a K_o of 1.0 as recommended by the investigative report. Concrete is assigned a typical density of 24kN/m^3.

As research efforts and references on the nonlinear stiffness characteristics (within the small strain region) for local granitic residual soils are few, published data on similar Hong Kong residual soils with equivalent weathering grades (Ng et al., 2000) are used to obtain the necessary soil parameters for analysis. Figure 5.8 shows data from laboratory test results of normalized shear stiffness variation with deviatoric strain for completely decomposed granite (Grade V) and the corresponding curve used to fit the data. An *n* value of -0.5 was adopted to represent the stiffness degradation pattern beginning from a $\varepsilon_{q(min)}$ of 0.0015% to a $\varepsilon_{q(max)}$ of 1%. Due to the high variability of G4 soil stiffness, computed results are presented for a G_{max}/p' of 1400 (upper bound), 800 (mid range) and 400 (lower bound) based on reference to lab test data as shown in Figure 5.9 by Ng et al. (2000). G3 soil and concrete are

prescribed with a linear elastic stiffness of 5.5GPa (Ng and Wang, 2001) and 30GPa respectively.

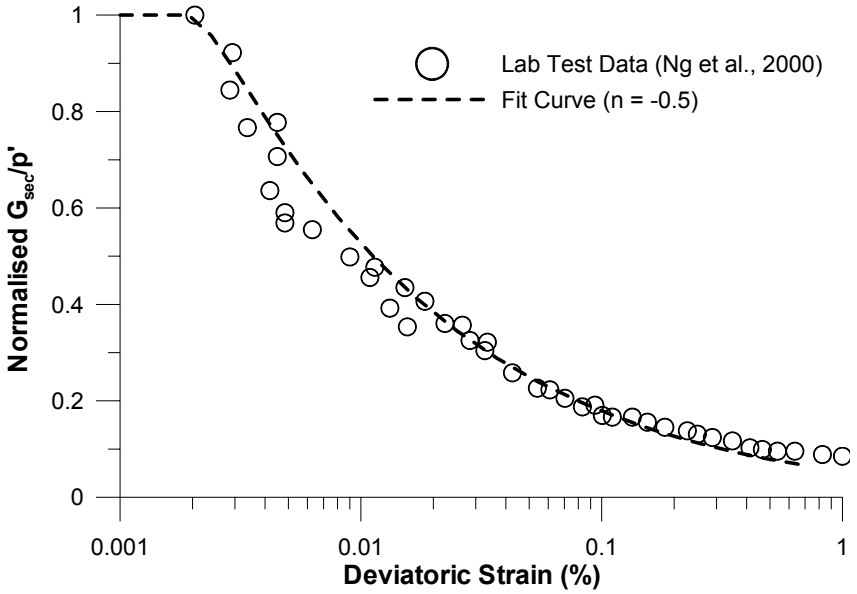

Fig. 5.8. Variation of normalised stiffness with deviatoric strain for Hong Kong Completely Decomposed Granite (Grade V)

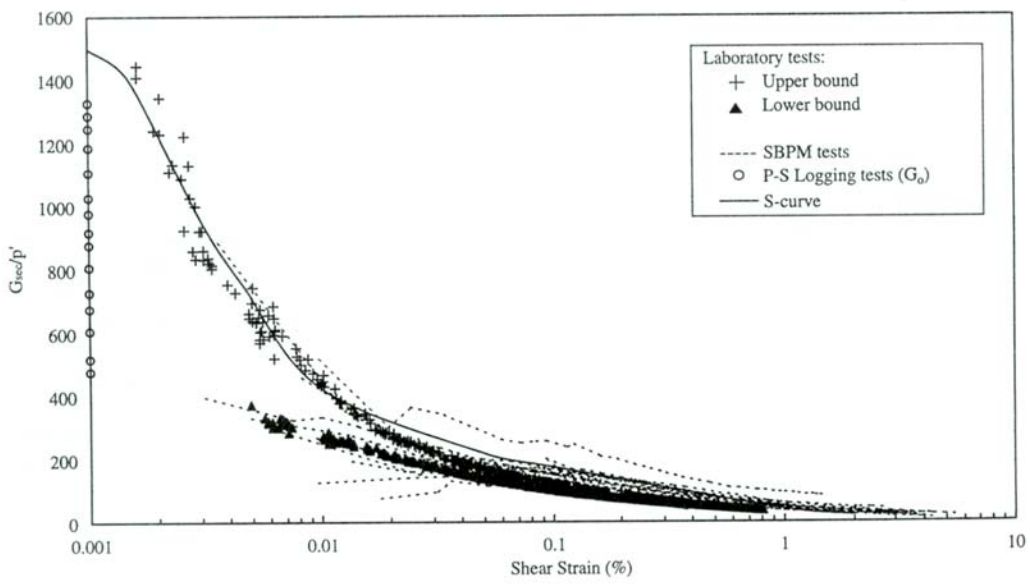

Fig. 5.9. Nonlinear stiffness variation of weathered Hong Kong granitic soil (Ng et al., 2000)

A friction angle of 35° (μ=0.7) was assigned to the interface elements to model soil-pile interface behaviour. This value was chosen based on a summary of research efforts (Leong et al., 2003) to characterize the properties of Bukit Timah granite soils which reveal a wide range of effective friction angles from 20° to 40°. No reduction in μ value was performed as soil around the pile is assumed to have consolidated back to its original stress state and strength before the tunnels are excavated along side it. Table 5.2 summarises the physical and mechanical properties of the soil, pile and soil-pile interface.

Table 5.2. Summary of properties assigned to soil, pile and soil-pile interface for NEL analysis

Material	Bulk Density (kN/m3)	E (GPa)	G_{max}/p'	n	μ	γ_{lim} (mm)
G4	20	-	1400 (upper) 800 (mid) 400 (lower)	-0.5	-	-
G3	22	5	-	-	-	-
Pile	24	30	-	-	-	-
Soil-Pile Interface	-	-	-	-	0.7	4

5.2.2.3. Volume loss and convergence point

Table 5.3 shows the input parameters required for the application of DCM to the NEL analysis. Maximum surface settlements are obtained from field readings while i values are assumed to be half of the depth to tunnel axis level (i.e. i=0.5z_o).

Table 5.3. Input volume loss and β magnitudes for analysis

Tunnel	S_{max} (mm)	i (m)	V_l(%)	C/D_t	β
SB	16	12.55	1.565	3.42	0.58*
NB	18	12.55	1.760	3.42	0.58*

* obtained from Figure 3.26

5.2.3 Results and Discussion

Induced pile bending moments and axial forces are first presented along with field data to justify the choice of G4 soil stiffness (G_{max}/p' of 400, 800 and 1400) used for the presentation of subsequent computed results (pile and soil displacements). Field data presented for bending moments and axial forces (Coutts and Wang, 2000) are maximum values converted from strain gauge readings, therefore the tunnel excavation stage at which these magnitudes are recorded are unknown.

5.2.3.1. Induced Pile Stresses (BM and P)

Figures 5.10 and 5.11 show the computed bending moments for piles P1 (alongside SB tunnel) and P2 (alongside NB tunnel) respectively due to the excavation of the SB tunnel followed by the NB tunnel. Similar to findings from parametric studies in Chapter 4, induced pile bending moment is greater for a given volume loss when higher soil stiffness is assigned to the G4 material. For a given soil stiffness, it is observed for pile P1 that maximum bending moment occurs after the SB tunnel excavation (Figure 5.10(a)) while maximum bending moment is induced for pile P2 after the NB tunnel excavation (Figure 5.11(b)). This behaviour appears reasonable and is explained further on in this study. Maximum computed bending moment is generated at a level slightly above tunnel axis level as compared to field data which indicate maximum values occurring at the invert level. Analysis performed using a G_{max}/p' value of 800 (mid range) appears to provide the closest prediction of induced bending moment magnitudes to field results.

Figures 5.12 and 5.13 show the computed axial forces for piles P1 and P2 respectively due to the excavation of the SB tunnel followed by the NB tunnel. Maximum computed pile axial forces for the analyses employing G_{max}/p' values of 400 and 1400 generally provide a reasonable upper and lower bound to which field results fall well within as shown in Figures 5.12(b) and 5.13(b). Largest pile axial forces are observed after the excavation of the NB tunnel. This behaviour is reasonable as the excavation of both tunnels generally result in soil settlement thus contributing to the development of skin friction along the shaft of the pile. Maximum computed pile axial forces are generally induced at tunnel axis level as compared to the field where corresponding values occur at the invert level. Similar to bending moments, computed results using a G4 soil G_{max}/p' value of 800 provided the best fit to field data.

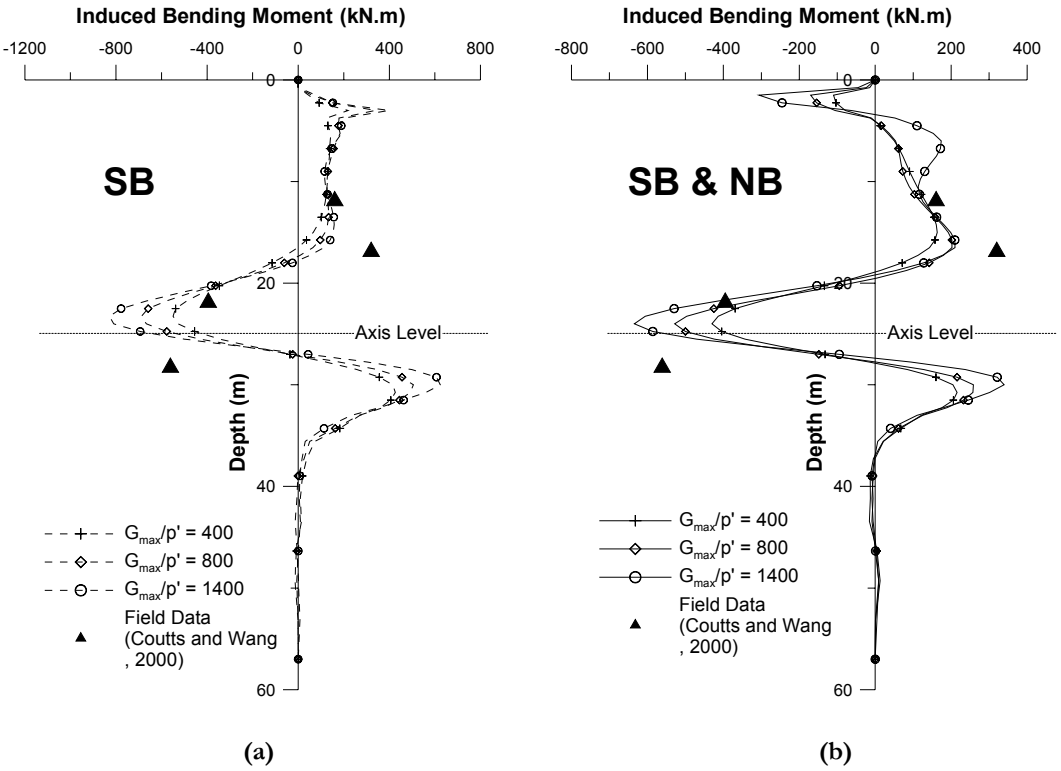

Fig. 5.10. Induced bending moment along pile P1 for different soil stiffness due to (a) SB and (b) subsequent NB tunnel excavation

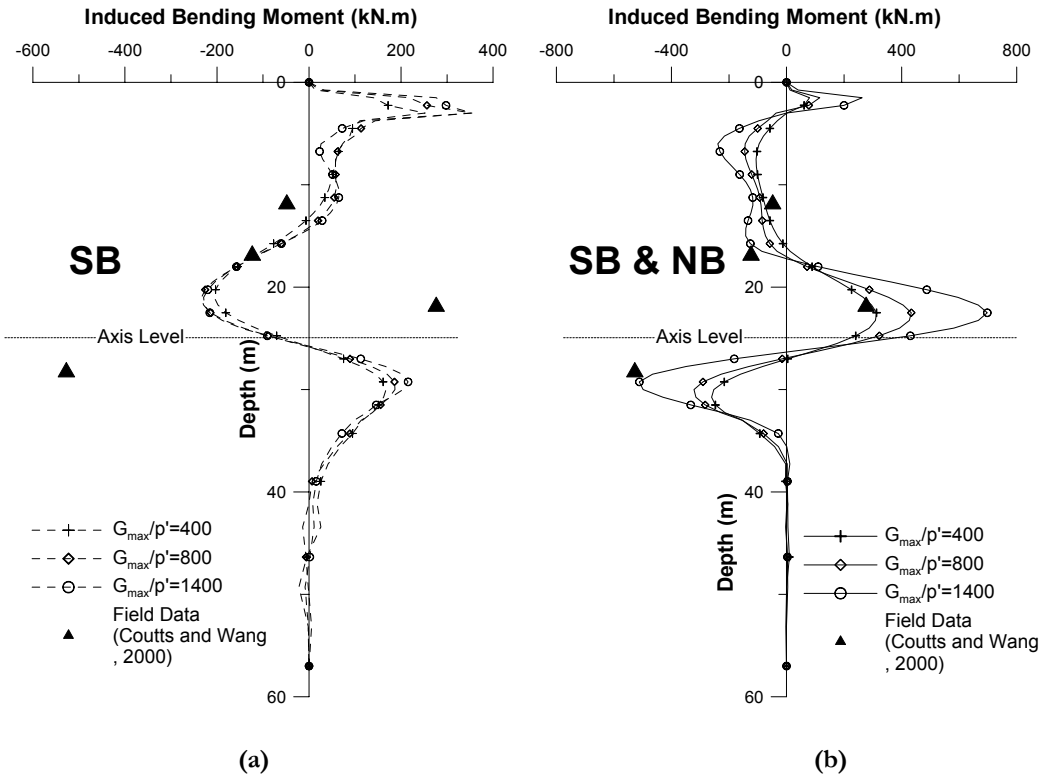

Fig. 5.11. Induced bending moment along pile P2 for different soil stiffness due to (a) SB and (b) subsequent NB tunnel excavation

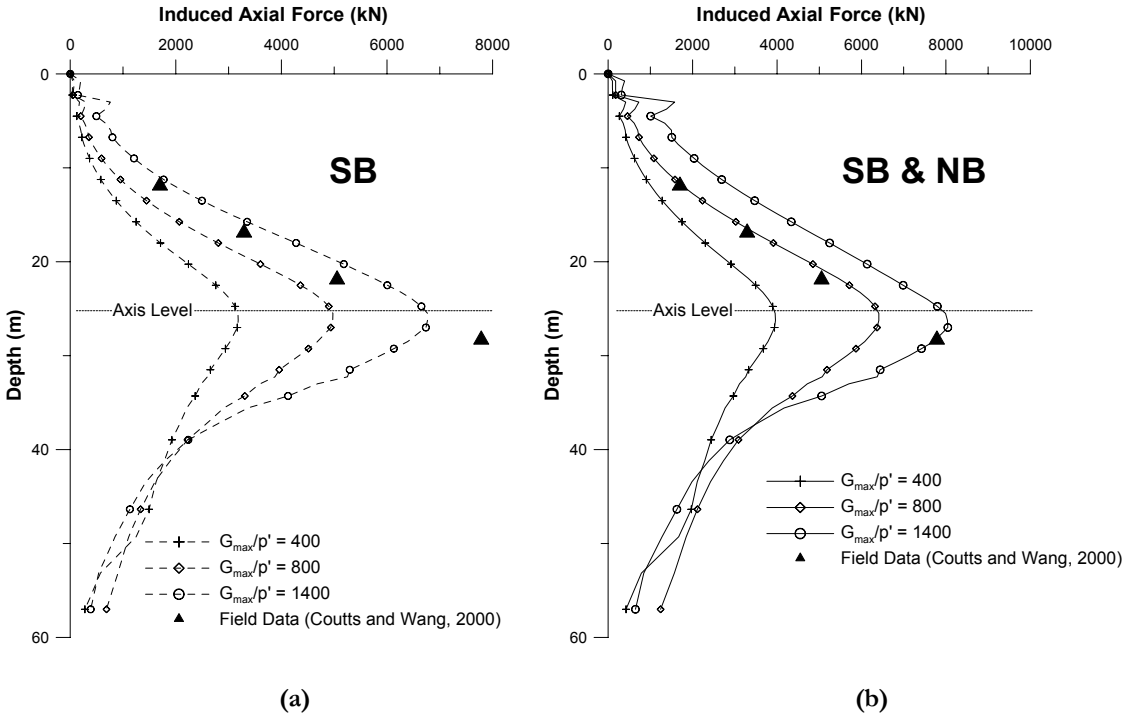

Fig. 5.12. Induced axial force along pile P1 for different soil stiffness due to (a) SB and (b) subsequent NB tunnel excavation

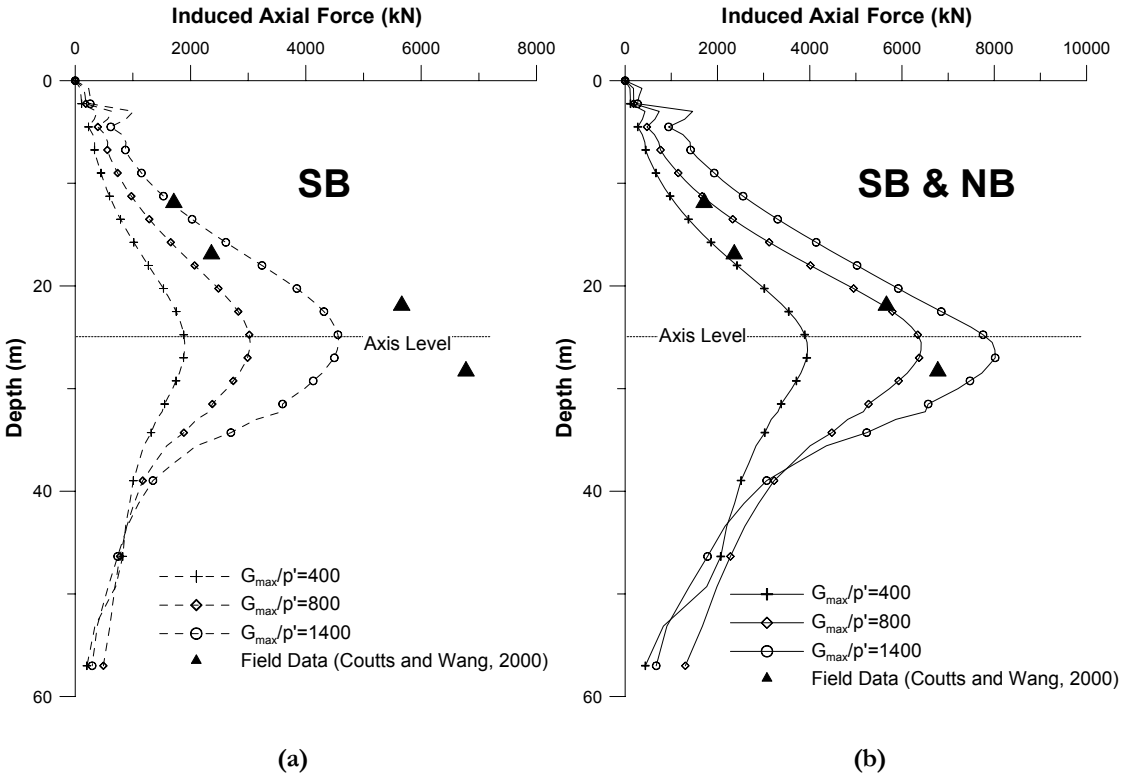

Fig. 5.13. Induced axial force along pile P2 for different soil stiffness due to (a) SB and (b) subsequent NB tunnel excavation

5.2.3.2. Induced Pile and Soil Displacements

Computed pile and soil displacement results are presented for the case where G4 soil is prescribed with a G_{max}/p' value of 800. This value was chosen as induced pile bending moments and axial forces provided the best fit to field data based on results from the previous section. Contour plots of soil and pile displacements are presented in Appendix A.

Figure 5.14 shows the development of surface settlement trough with the excavation of the SB tunnel followed by the NB tunnel. The SB and NB tunnel convergence resulted in a S_{max} of approximately 14mm and 17mm respectively as compared to corresponding field results of 16mm and 18mm. The lower computed values can be explained by the development of

far field settlements of about 2.5mm at both ends of the transverse mesh boundary. Nevertheless, settlement trough magnitudes and profiles are predicted to a reasonable degree of accuracy. A resultant S_{max} of 24mm is obtained from the simulated excavation of both tunnels.

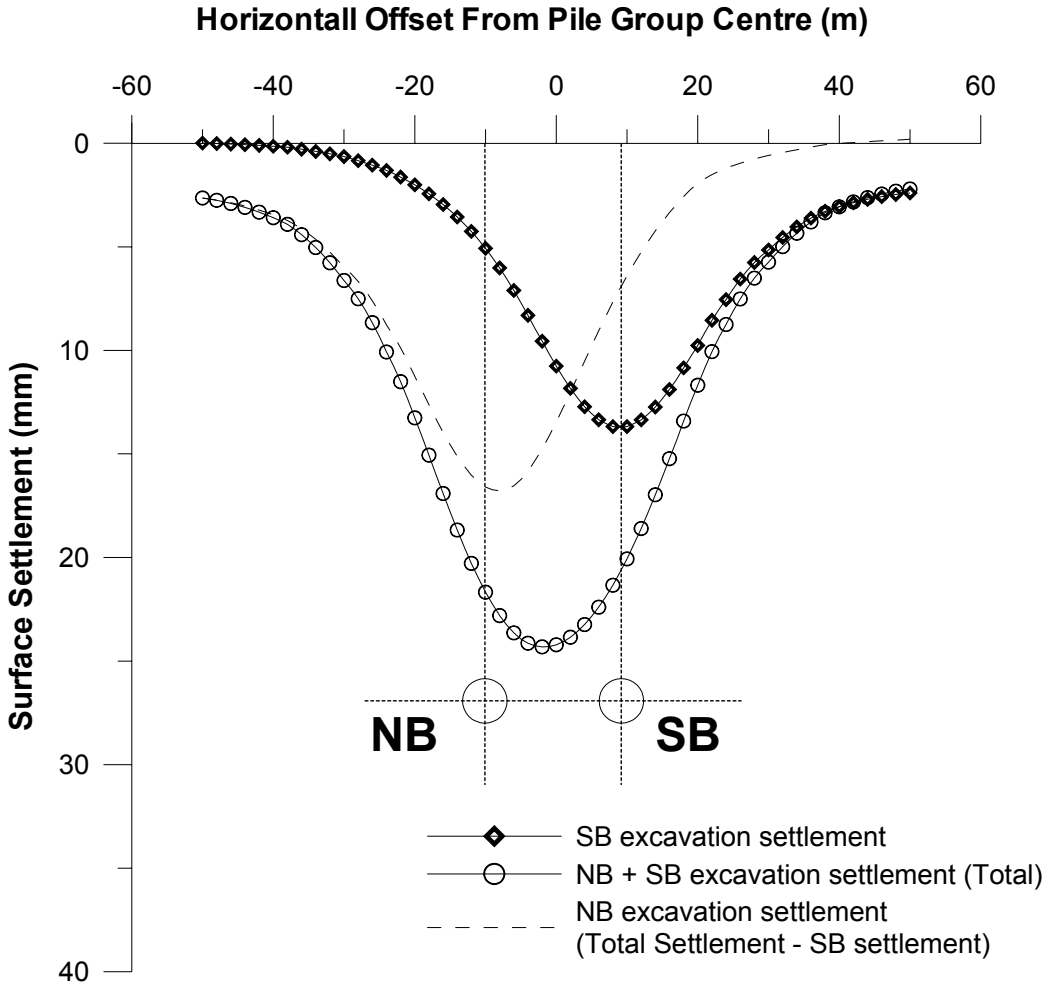

Fig. 5.14. Development of surface settlement trough with SB and NB tunnel excavation

Pile horizontal displacements with respect to pile group centre after SB and NB tunnel excavation is presented in Figure 5.15. In the subsequent plots, positive pile displacement

would indicate movement towards the SB tunnel. Results from the analysis are discussed according the sequence of tunnel being excavated.

SB tunnel excavation

The pile heads (P1 and P2) are observed to displace horizontally towards the SB tunnel with similar magnitudes as they are connected by a rigid pile cap. Pile P1 (X_{SB}=1.13D_t) experiences significantly larger horizontal displacement and curvature around the tunnel level than pile P2 (X_{SB}=1.69D_t) due to their respective horizontal distances from the SB tunnel. This observation agrees well with higher maximum induced bending moment obtained for pile P1 (687kN.m) compared to pile P2 (354kN.m) as shown previously in Figure 5.10(a) and 5.11(a). Both piles which are embedded in 8m of stiff G3 material experiences kickback of slightly less than 1mm.

NB after SB tunnel excavation

The pile heads (P1 and P2) translated approximately 6mm towards the NB tunnel as soil horizontal displacements changed direction. As horizontal soil movements are reversed in the opposite direction (towards the NB tunnel), pile P2 (X_{NB}=1.29D_t) experiences greater displacements and change in shape than pile P1 (X_{NB}=1.85D_t) around the tunnel level. Maximum horizontal displacement slightly above tunnel axis level for pile P1 is reduced by approximately 4mm when the NB tunnel is excavated. This observation explains the occurrence of largest induced bending moments during the SB tunnel excavation for pile P1 as mentioned earlier in the previous section. Pile lengths below tunnel axis level return to an nearly vertical position similar to its original state.

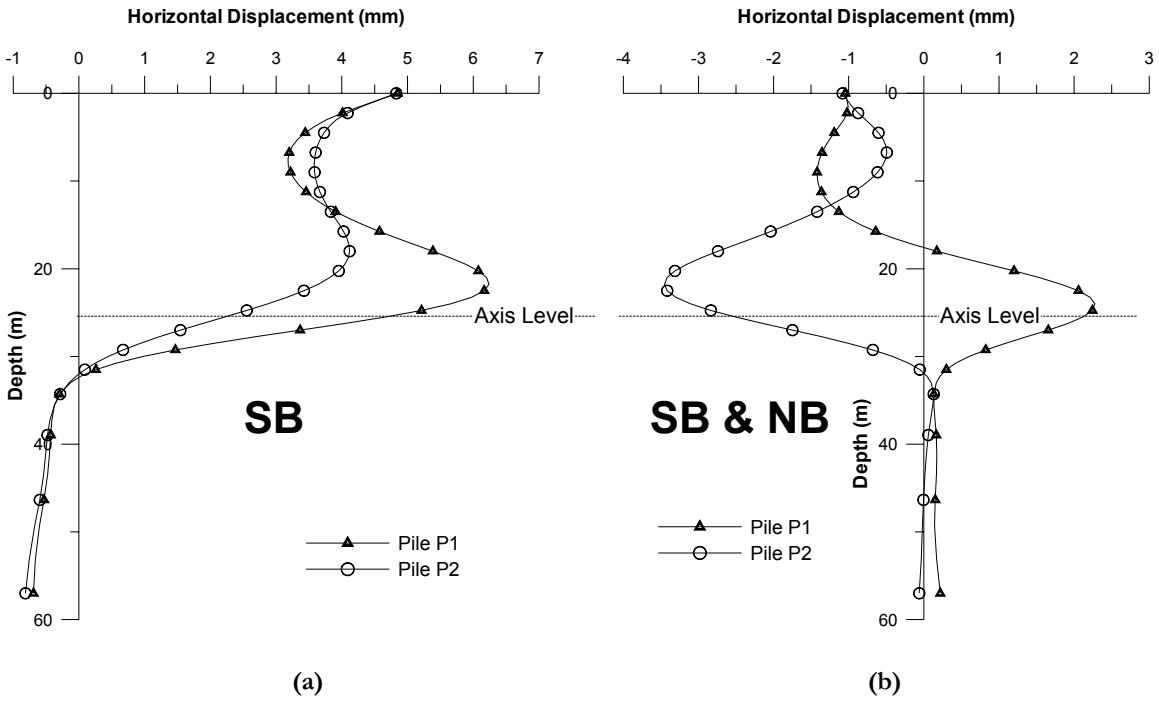

Fig. 5.15. Pile horizontal displacement after (a) SB and (b) NB tunnel excavation

A comparison of pile and far field soil horizontal displacements are as shown in Figure 5.16 for piles P1 and P2. Far field soil displacements are obtained at the opposite end of the half mesh from the face of transverse symmetry to minimize the influence of the pile group on soil movements. When the SB tunnel is excavated, far field soil is observed to deform with magnitudes greater than the corresponding piles. This behaviour is similar to findings in the previous chapter and can be attributed to the influence of the pile group which produces a stiff foundation system in the ground to resist the soil movements. However, when the NB tunnel is excavated, resulting in a reversal of soil displacement vectors, piles P1 and P2 are observed to experience greater movements than the far field soil at certain sections along its length. An explanation for such behaviour is as discussed below.

1. The greater pile displacement at the top 18m of pile P2 compared to the far field soil could be explained by the influence of the pile group to produce

similar pile head displacements for piles P1 and P2. Far field soil horizontal movements at the ground surface corresponding to location of pile P1 have a predominant effect on the behaviour/displacement of the pile cap as magnitudes are greater than that of far field soil displacements at pile P2. Thus, the upper 18m of pile P2 is "pulled" along as pile P1 displaces towards the NB tunnel.

2. Figure 5.16(a) shows that the net horizontal displacements of pile P1 and the corresponding far field soil due to the component of NB induced ground movements to be approximately similar. This behaviour is different compared to pile P2 where net soil displacement is greater than the pile at tunnel level and can be explained by their relative distances from the NB tunnel. At an X_{NB} distance of $1.85D_t$, far field soil horizontal displacements are expected to decrease steadily with depth thus resulting in changes of curvature with depth similar to results presented in Figure 4.18. Thus soil and pile appears to rebound back to its original state of zero curvature (i.e. free from bending induced stresses)

Pile settlements along with their corresponding far field soil vertical displacements are presented in Figure 5.17. Results are intuitively correct as pile P1 and P2 experiences largest settlement and axial compression after the excavation of the both the SB and NB tunnel. Far field soil settlements are significantly greater than that of the piles at both stages of tunnel excavation thus resulting in large downdrag forces (6414kN as shown in Figure 5.12(b))) along lengths above tunnel invert level.

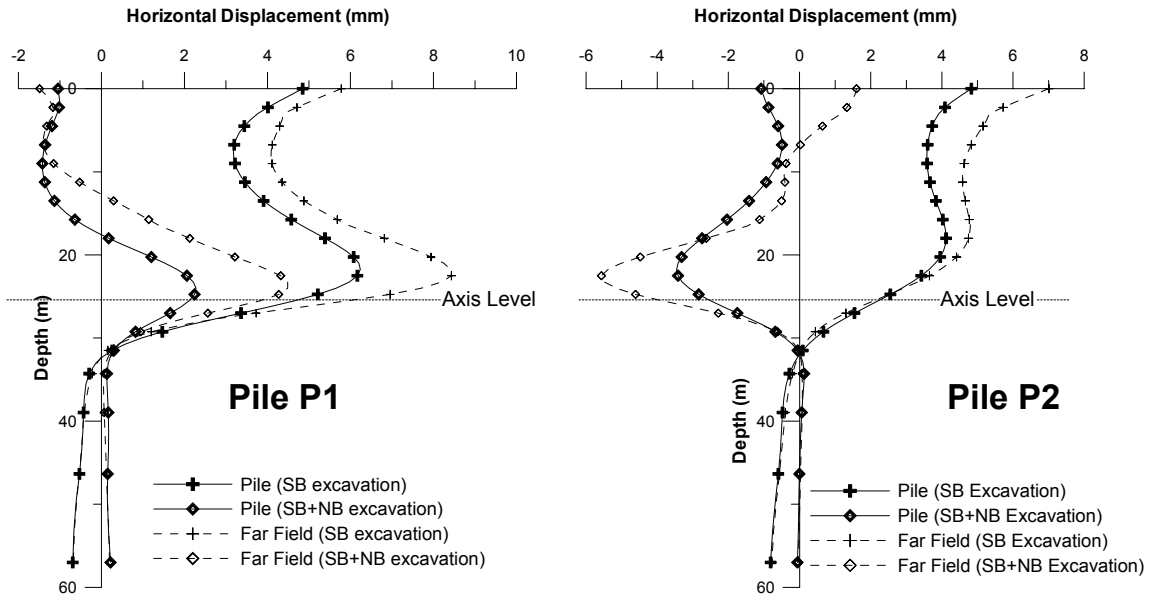

(a) **(b)**

Fig. 5.16. Comparison of horizontal displacement for pile (a) P1 and (b) P2 with corresponding far field soil displacements

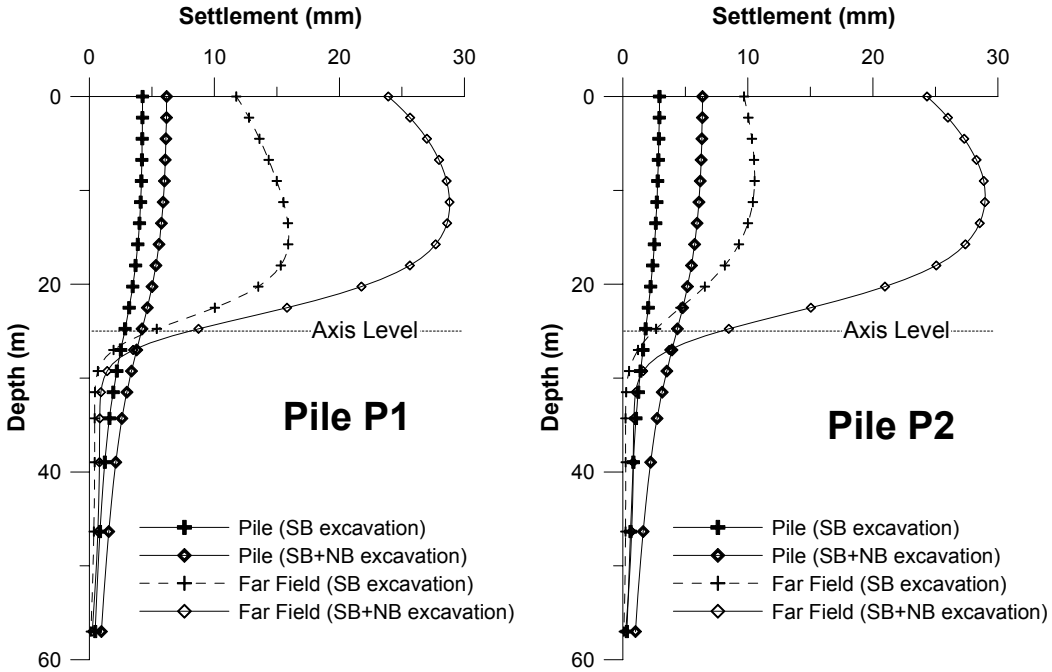

(a) **(b)**

Fig. 5.17. Comparison of settlement for pile (a) P1 and (b) P2 with corresponding far field settlement

Figure 5.18 shows the progressive deformation of the pile group (magnified by 1000 times) with tunnel excavation sequence. The piles are being compressed axially due to the development of negative skin friction from the settlement of the surrounding soil. The pile cap is also observed to rotate producing a small inclination of approximately 1:19000 to the horizontal when the SB tunnel is excavated.

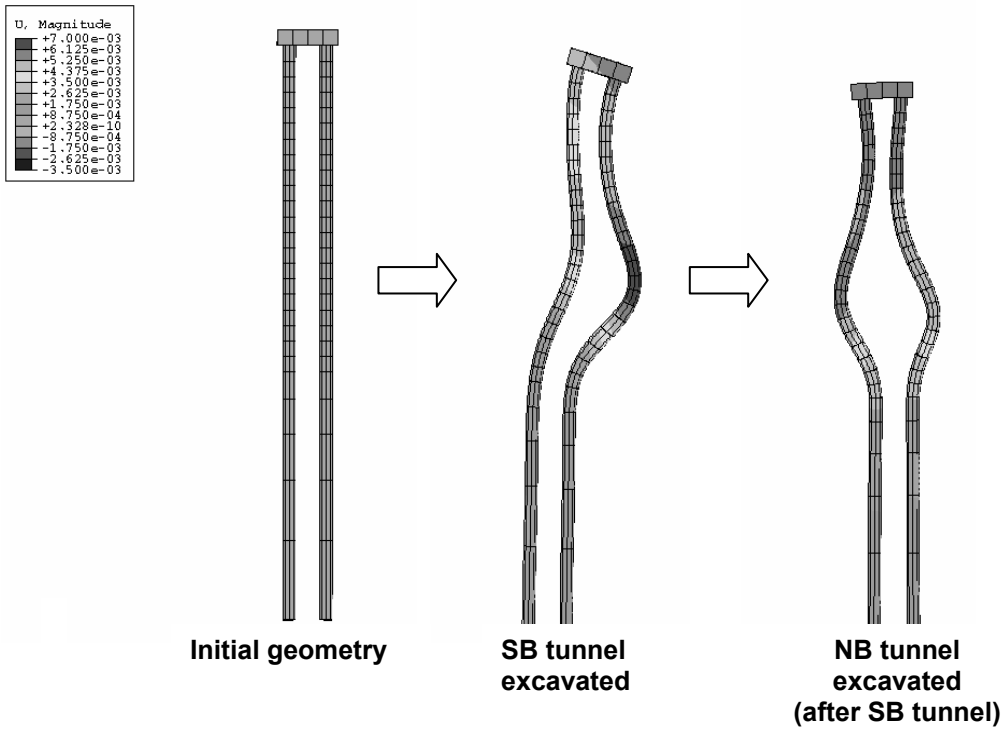

Fig. 5.18. Contour plot of displacements for deformed pile group mesh (x1000)

5.3 Summary

The backanalysis of Loganathan's centrifuge experiment (Test3) and the twin tunnel NEL project in Singapore yielded results that are in close agreement to recorded data. Magnitudes and trends of induced pile bending moment and axial force are reasonably well predicted thus demonstrating the high potential of the developed DCM to analyse tunnel-soil-structure interaction problems. Although field displacement data from the NEL project were not

available to the author for comparison at the time of thesis completion, the predicted behaviour of the pile group with tunnel excavation sequence appears to be realistic.

It has to be noted that although computed results for the NEL tunnel project are being predicted to a reasonable degree of accuracy (magnitude and trend) it does not serve as proof to the correctness of the soil and interface material properties due to (i) the absence of detailed soil investigation reports at Pier14 and (ii) the highly variable mechanical properties of weathered granite material in Singapore. In short, similar results could be obtained using a different combination of material parameters.

CHAPTER 6

CONCLUSIONS

6.1 Work reported in the thesis

6.1.1 Displacement Controlled Method

A novel kinematic approach to simulate uniform soil displacements along the tunnel boundary in the longitudinal direction has been developed in this study. This alternative approach aims to provide improved displacement predictions of soil around a deforming tunnel compared to the more popular stress based[2] methods which typically yield wider settlement troughs and high far field settlement when compared to field or test data.

The kinematic method is conceived based on observation of displacement vector plots from centrifuge tests. Two important characteristics of soil displacement observed from the tests were the non-uniform convergence of soil at the tunnel boundary and small invert heave compared to crown settlement. These observations provided the basis for the three assumptions made in the displacement controlled method. Small invert heave is assigned along with converged tunnel profile assumed to be similar to excavated shape. Lastly, soil around the excavated tunnel perimeter is assumed to converge to a single focus point on the tunnel centre line whose location is primarily dependant on cover to tunnel diameter ratio. A nonlinear stiffness constitutive model was required for the displacement control method to successfully predict tunneling induced ground movements.

[2] Stress based methods are implemented by reducing a proportion of the initial equilibrium stress around the excavated tunnel either by releasing fixities or removing soil elements within the tunnel

Computed results from 6 case studies in 4 different soils compare reasonably well with field and centrifuge test data. Narrow settlement trough widths with minimal far field settlements are favourably predicted by the Displacement Control Model (DCM). In addition, horizontal displacement profiles with depth are also well predicted in trend and magnitude consequently increasing the confidence of simulating realistic pile responses due to tunneling induced ground movements.

It is noted here that the proposed DCM model is currently unsuitable for the prediction of stresses induced in tunnel linings as (i) the stress distribution field around the excavated tunnel is not studied and (ii) it is a stress based (unloading) problem rather than a kinematic one. Further research efforts are required to extend the possibility of DCM to predict induced tunnel lining stresses.

6.1.2 Tunnel-Soil-Pile Interaction Studies

A total of sixty-five tunnel-soil-pile simulations were performed to study the various factors influencing pile performance and the conditions that would be critical to its structural integrity. The simulations were carried out in three dimensional space with the application of uniform soil movements along the tunnel longitudinal axis as documented field cases and numerical studies have shown that pile bending and axial response are most critical under this condition. Soil-pile interaction was modeled in this study by introducing zero thickness interface elements between pile and soil thus allowing for relative slip to occur.

The computed bending and axial response of the pile generally conform in trend to recent findings. For a given pile horizontal distance from tunnel centre, largest induced bending

moment occurs for the case in which pile tip is located one tunnel diameter below tunnel axis level. Below this relative pile tip-tunnel axis level, maximum induced bending moment along the pile length remains approximately constant in magnitude. Results also indicate that pile cracking and ultimate moments are easily exceeded at respective volume losses of 1.5% and 5%, even when the pile is installed in soft ground. At a pile horizontal offset of two tunnel diameters from the tunnel centre, experiencing a moderately high volume loss of 3%, magnitudes of induced bending moments are generally small and negligible relative to pile cracking moment.

Under circumstances where pile head is fixed against rotation and horizontal displacement, maximum induced bending moment is induced at the pile head thus demonstrating the slender behaviour of the pile in conforming to soil movements. This magnitude of bending moment is approximately constant for all relative pile tips to tunnel axis levels and larger in magnitude compared to corresponding free head pile case.

Unlike the bending response of piles caused by tunneling induced ground movement, its axial response is more complicated. The axial behaviour of the pile is primarily dependant upon two main factors. First would correspond to pile head fixity conditions where complete vertical restraint (ie. pile head fixed vertically) would induce tensile forces in the pile while free headed piles would experience compressive forces. In both cases, negative skin friction occurs along the pile shaft.

The second factor affecting the axial behaviour of single piles is the location of the pile and pile tip relative to the zone of large displacements. This factor is only investigated for piles with free head conditions. The zone of large displacements is approximately enveloped by a

forty five degree line extending upwards from the tunnel boundary at the springline. Should the pile tip be located within this zone, small compressive forces or even tensile forces could be induced as end bearing reaction is not able to develop. High compressive forces are expected for piles with tips below and outside the zone of large displacements. In addition, should the pile be located a further horizontal offset from the tunnel centre, shorter lengths of the pile would be situated within the zone of large displacements. Consequently, this results in smaller induced axial forces as shorter lengths of the pile experience mobilization of negative skin friction.

Computed axial forces for the fixed head pile case indicate that ultimate pile structural capacity in tension could be easily exceeded depending on relative position of pile and pile tip to the tunnel. Magnitudes of compressive forces are generally small compared to ultimate pile capacity in compression.

Back analysis of a centrifuge and field case study has demonstrated the ability of the displacement control method in simulating tunnel-soil-pile interaction problems. Maximum magnitudes of induced pile bending moment and axial force are reasonably well predicted when compared with test data.

6.2 Recommendations for further work

There is much scope for further research in this area, both in extending and supplementing the work described here.

6.2.1 Consolidation analysis

The displacement control method could be extended to predict stress and pore pressure changes around a deforming tunnel under plane strain conditions. The large number of centrifuge modeling of tunnel excavation in clays within recorded pore pressure changes would present a good opportunity to test the applicability of the kinematic method.

6.2.2 Pile groups

As the factors affecting the performance of single piles subject to tunneling induced ground movements are generally well covered and understood in this study, subsequent work could be performed to investigate pile group response. Group effects and pile head fixity conditions can be directly accounted for and modeled in three dimensional space thus providing important insight into the stresses generated in the pile and pile cap (due to differential settlement).

6.2.3 Tunnel-Soil-Structure Interaction

The displacement control method could be extended to predict the response of structures other than pile foundations subject to tunneling induced ground movement. Structural response of buildings, bridges etc. could be evaluated accordingly with damage classifications charts being proposed.

6.2.4 Improvements in Deformation Mechanics

The current kinematic model assumes soil displacement vectors on the excavated tunnel boundary to focus on a single point located within the bounds of the tunnel centre and

invert. It also assumes invert displacement to be zero to obtain a good match to surface S_{max}. This model could be improved by assuming a moving focus point for soil on the excavated boundary above a certain level relative to tunnel springline. Below this level, soil could be assumed to converge to a single focus point. The proposed deformation mechanism is as shown in Figure 5.1. This would enable more realistic invert heave values to be assigned for analysis.

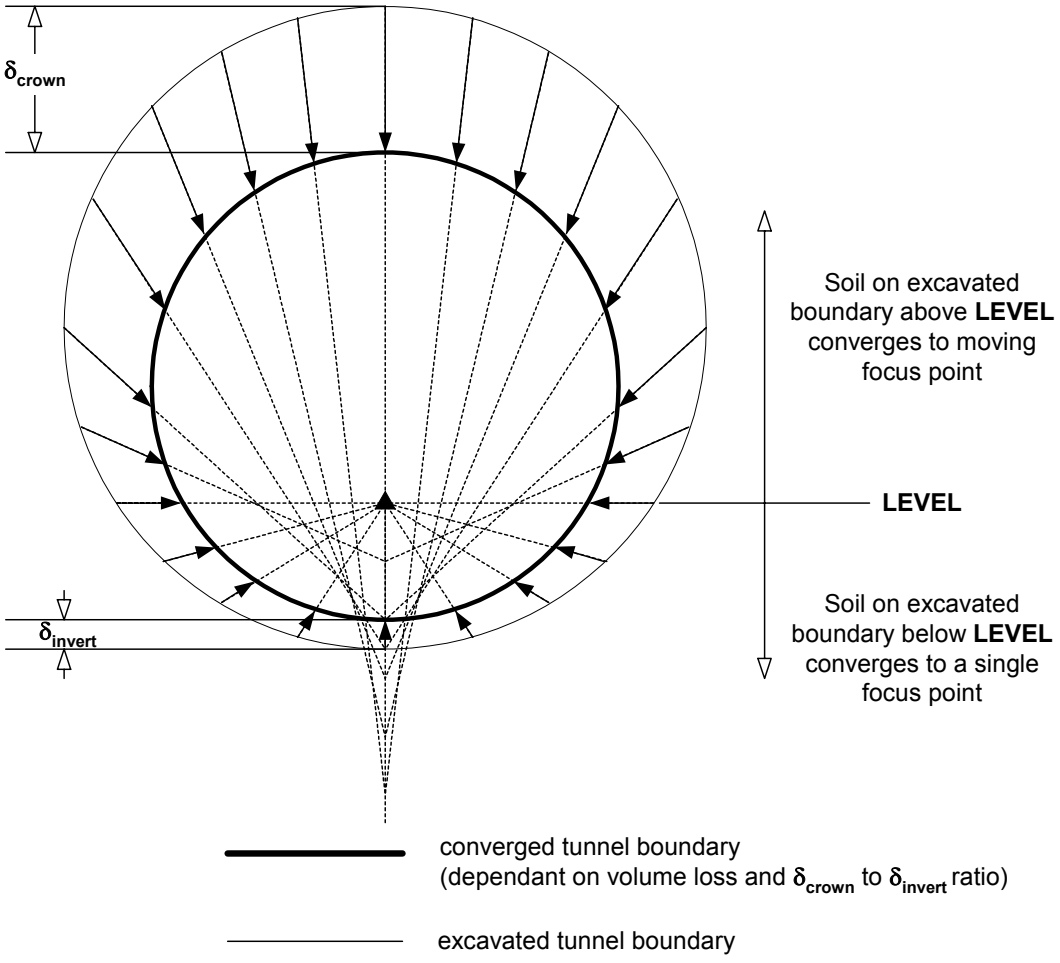

Fig. 6.1. Improved kinematic model to simulate tunnel convergence

REFERENCES

ABAQUS v. 6.3 (2002). Hibbitt, Karlsson and Sorenson, Inc.

Addenbrooke, T. I., Potts, D. M. and Puzrin, A. M. (1997). The influence of pre-failure soil stiffness on the numerical analysis of tunnel construction. *Geotechnique,* Vol. 47, No. 3, pp. 693-712.

Attewell, P. B. and Farmer I. W. (1974). Ground deformations resulting from shield tunneling in London Clay. *Canadian Geotechnical Journal*, Vol. 11, No. 3, pp. 380-395.

Attewell, P. B., Glossop, N. H. and Farmer, I. W. (1978). Ground deformations caused by tunneling in a silty alluvial clay. *Ground Engineering*, Vol. 11, No. 8, pp. 32-41.

Broms, B. (1979). Negative skin friction. *Proc. 6th Asian Regional Conf. Soil Mechanics and Foundation Engineering*, Singapore, Vol. 2, 41-75.

Chen, L. T., Poulos, H. G. and Loganathan, N. (1999). Pile responses caused by tunneling. *Journal of Geotechnical and Geoenvironmental Engineering*, Vol. 125, No. 3, pp. 207-215

Cheng, C.Y., Dasari, G. R., Leung C. F. and Chow, Y. K. (2002). A Novel FE Technique to Predict Tunnelling Induced Ground Movements in Clays. *Proc. Fifteenth KKCNN Symposium on Civil Engineering* (eds. S. T. Quek and D. W. S. Ho).

Chow, Y. K., Chin J. T. and Lee S. L (1990). Negative skin friction on pile groups. *Int. Journal for Numerical and Analytical Method in Geomechanics*. Vol. 14, pp. 75-91.

Cording, E. J. and Hansmire, W. H. (1975). Displacement around soft ground tunnels, general report: session IV, tunnels in soil. *Proc. 5th Panamerican Congr. on Soil Mech. And Foundations Engrg.*

Coutts, D. R. and Wang, J. (2000). Monitoring of reinforced concrete piles under horizontal and vertical loads due to tunneling. *Tunnels and Underground Structures* (eds. Zhao, Shirlaw & Krishnan), Balkema.

Dames and Moore (1983). Singapore mass rapid transit system: Detailed geotechnical study. Interpretive Report. *Provisional Mass Rapid Transit Authority, Singapore*.

Dasari, G. R., Rawlings, C. G. and Bolton, M. D. (1996). Numerical modeling of a NATM tunnel construction in London Clay. *Proc. Int. Symposium on Geotechnical Aspects of Underground Construction in Soft Ground,* London (eds. R. J. Mair and R. N. Taylor), Balkema. pp. 491-496.

Deane, A. P. and Bassett, R. H. (1995). The Heathrow Express Trial Tunnel. *Proc. Inst. Civil Engineers*, Vol. 113, July, pp. 144-156.

Diaz-Rodriguez, J. A. (1992). On the dynamic properties of Mexico City clay for wide strain range. 10th World Conf. On Earthquake Engineering, Madrid Vol. 1, pp. 1257-1262.

Diaz-Rodriguez, J. A., Leroueil, S. and Aleman, J. D. (1992). Yielding of Mexico City clay and other natural clays. *Journal of Geotechnical Engineering*, ASCE, Vol. 118, No. 7, pp. 981-995.

Dyer, M. R., Hutchinson, M. T. and Evans, N. (1996). Sudden Valley Sewer: a case history. *Proc. Int. Symposium on Geotechnical Aspects of Underground Construction in Soft Ground*, London (eds. R. J. Mair and R. N. Taylor), Balkema, pp. 671-676.

Fujita, K. (1981). On the surface settlements caused by various methods on shield tunneling. *Proc. XIth Int. Conf. On Soil Mechanics and Foundations Engineering*, Vol. 4, pp. 609-610.

Grant, R. J. and Taylor, R. N. (2000). Tunneling-induced ground movements in clay. *Geotechnical Engineering, Proc. Institutions of Civil Engineers*, Vol. 143, No. 1, pp. 43-55.

Gunn, M. J. (1993). The prediction of surface settlement profiles due to tunneling. *Predictive Soil Mechanics, Proc. Wroth Memorial Symposium*, Oxford 1992, Thomas Telford, pp. 304-316.

Hagiwara, T., Grant, R. J., Calvello, M. and Taylor, R. N. (1999). The effect of overlying strata on the distribution of ground movements induced by tunneling in clay. *Soils and Foundaions*, Vol. 39, No. 3, pp. 63-73.

Hegarden, H. J. A. M., van der Poel, T. J. and van der Schrier, J. S. (1996). Ground movements due to tunneling: influence on pile foundations. *Proc. Int. Symposium on Geotechnical Aspects of Underground Construction in Soft Ground*, London (eds. R. J. Mair and R. N. Taylor), Balkema, pp. 519-524.

Jacobsz, S. W., Standing, J. R., Mair, R. J., Soga, K., Hagiwara, T. and Sugiyama, T. (2001). The effects of tunneling near single driven piles in dry sand. *Proc. of Asian Regional Conf. on Geotechnical Aspects of Underground Construction in Soft Ground*, Tongji University Press, Shanghai, pp. 29-35.

Jardine, R. J., Potts, D. M., Fourie, A. B. and Burland, J. B. (1986). Studies of the influence of non-linear stress-strain characteristics in soil-structure interaction. *Geotechnique*, Vol. 36, No. 3, pp. 377-396.

Jardine, R. J., Potts, D. M., StJohn, H. D. and Hight, D. W. (1991). Some practical applications of a non-linear ground model. *Xth European Conf. on Soil Mechanics and Foundation Engineering, Florence*, Vol. 1, pp. 223-228.

Kovacevic, N., Edmonds H. E., Mair, R. J., Higgins, K. G. and Potts, D. M. (1996). Numerical modeling of the NATM and compensation grouting trials at Redcross Way. *Proc. Int. Symposium on Geotechnical Aspects of Underground Construction in Soft Ground*, London (eds. R. J. Mair and R. N. Taylor), Balkema, pp. 553-559.

Kuwabara, F. and Poulos, H. G. (1989). Downdrag forces in group of piles. *ASCE Journal of Geotechnical Engineering*, Vol. 115, No. 6, pp. 806-818.

Lake, L. M., Rankin, W. J. and Hawley, J. (1992). Prediction and effects of ground movements caused by tunneling in soft ground beneath urban areas. CIRIA *Project Report 30*, Construction Industry Research and Information Association, London.

Lee, C. J., Bolton, M. D. and Al-Tabbaa, A. (2002). Numerical modeling of group effects on the distribution of dragloads in pile foundations. *Geotechnique*, Vol. 52, No. 5, pp. 325-335.

Lee, K. M. and Rowe, R. K. (1989). Deformations caused by surface loading and tunneling: the role of elastic anisotropy. *Geotechnique*, Vol. 39, No. 1, pp. 125-140.

Lee, K. M., Rowe, R. K. and Lo, K. Y. (1992). Subsidence due to tunneling: Part I – Estimating the gap parameter. *Canadian Geotechnical Journal*, Vol. 29, No. 5, pp. 929-940.

Lee, R. G., Turner, A. J. and Whitworth, L. J. (1994). Deformations cased by tunneling beneath a piled structure. *Proc. XIII Int. Conf. Soil Mechanics and Foundation Engineering.*, University Press, London, pp. 873-878.

Lee, S.-W. (2002). The use of compensation grouting in tunneling: a case study. *Geotechnical Engineering*, Vol. 155, Issue 2, pp. 101-109.

Leong, E. C., Rahardjo, H. and Tang, S. K. (2003). Characterisation and engineering properties of Singapore residual soils. *Characterisation and Engineering Properties of Natural Soil* (eds. Tan et al), Vol. 1. pp. 1279-1304.

Loganathan, N. and Poulos, H. G. (1998). Analytical prediction for tunneling-induced ground movements in clays. *Journal of Geotechnical and Geoenviromental Engineering*, Vol. 124, No. 9, pp. 846-856.

Loganathan, N., Poulos, H. G. and Stewart, D. P. (2000). Centrifuge model testing of tunneling induced ground and pile deformations. *Geotechnique*, Vol. 50, No. 3, 283-294.

Loganathan, N., Poulos, H. G. and Xu, K. J. (2001). Ground and pile-group response due to tunneling. *Soils and Foundations*, Vol. 41, No. 1, pp. 57-67.

Mair, R. J. (1979). Centrifugal modeling of tunneling construction in soft clay. *PhD Thesis*, University of Cambridge.

Mair, R. J. (1992). Developments in geotechnical engineering research: application to tunnels and deep excavation, Unwin Memorial Lecture 1992. *Proc. Institution of Civil Engineers and Civil Engineering*, Vol. 93, pp. 27-41.

Mair, R. J., Taylor, R. N. and Bracegirdle, A. (1993). Subsurface settlement profiles above tunnels in clay. *Geotechnique*, Vol. 43, No. 2, pp. 315-320.

Moh, Z-C., Ju, D. H. and Hwang, R. N. (1996). Ground movements around tunnels in soft ground. *Proc. Int. Symposium on Geotechnical Aspects of Underground Construction in Soft Ground*, London (eds. R. J. Mair and R. N. Taylor), Balkema, pp. 725-730.

Morton, J. D. and King, K. H., (1979). Effect of tunneling on the bearing capacity of and settlement of piled foundations. *Proc. Tunneling '79*, (ed. M. J. Jones), pp. 57-58. London: IMM

Mroueh, H. and Shahrour, I. (2002). Three-dimensional finite element analysis of the interaction between tunneling and pile foundations. *Int. Journal for Numerical and Analytical Methods in Geomechanics.*, Vol. 26, pp. 217-230.

Ng, C. W. W., Pun, W. K. and Pang, R. P. L. (2000). Small strain stiffness of natural granitic saprolite in Hong Kong. *Journal of Geotechnical and Geoenviromental Engineering*, Vol. 126, No. 9, pp. 819-833.

Ng, C. W. W. and Wang, Y. (2001). Field and laboratory measurements of small strain stiffness of decomposed granites. *Soils and Foundations*, Vol. 41, No. 3, pp. 57-71.

O'Reilly, M. P. and New, B. M. (1982). Settlements above tunnels in the United Kingdom – their magnitude and prediction. *Tunneling '82*, London, IMM, pp. 173-181.

Panet, M. and Guenot, A., (1982). Analysis of convergence behind the face of a tunnel. *Proc. Tunnelling 82, Institution of Mining and Metallurgy*, London, pp. 197-204.

Peck, R. B. (1969). Deep excavations and tunneling in soft ground. *Proc. 7th International Conference Soil Mechanics and Foundation Engineering*, Mexico City, State of the Art Volume, pp. 225-290.

Phienwej, N. (1997). Ground movements in shield tunneling in Bangkok soils. *Proc. XIV th Int. Conf. on Soil Mechanics and Foundation Engineering*, Hamburg, Vol. 3, pp. 1469-1472.

Ramasamy, N. (1992). Soft ground tunneling Bangkok subsoils. *M. Eng Thesis*, Asian Inst. of Technology, Bangkok, Thailand.

Randolph, M. F. and Wroth, C. P. (1981). Application of the failure state in undrained simple shear to the shaft capacity of driven piles. *Geotechnique*, Vol. 31, No. 1, pp. 143-157.

Ng, R. M. C., Lo, K. Y. and Rowe, R. K. (1986). Analysis of field performance - the Thunder Bay tunnel. *Canadian Geotechnical Journal*, Vol. 23, pp. 30-50.

Romo, M. P. (1997). Soil movements induced by slurry shield tunneling. *Proc XIV th Int. Conf.e on Soil Mechanics and Foundation Engineering*, Hamburg, Vol. 3, pp. 1473-1481.

Rowe, R. K. and Lee, J. M. (1992). Subsidence due to tunneling: Part II – evaluation of a prediction technique. *Canadian Geotechnical Journal*, Vol. 29, No. 5, pp. 941-954.

Rowe, R. K., Lo, K. Y. and Kack, G. J. (1983). A method of estimating surface settlement above tunnels constructed in soft ground. *Canadian Geotechnical Journal*, Vol. 20, No. 8, pp. 11-22.

Sagaseta, C. (1987). Analysis of undrained soil deformation due to ground loss. *Geotechnique*, Vol. 37, No. 3, pp. 301-320.

Shibuya, S. and Tamrakar, S. B. (2003). Engineering properties of Bangkok clay. *Characterisation and Engineering Properties of Natural Soil* (eds. Tan et al), Vol. 1. pp. 645-694.

Simpson, B., Atkinson, J. H. and Jovicic, V. (1996). The influence of anisotropy on calculations of ground settlements above tunnels. *Proc. Int. Symposium on Geotechnical Aspects of Underground Construction in Soft Ground*, London (eds. R. J. Mair and R. N. Taylor), Balkema, pp. 591-594.

Stallebrass, S. E., Jovicic, V. and Taylor, R. N. (1994). The influence of recent stress history on ground movements around tunnels. *Prefailure Deformation of Geomaterials* (eds. S. Shibuya, T. Mitachi and S. Miura), Balkema, Vol. 1, pp. 612-620.

Stallebrass, S. E., Grant, R. J. and Taylor, R. N. (1996). A finite element study of ground movements measured in centrifuge model tests of tunnels. *Proc. Int. Symposium on Geotechnical Aspects of Underground Construction in Soft Ground*, London (eds. R. J. Mair and R. N. Taylor), Balkema, pp. 595-600.

Stewart, D. P. (1992). Lateral loading of piled bridge abutments due to embankment construction. *PhD Thesis*, University of Western Australia.

Subba Rao, K. S., Allam, M. M. and Robinson, R. G. (2000). Drained shear strength of fine-grained soil-solid surface interfaces. *Geotechnical Engineering, Proc. Institutions of Civil Engineers*, Vol. 143, No. 2, pp. 75-81.

Taylor, R. N. (1995). Tunneling in soft ground in the UK. *Underground Construction in Soft Ground* (eds. K. Fujita and O. Kusakabe), Balkema, pp. 123-126.

Teh, C. I. and Wong, K. S. (1995). Analysis of downdrag on pile groups. *Geotechnique*, Vol. 45, No. 2, pp. 191-207.

Teunissen, E. A. H. and Hutteman, M. (1998). Pile and surface settlements at full scale tests North/South metro line Amsterdam. *Tunnels and Metropolises* (eds. Negro Jr. and Ferreira), Balkema, Rotterdam.

Tham, K. S. and Deutscher, M. S. (2000). Tunnelling under Woodleigh Workers' Quarters on Contract 705. *Tunnels and Underground Structures* (eds. Zhao, Shirlaw and Krishnan), Balkema.

Tsubakihara, Y. and Kishida, H. (1993). Frictional behaviour between normally consolidated clay and steel by two direct shear type apparatuses. *Soils and Foundations*, Vol. 33, No. 2, pp. 1-13.

Verrujit, A. and Booker, J. R. (1996). Surface settlements due to deformation of a tunnel in an elastic half plane. *Geotechnique*, Vol. 46, No. 4, pp. 753-756.

Viggiani, G. and Atkinson, J. H. (1995). Stiffness of fine-grained soil at very small strains. *Geotechnique*, Vol. 45, No. 2, pp. 249-295.

Zytynski, M., Randolph, M. F., Nova, R. and Wroth, C. P. (1978). On modelling the unloading-reloading behaviour of soils. *Int. Journal for Numerical and Analytical Method in Geomechanics*. Vol. 2, pp. 87-94.

APPENDIX A

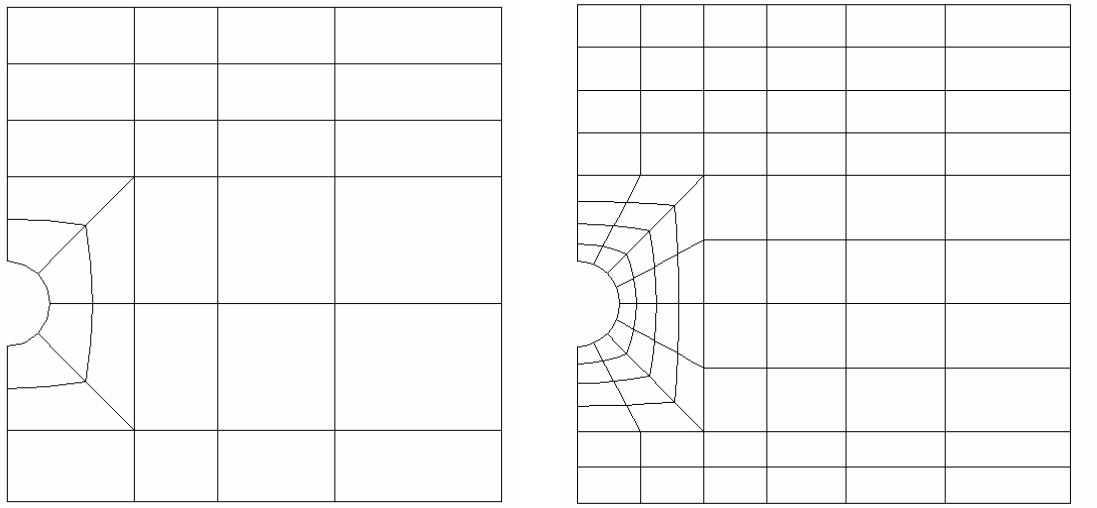

(a) **(b)**

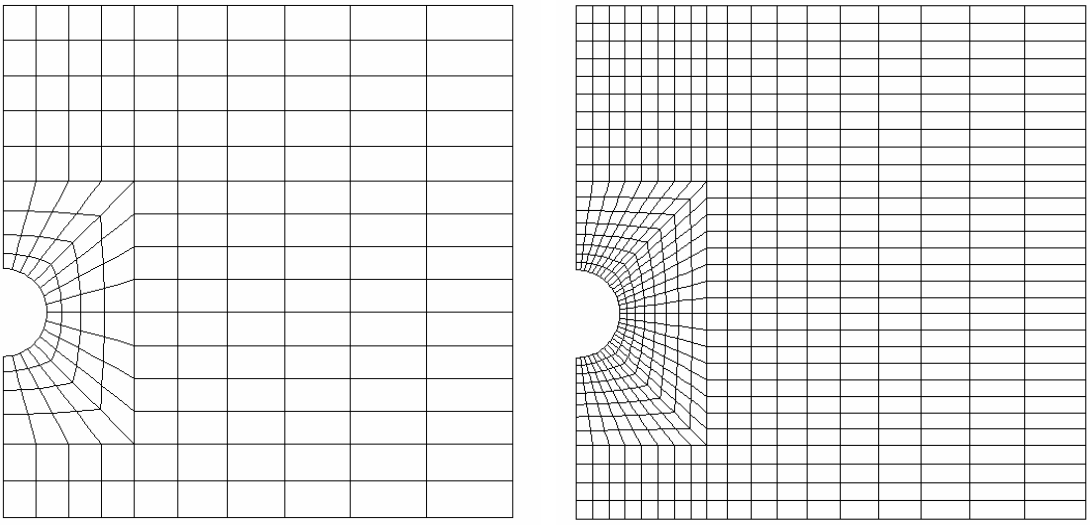

(c) **(d)**

Fig. A.1. Mesh density of (a) 30, (b) 84, (c) 182 and (d) 668 elements used for convergence study

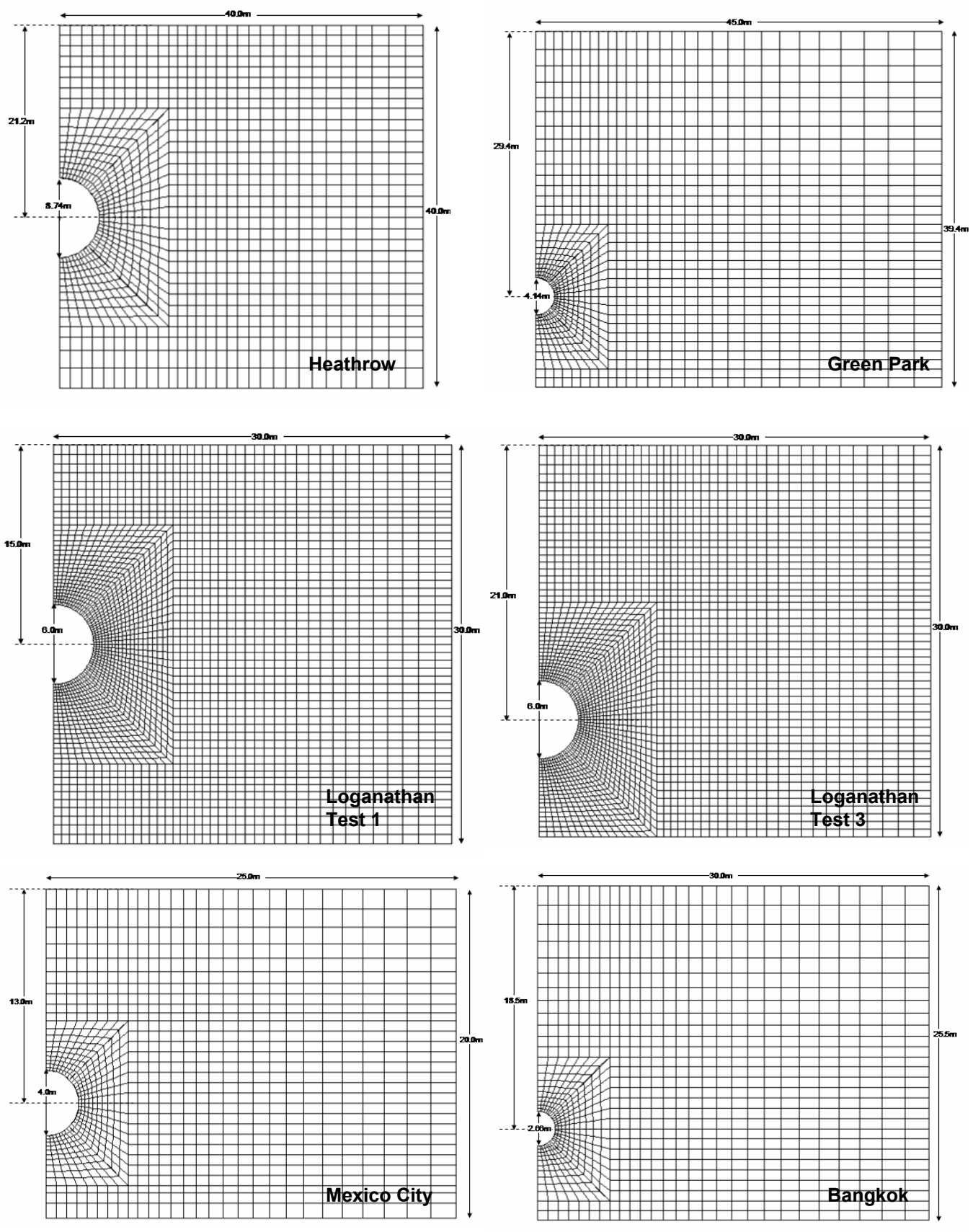

Fig. A.2. Mesh dimension for all analysed case histories in Chapter 3

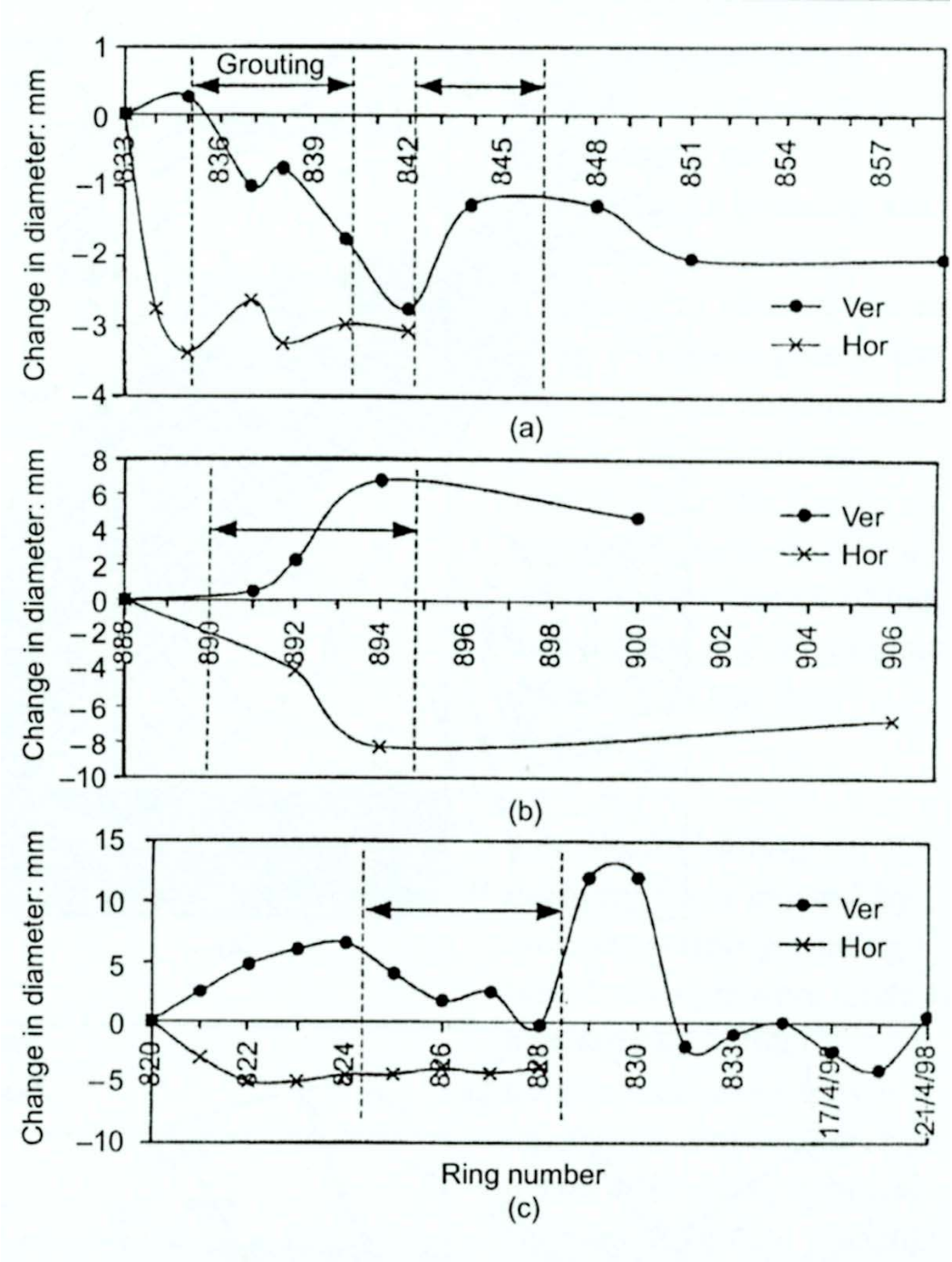

Fig. A.3. Vertical and horizontal changes in tunnel lining diameter before and after compensation grouting for London Docklands Light Railway Lewisham Extension twin tunnel project (Lee, 2002)

Implementation of DCM to Finite Element Analysis

Step 1: Create mesh and extract coordinates of nodes of excavated boundary.

Step 2: Calculate displacement magnitudes of nodes on excavated boundary to form converged tunnel profile

Excavated tunnel radius = R
Converged tunnel radius = R_c

Tunnel volume loss = V_l (%) = $\dfrac{100\left(R^2 - {R_c}^2\right)}{R^2}$ $\Rightarrow$ $R_c = R\sqrt{\dfrac{100 - V_l}{100}}$

Ratio of crown to invert displacement = $\alpha = \dfrac{\Delta_c}{\Delta_i}$ $\Rightarrow$ $\Delta_c = \alpha\Delta_i$

From tunnel geometry, $\Delta_c + \Delta_i = 2\left(R - R_c\right)$

$$\Rightarrow \quad \Delta_i\left(1+\alpha\right) = 2R\left(1 - \sqrt{\frac{100 - V_l}{100}}\right)$$

$$\Rightarrow \quad \Delta_i = \frac{2R\left(1 - \sqrt{\dfrac{100 - V_l}{100}}\right)}{\left(1+\alpha\right)}$$

To shift converged tunnel center to coordinate (0,0), translate existing coordinates of nodes on the excavated tunnel boundary (x_o,y_o) upward by the following magnitude:

Let $R - R_c - \Delta_i = \lambda$

$\Rightarrow$ translated coordinate is $\left(x_o, y_o + \lambda + \beta R\right)$

gradient, $m = \dfrac{y_o + \lambda + \beta R}{x_o}$ $\Rightarrow$ equation of intersecting line, $y = mx - \beta R$

To find coordinate of intersecting line with converged tunnel profile, substitute
$y = mx - \beta R$ into $y^2 + x^2 = R^2$

$\Rightarrow$ $\left(1 + m^2\right)x^2 - \left(2\beta R m\right)x - \left(1 - \beta^2\right)R^2 = 0$

$\Rightarrow$ solve for x ($x \geq 0$) and y

Step 3: Perform first step of analysis to attain geostatic equilibrium by constraining nodes on excavated tunnel in all directions.

Step 4: Impose corresponding node displacement on excavated boundary to simulate stress relief and tunnel convergence.

Calculation of mean normal effective stress for soil constitutive model

As total vertical and horizontal stresses are called at each calculation step to determine soil stiffness $\left[G = f\left(p', \varepsilon_q{}^n\right)\right]$, a modification factor (λ) is introduced to convert mean effective stress to mean total stress. Derivations for the conversion are as shown below:

γ_{bulk} = soil bulk unit weight

γ_w = water unit weight

λ = effective stress modification factor

$$p = \frac{(2K_o + 1)}{3}.(\gamma_{bulk} - \gamma_w) + \gamma_w \quad ; \quad p' = \frac{(2K_o + 1)}{3}.(\gamma_{bulk} - \gamma_w)$$

$$\lambda = \frac{p'}{p} = \frac{\frac{(2K_o + 1)}{3}.(\gamma_{bulk} - \gamma_w)}{\frac{(2K_o + 1)}{3}.(\gamma_{bulk} - \gamma_w) + \gamma_w} = \frac{(2K_o + 1).(\gamma_{bulk} - \gamma_w)}{(2K_o + 1)(\gamma_{bulk} - \gamma_w) + 3\gamma_w}$$

$$\Rightarrow \quad G = A.p'.\varepsilon_q{}^n = A.(\lambda p).\varepsilon_q{}^n$$

Example calculation – Loganathan et al. (2000) Test 3 Analysis

$\gamma_{bulk} = 16.5kN/m^3$

$\phi' = 23^\circ$

$OCR_{springline} \approx 5.2$

$$K_{o(OCR)} = K_{o(NC)}.OCR^{\sin\phi'} = (1 - \sin 23^\circ)(5.2)^{\sin 23^\circ} = 1.16$$

$$\Rightarrow \quad \lambda = 0.4184$$

$$\Rightarrow \quad G = 550.p'.\varepsilon_q{}^n \approx 230.p.\varepsilon_q{}^n$$

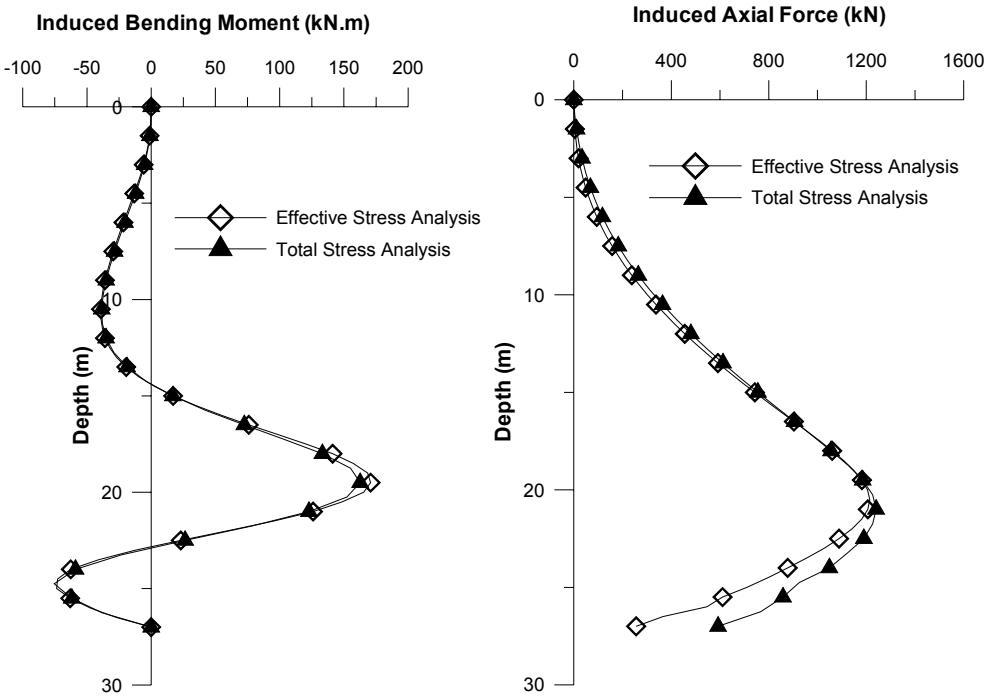

Fig. A.4. Comparison of BM and P for total stress and effective stress analysis (V_l = 1%, G_{max}/p'=400, Y_p = -1D_t, X=1D_t)

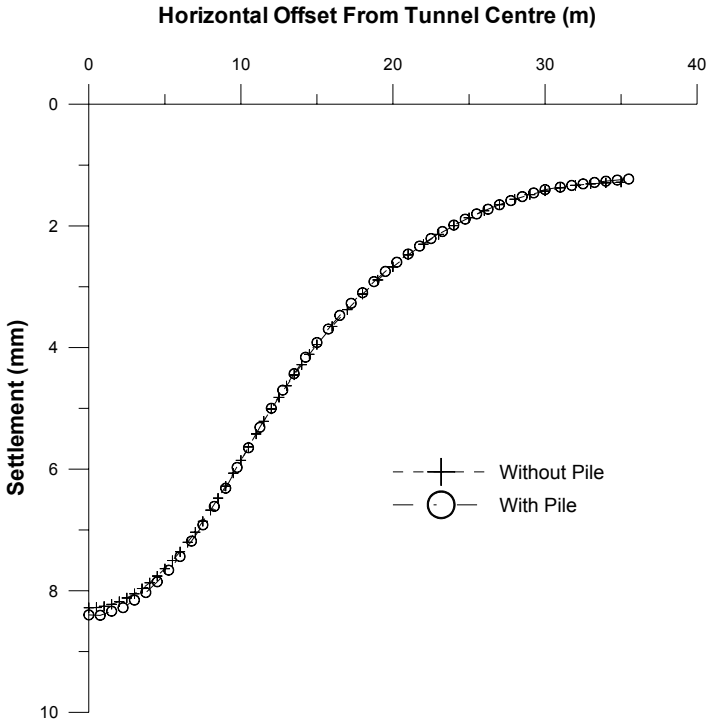

Fig. A.5. Surface settlement trough for with (far field) and without presence of pile

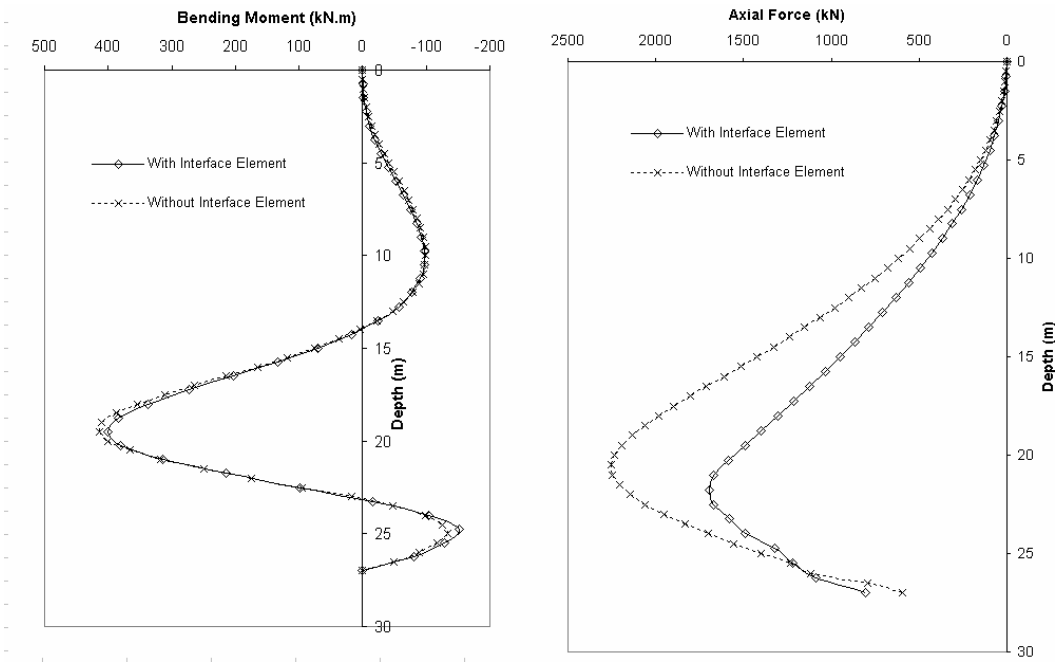

(a) **(b)**

Fig. A.6. Effect of modeling slip between pile and soil using interface elements for (a) bending moment and (b) axial force (V_I = 3%, Y_P = -1D_t, X=1D_t)

Structural Strength of Pile for Parametric Analysis

1. Pile cracking moment (M_{cr})

Assuming concrete compressive strength (f_{cu}) of 30 MPa and tensile strength $\frac{f_{cu}}{10}$

$$\Rightarrow \qquad M_{cr} = \frac{f_{cu} I}{y} = \frac{f_{cu} \pi D_p^{\ 3}}{32} = 151 kN.m$$

2. Pile ultimate moment (M_{ult}) (BS 8110)

Assumptions:

Concrete ultimate strain (ε_o) = 0.35%
Concrete ultimate design stress = 0.45f_{cu} (partial factor of safety = 1.5)
Steel ultimate limit = 0.87f_y (partial factor of safety = 1.15)
12T25 steel bar reinforcement (cover 50mm)
No axial load on pile head

From equilibrium of forces $\left(\sum F = 0\right)$, Neutral Axis (N.A) is approximately 180mm above pile centre.

Centroidal point for equivalent rectangular stress block (0.9x) is located approximately 82mm above N.A.

Moment arm ≈ 448mm

$\Rightarrow \quad M_{ult} \approx 632\text{kN.m}$

3. Pile limiting tensile force (P_{ult})

$$P_{ult} = f_{cu}\left(\frac{\pi D_p^{\,2}}{4}\right) = 1508kN$$

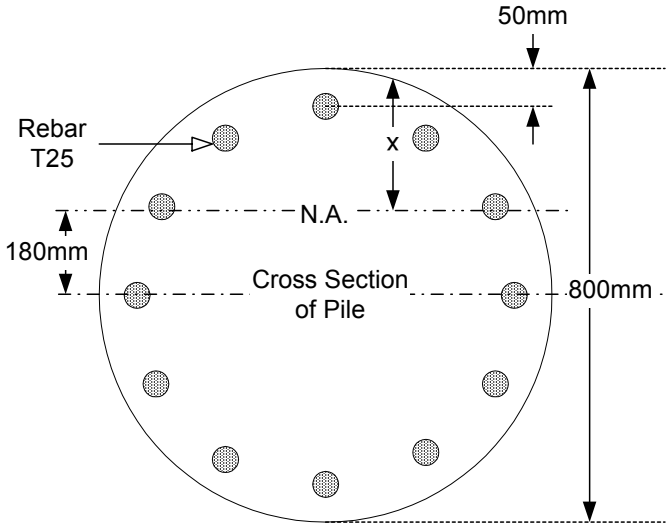

Fig. A.7. Pile and rebar dimensions

Pile response along length for X = 2D_t and V_l = 1%

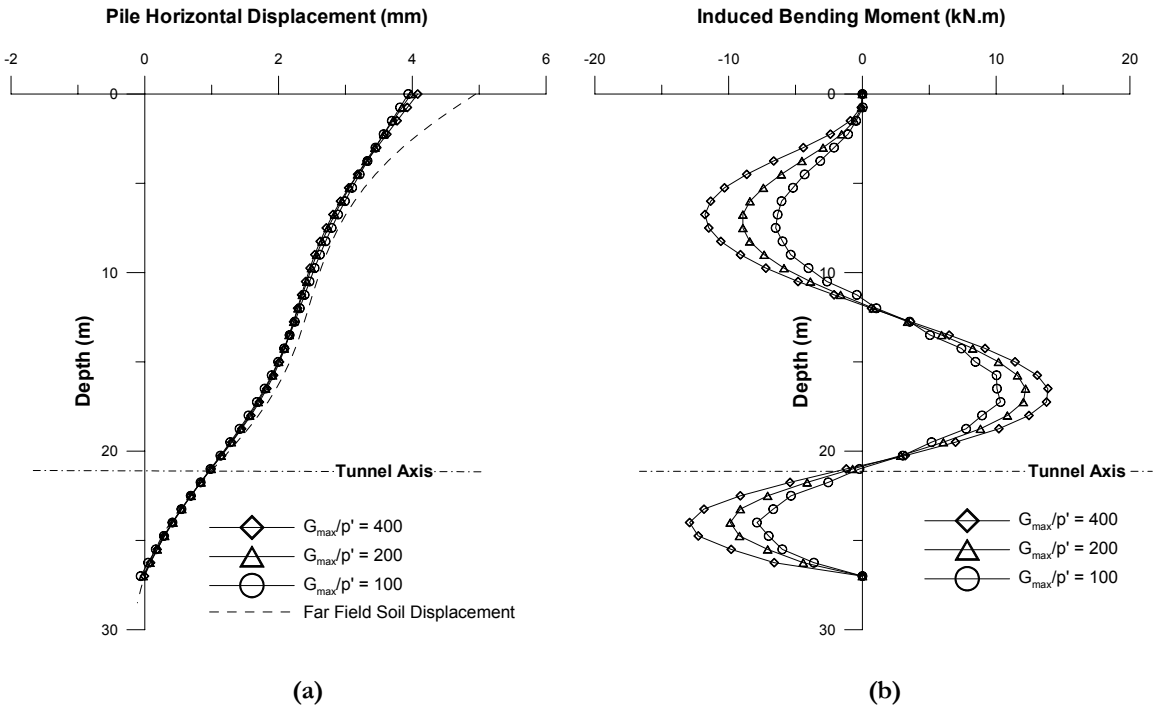

Fig. A.8. Pile (a) horizontal displacement and (b) bending moment profile for Y_p = -1D_t

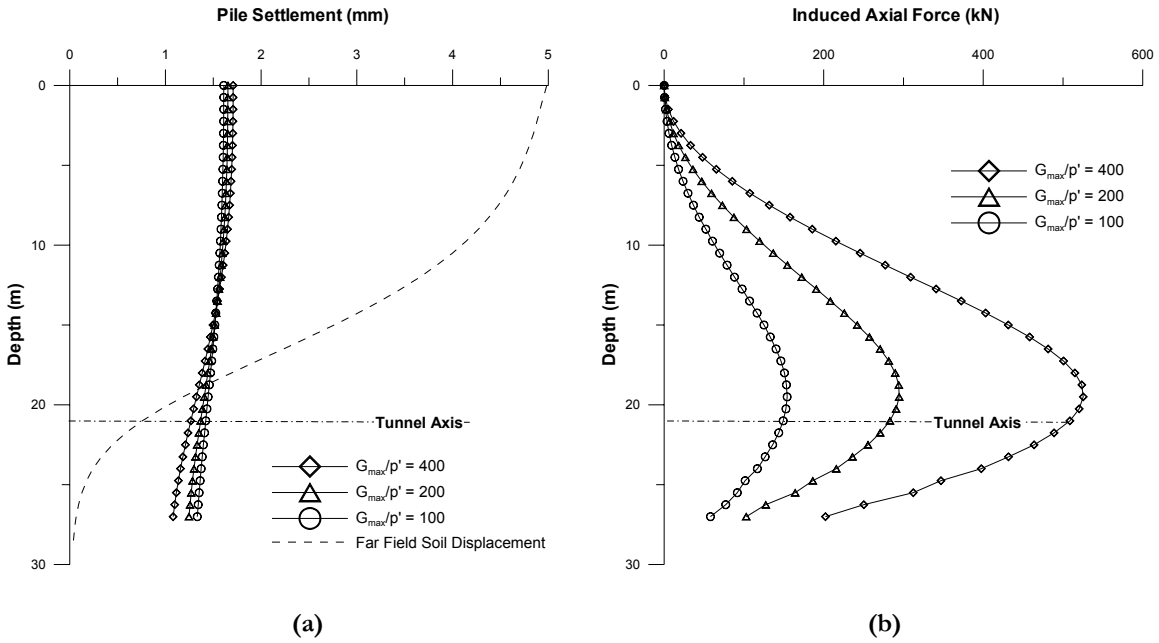

(a) **(b)**

Fig. A.9. Pile (a) settlement and (b) axial force profile for Y_p = -1D_t

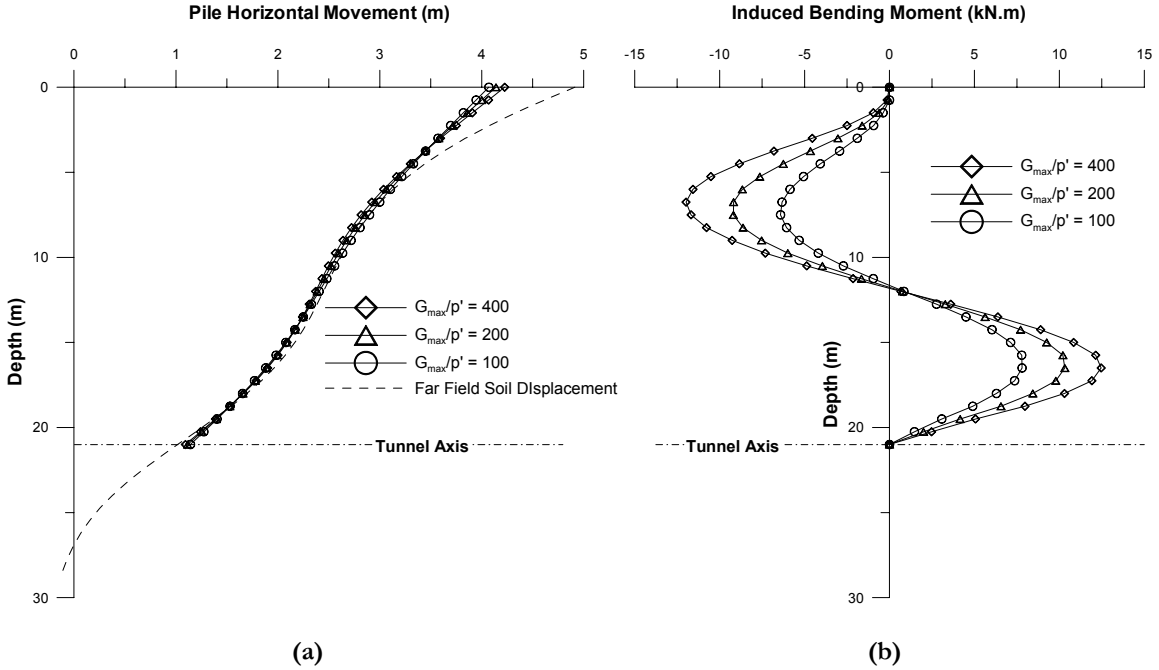

(a) **(b)**

Fig. A.10. Pile (a) horizontal displacement and (b) bending moment profile for Y_p = -1D_t

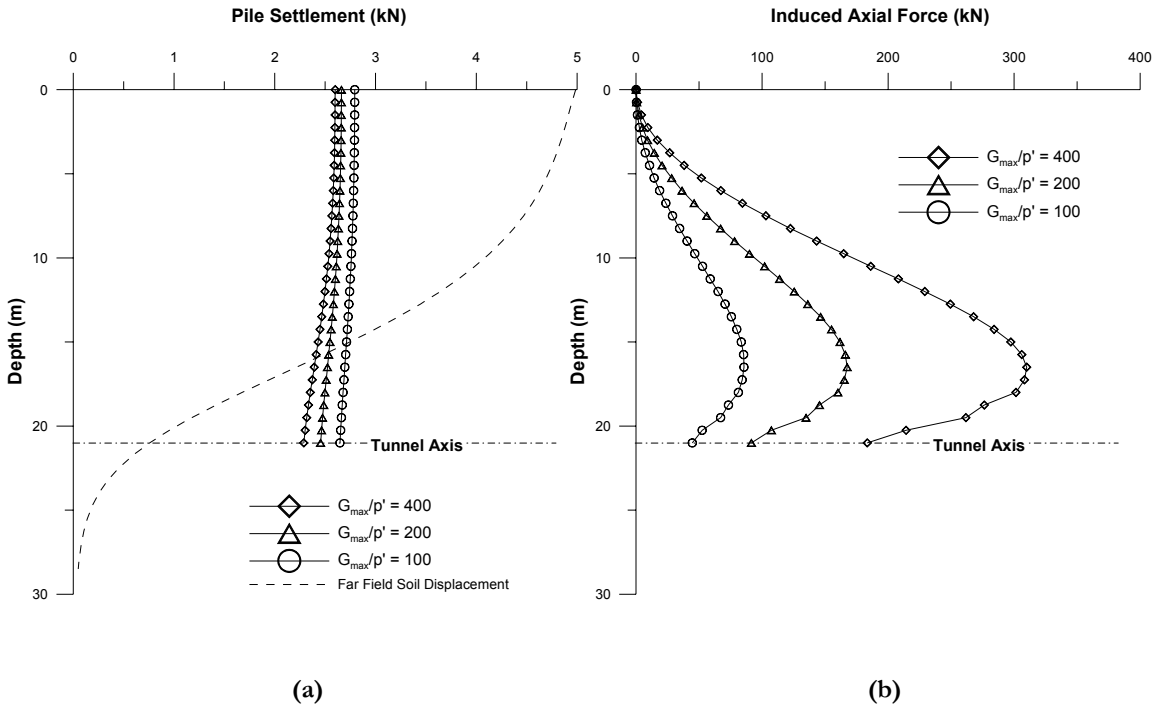

Fig. A.11. Pile (a) settlement and (b) axial force profile for $Y_p = 0D_t$

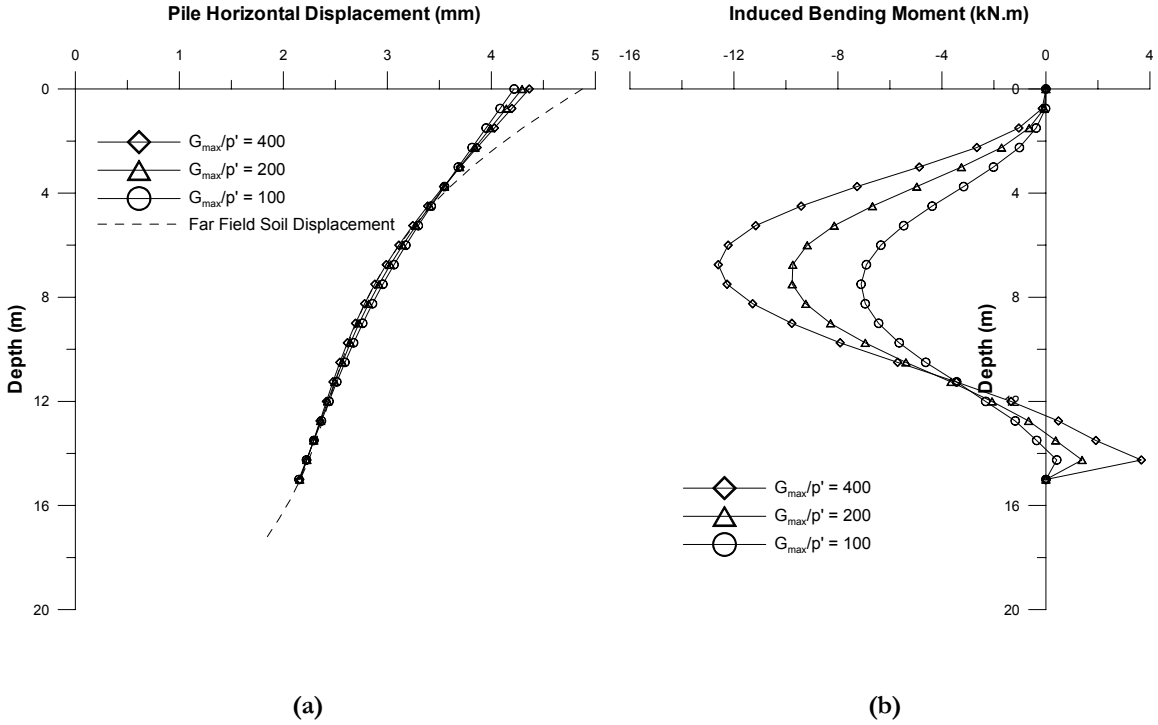

Fig. A.12. Pile (a) horizontal displacement and (b) bending moment profile for $Y_p = +1D_t$

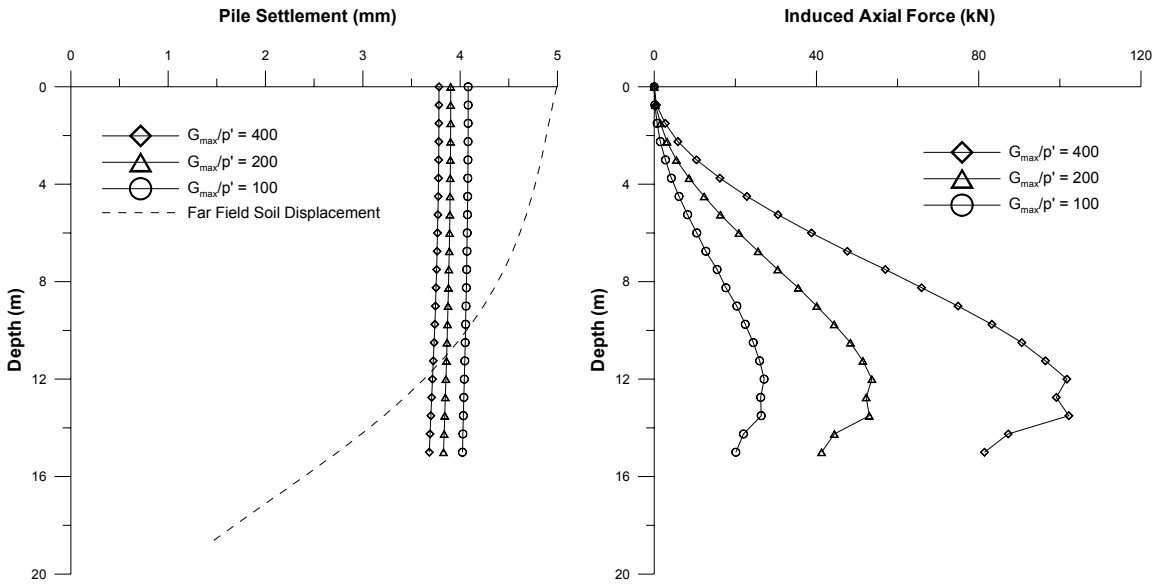

Fig. A.13. Pile (a) settlement and (b) axial force profile for $Y_p = +1D_t$

Variation of pile performance with volume loss ($X = 2D_t$)

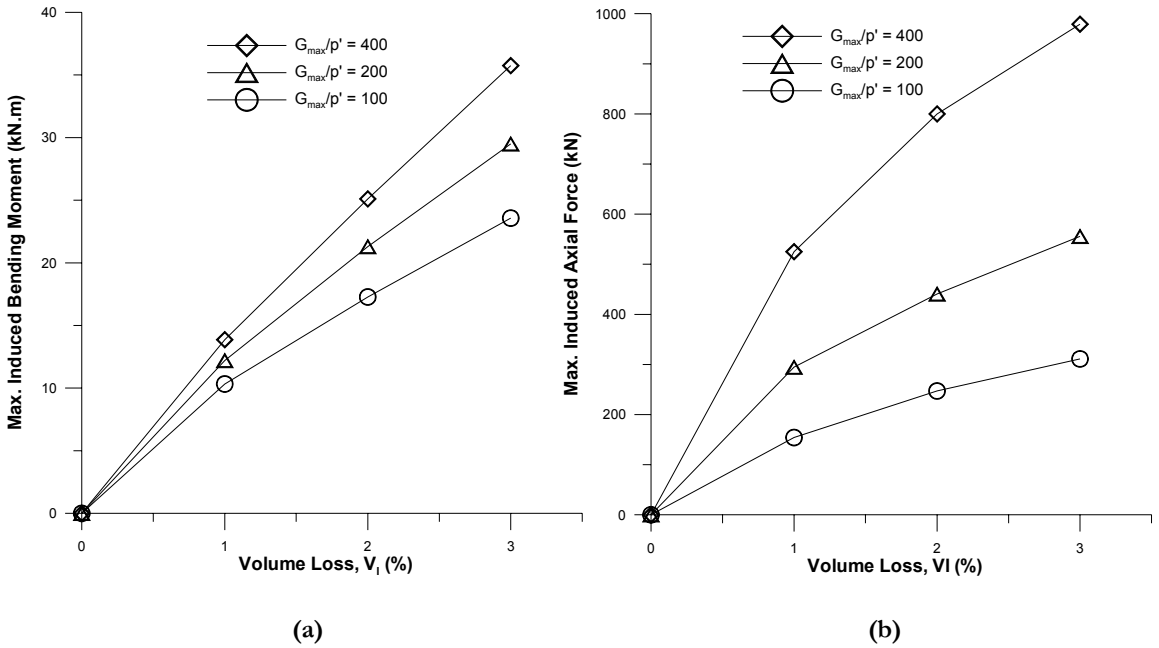

Fig. A.14. Variation of maximum induced pile (a) bending moment and (b) axial force for $Y_p = -1D_t$

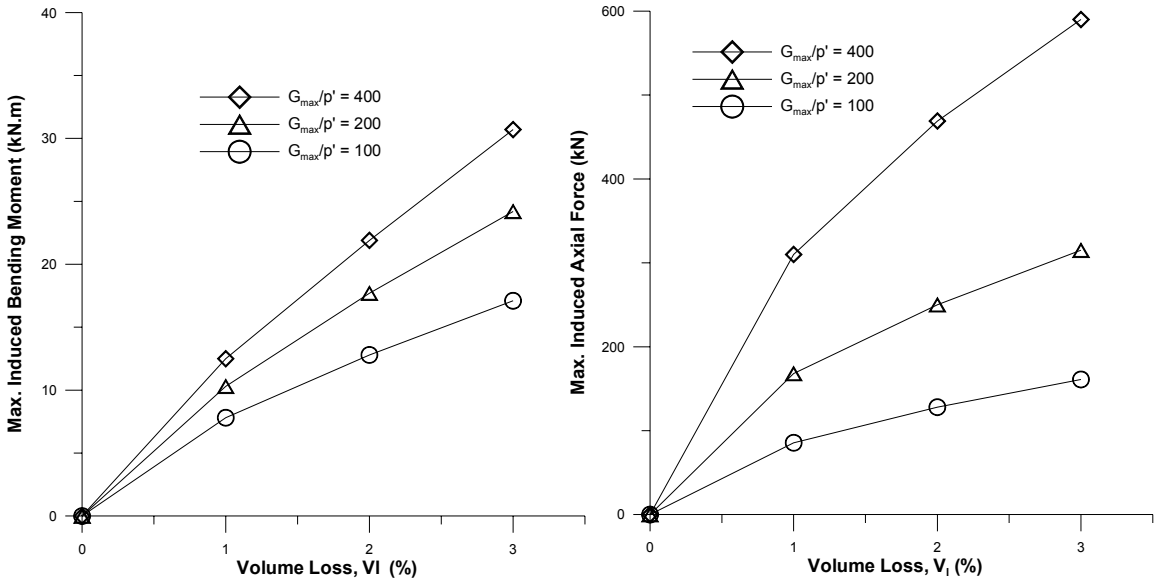

(a) (b)

Fig. A.15. Variation of maximum induced pile (a) bending moment and (b) axial force for $Y_p = 0D_t$

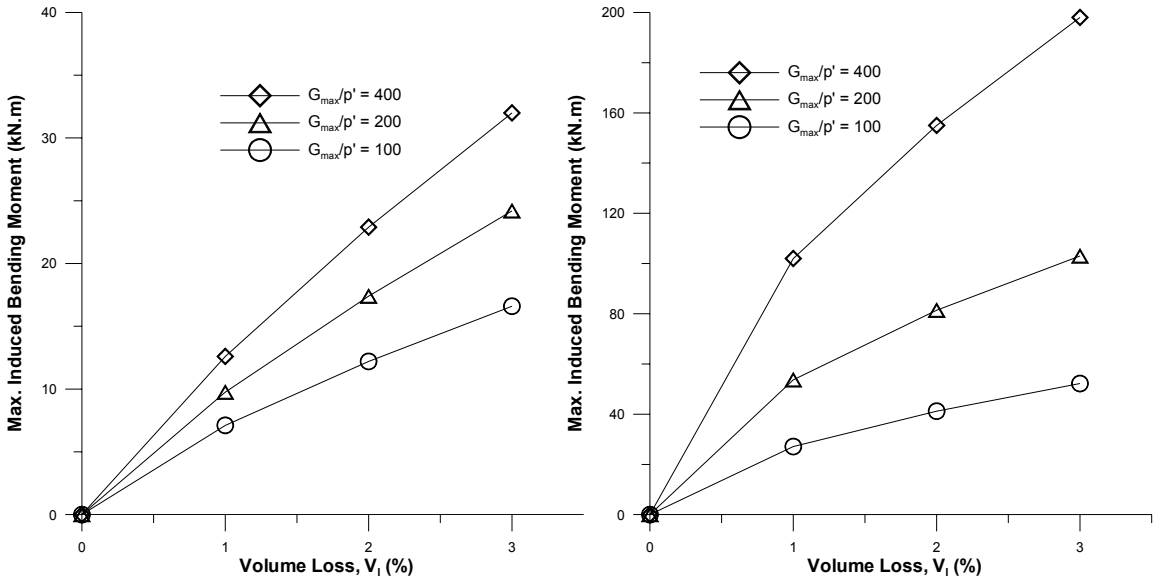

(a) (b)

Fig. A.16. Variation of maximum induced pile (a) bending moment and (b) axial force for $Y_p = +1D_t$

Comparison of fixed and free head pile response for X=1D_t and V_t = 1%

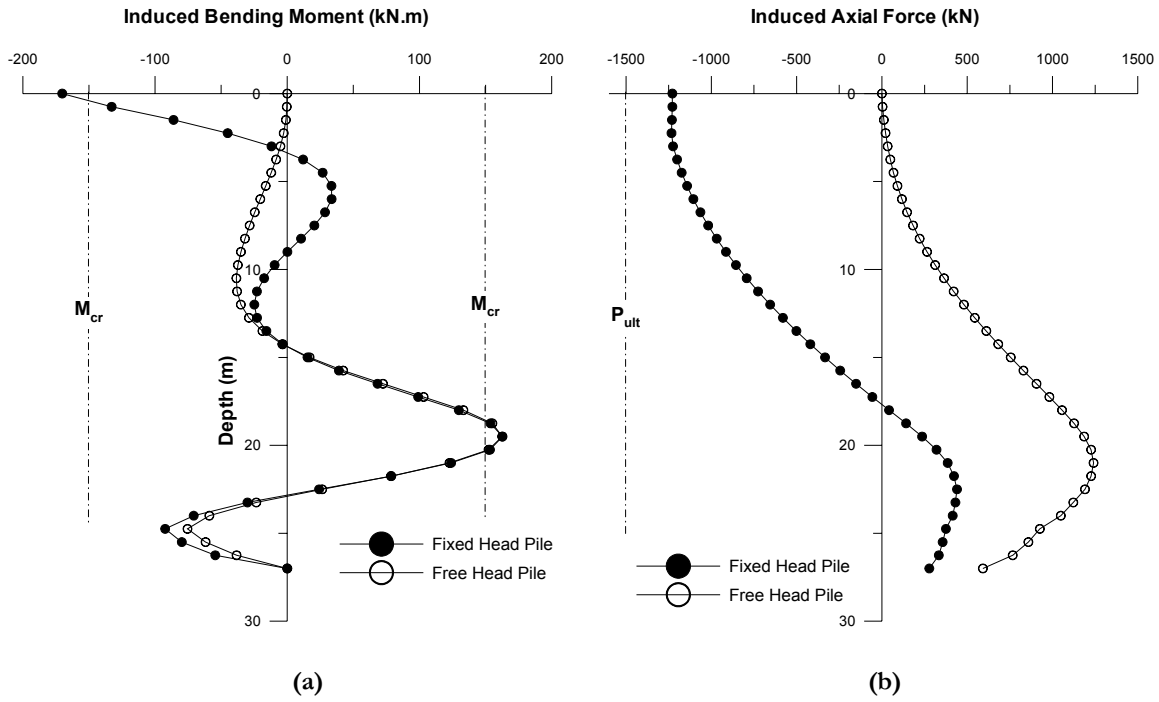

Fig. A.17. Pile (a) bending moment and (b) axial force variation for Y_p = -1D_t

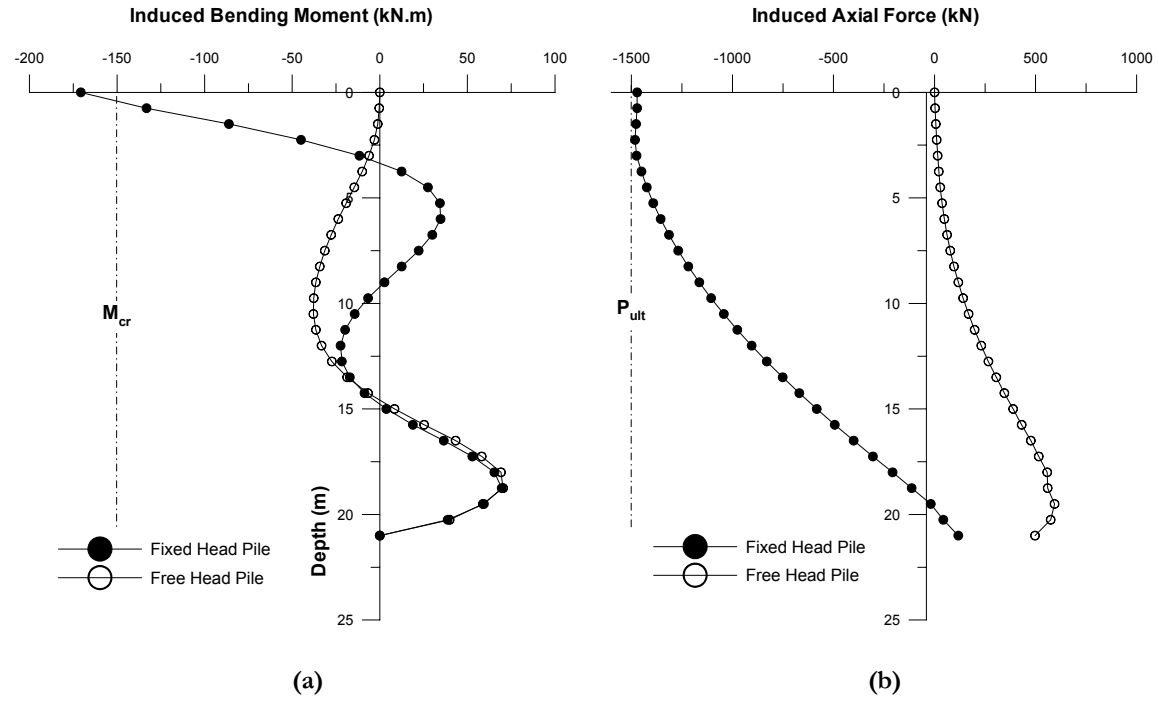

Fig. A.18. Pile (a) bending moment and (b) axial force variation for Y_p = 0D_t

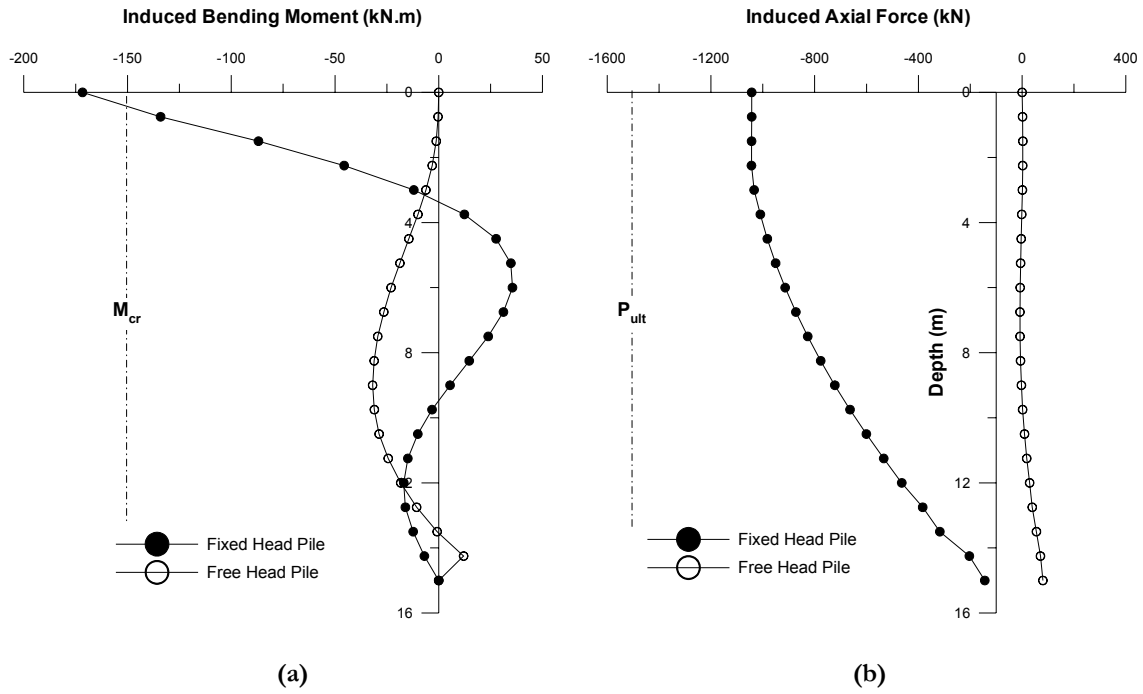

Fig. A.19. Pile (a) bending moment and (b) axial force variation for $Y_p = +1D_t$

Fixed head pile response with volume loss

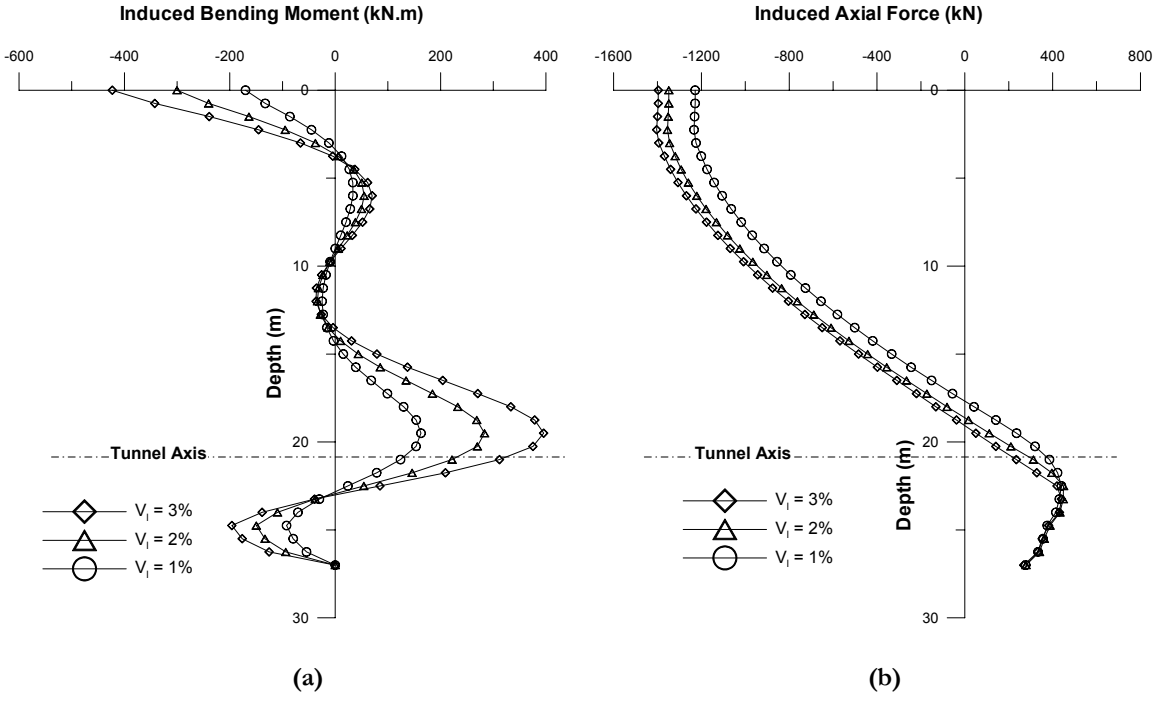

Fig. A.20. Pile (a) bending moment and (b) axial force variation for $Y_p = -1D_t$

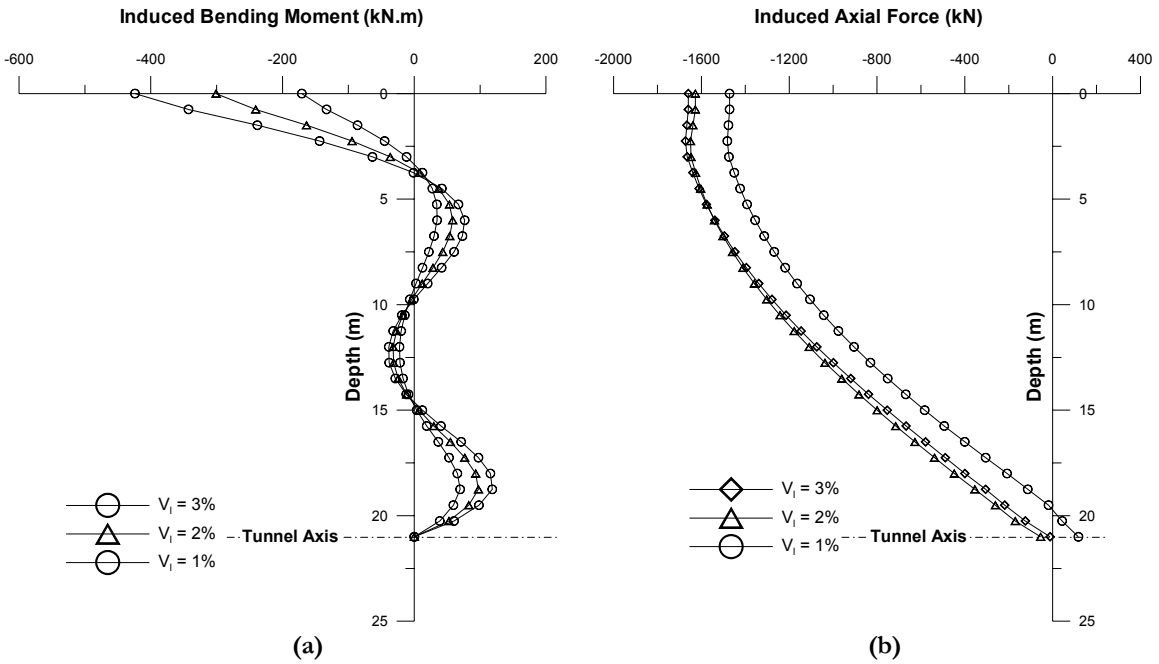

Fig. A.21. Pile (a) bending moment and (b) axial force variation for $Y_p = 0D_t$

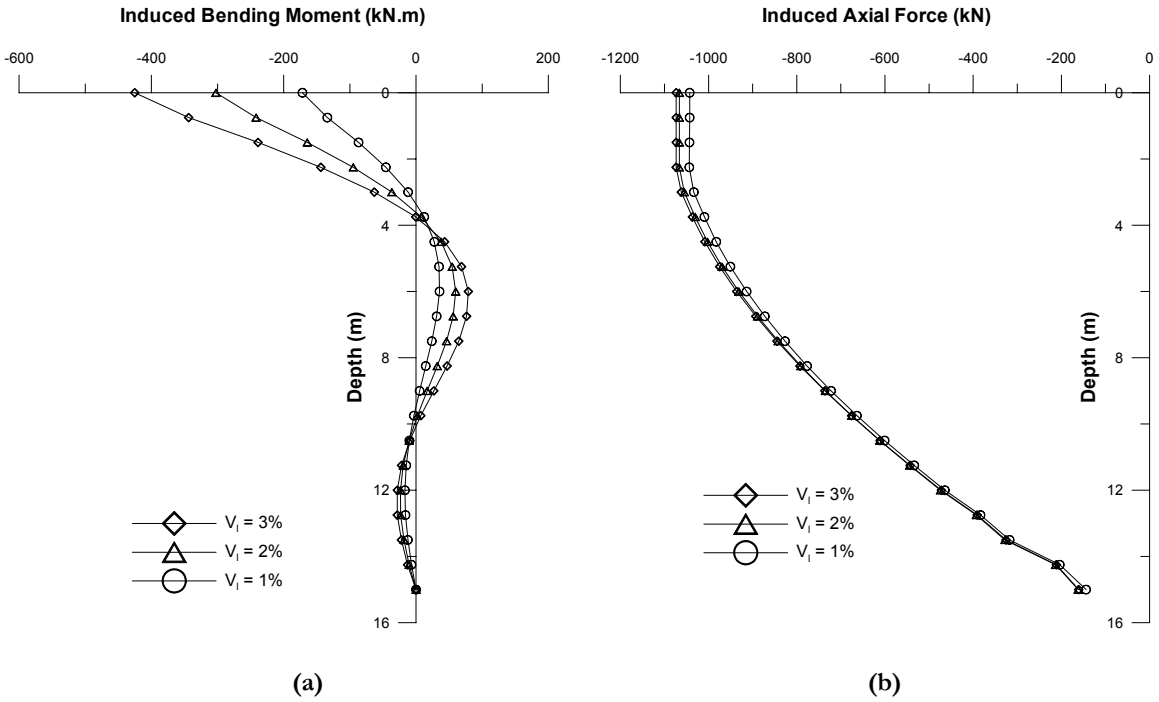

Fig. A.22. Pile (a) bending moment and (b) axial force variation for $Y_p = +1D_t$

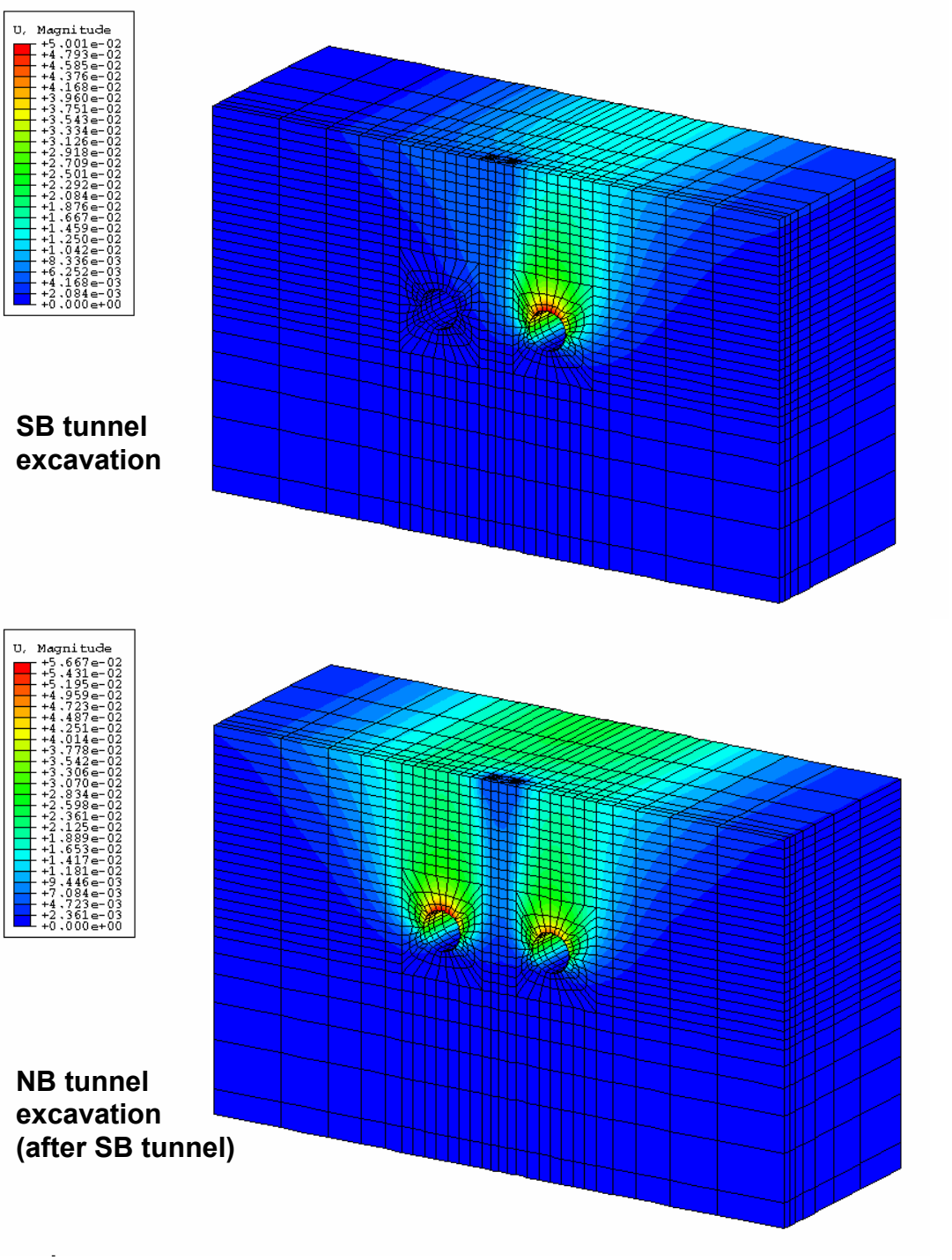

Fig. A.23. Contour plot of displacement magnitudes after SB and NB tunnel excavation

Calculation of average Gmax/p' ratio for kaolin clay in Loganathan's centrifuge case study

Depth (m)	σ_v ' (kPa)	OCR	K_o	p' (kPa)	p_c' (kPa)	R_o	G_{max} (kPa)	G_{max}/p'
5	32.5	18.46	1.91	52.16	444	8.51	4.20E+04	805.57
10	65	9.23	1.45	84.70	444	5.24	5.24E+04	619.13
15	97.5	6.15	1.24	113.19	444	3.92	5.99E+04	528.94
20	130	4.62	1.11	139.47	444	3.18	6.59E+04	472.24
25	162.5	3.69	1.02	164.30	444	2.70	7.10E+04	432.05
30	195	3.08	0.95	188.06	444	2.36	7.55E+04	401.49
							Average	**543.24**

Density	16.5 kN/m^3
ϕ'	23°
OCR	$\sigma_{v\,max}' / \sigma_v'$
$K_{o\,nc}$	1-sin(ϕ')
$K_{o\,oc}$	$K_{o\,nc}$*OCR$^{\sin\phi}$
R_o	p_c'/p'
G_{max}	2088*$p'^{0.653}$*$R_o^{0.196}$

Table A.1. Calculation of G_{max}/p' ratio for input in analysis (Viggiani and Atkinson, 1995)